Development of Separation-Based Microfluidic Platforms to Study Intracellular Nitrosative and Oxidative Stress

By

Joseph M. Siegel
B.S. Chemistry, Truman State University, 2011

Submitted to the graduate degree program in the Department of Chemistry and the Graduate Faculty of the University of Kansas in partial fulfillment of the requirements for the degree of Doctor of Philosophy.

_____
Chair: Dr. Susan M. Lunte

_____
Dr. Robert C. Dunn

_____
Dr. Steven A. Soper

_____
Dr. Christopher G. Elles

_____
Dr. Karen J. Nordheden

Dissertation Defense: July 11, 2017
10:00 am
Simons Auditorium

The Dissertation Committee for Joseph M. Siegel
certifies that this is the approved version of the following dissertation:

Development of Separation-Based Microfluidic Platforms to Study Intracellular Nitrosative and Oxidative Stress

_____

Dr. Susan M. Lunte

Date approved: July 11, 2017

Abstract

Nitrosative and oxidative stress are conditions caused by the overproduction of reactive nitrogen and oxygen species (RNOS), respectively. Nitric oxide (NO) and superoxide ($O_2^{\bullet -}$) are the main sources of all RNOS. Macrophages are immunes cells that are known to produce large amounts of RNOS as part of the immune response. RNOS are capable of nitration, nitrosylation, oxidation, and peroxidation of crucial biomolecules, thereby inhibiting cellular function and causing cytotoxicity. Nitrosative and oxidative stress have been linked to neurodegenerative diseases, cardiovascular disease, and cancers. Therefore, a method to detect and monitor RNOS in macrophages is of the utmost importance. This dissertation describes the progress in developing separation-based microfluidic platforms to directly and indirectly measure RNOS *in vitro*.

Most RNOS are highly reactive and unstable under physiological conditions and therefore extremely difficult to accurately quantitate. Microchip electrophoresis (ME) provides sub-minute separation times, making it possible to separate multiple RNOS in a single analysis before significant degradation occurs. First, methods were developed that utilized ME with electrochemical detection (EC) since many RNOS are electrochemically active. NO was detected indirectly through its degradation product nitrite (NO_2^-). NO_2^- and glutathione (common antioxidant) were separated and detected in macrophage cell lysates after stimulation with lipopolysaccharides (LPS) using ME-EC. Then this method was improved with the combination of transient isotachophoresis to stack NO_2^- and a platinum working electrode modified with platinum black to increase sensitivity. A cellulose acetate decoupler for ME-EC was also developed to reduce noise from the electric field. This approach should improve future

separations through the use of higher electric field strengths and also allow coupling of ME-EC with single cell analysis devices.

RNOS were also separated and detected with ME coupled to laser-induced fluorescence (LIF). LIF provides lower limits of detection compared with EC, but it requires derivatization of analytes prior to analysis. A method utilizing MitoSOX Red, a fluorescent probe specific for $O_2^{\bullet-}$, was developed. $O_2^{\bullet-}$ production was monitored in macrophage cells stimulated with phorbol 12-myristate 13-acetate (PMA) while inhibiting superoxide dismutase, the primary cellular defense against $O_2^{\bullet-}$ production. Then DAF-FM DA, a NO-specific fluorescent probe, was added to this method. This allowed for the simultaneous detection of NO and $O_2^{\bullet-}$ in macrophages stimulated with both nitrosative and oxidative stress agents.

In the future, both the ME-EC and ME-LIF developed in this dissertation will be applied to a single cell analysis (SCA) microfluidic system. SCA will provide information about the effects of cellular heterogeneity on RNOS production. Additionally, RNOS production due to disease-specific stimulants, such as amyloid-β for Alzheimer's disease, will be monitored.

Dedication

To Jenny, my amazing wife

Acknowledgements

I cannot overstate my gratitude for everybody that helped and supported me over the last five years to get to this point!

First of all, I would like to thank my advisor Dr. Susan Lunte. I cannot thank her enough for allowing me to join her group the summer before I started graduate school and then letting me continue to work in her group for the remainder of my graduate school career. Her guidance and support has ultimately allowed me to succeed in graduate school. She has always encouraged me to seek out and take advantage of opportunities, such as applying for fellowships and travel awards as well as attending a variety of conferences to present my research and network. I have learned so much from her throughout my last five years, and I will never cease to be amazed by her vast knowledge of analytical chemistry. Furthermore, I greatly appreciate her nominations for departmental and travel awards. Finally, thank you Sue for playing a huge part in molding me into the person and scientist I am today and will continue to be for the rest of my life.

Thank you Dr. Susan Lunte, Dr. Steve Soper, Dr. Bob Dunn, Dr. Chris Elles, and Dr. Karen Nordheden for being on my defense committee and reading my dissertation. I have always respected each of you as scientists and am grateful for such a prestigious committee. I would also like to thank all staff and faculty in the KU Department of Chemistry and the Ralph N. Adams Institute for Bioanalytical Chemistry. I am very grateful for all the help Susan Teague provided during our lab move. I would like to thank Ryan Grisby for his help in the cleanroom and his microfabrication advice. I would also like to thank Cady Bush. She was always there to answer any question (or know who to contact for the answer) regarding reimbursements, travel

planning, or Sue's sometimes chaotic schedule. She was also somebody I could always go to for a good conversation about life. I also appreciate all the editorial support that was provided by Nancy Harmony.

During my time in graduate school I also had the great pleasure of working with a number of brilliant group members: graduate students Tom Linz, Anne Regal, David Scott, Dulan Gunasekara Jessica Creamer, Nate Oborny, Abdullah Al-Hossaini, Rachel Saylor, Shamal Gunawardhana, Manjula Wijesinghe, Giuseppe Caruso, Claudia Fresta, Michael Hogard, Amanda Furness, Kelci Schilly, Galina Bulgakova, and Dhanushka Weerasekara; undergraduate students Pann Pichetsunnthorn, Erin Evans, Keelan Trull (REU), Jeff Bauman, Paige Skillett (REU), Esha Abbi (REU) Ricardo Gonzalez, Vince Florentino, Fergal O'Donnell (REU), Christian Davis (REU), and Sonia Schöneich; and visiting students and professors Diogenes Meneses dos Santos, Simon Pfeiffer, Bruno Lucca, Richard Piffer, Elton Melo Costa, Dr. Leena Suntornsuk, and Dr. Ebru Buyuktuncel. I considered all these group members my friends and I really enjoyed our conversations, both personal and scientific, in lab and at group lunches, dinners, and happy hours. I am grateful that I got to be part of a group that is very open and willing to help. I would like to especially thank Dulan for mentoring me during my first two years. He taught me all the basics about RNOS, ME-EC, and cell culturing.

I would specifically like to thank all the group members that were part of the RNOS/SCA minigroup: Dulan, Giuseppe, Claudia, Michael, Manjula, Kelci, Dhanushka, Pann, Keelan, Jeff, Paige, Ricardo, Fergal, and Richard. Richard picked up the superoxide project and I was lucky enough to work with him on that project throughout his time at KU. I would like to thank Paige, Jeff, and Ricardo for all their hard work on the detection of peroxynitrite with HKGreen-3 project. I also appreciate all the cell culturing help and advice that was provided by Giuseppe

and Claudia. I am also grateful that I got to work Kelci during my last two years on the Pt black project. I greatly enjoyed the opportunity to mentor Kelci and pass on my knowledge, as Dulan did for me.

Thank you to the Culbertson lab at Kansas State University for their help with single cell analysis. Dr. Chris Culbertson is a very knowledgeable scientist and always provided good advice on ways to advance my research. I would like to thank Damith Patabadige, Jay Sibbitts, and Jalal Sadeghi for all their help performing the single cell analysis experiments. I would also like to thank Anne Culbertson for her help with cell culturing at K-State.

I greatly appreciate the support that has been provided by the Madison and Lila Self Graduate Fellowship. This fellowship funded me for four years and provided me the opportunity to grow professionally and as a leader. I thank all the SGF staff that I have worked with: Sharon Graham, Cathy Dwigans, Patty Dannenberg, Stephani Buchwitz, Amy Benoit-Warlick, Tammie Zordel, and Michael Roberts. Thank you all for your encouragement and support during my time in the fellowship.

I am also grateful for all the close friends I've made within the chemistry department in other groups: Mary Smith, Mason Hart, Jude Lakbub, Tom Field, and Chris Otolski. We have always been there for each other through the highs and lows of graduate school. They have also been an invaluable source of knowledge since the majority of them are not in analytical chemistry.

Last, but certainly not least, I have to thank my family. My wife, Jenny, has been my rock throughout graduate school and always encouraged and pushed me to keep going so that I could achieve my goals after graduate school. This dissertation is dedicated to her because I

couldn't have done this without her. Another joy, was always getting to come home to my two dogs, Rocky and Lily, who were always excited to see me, which felt good after a tough day in lab. I am also grateful to my parents, John and Tracy, who have always been supportive and pushed me to be the best person I can be. Additionally, I want to thank my sister, Kirsten, for being a person I could always talk to and for constantly cheering me on. I also need to thank Jenny's side of the family, Tom, Helen, Aaron, and Rosanne, who have also always been there for me, along with Henry and Olivia who were always there to cheer me up. Thank you to everybody in my family who have listened to me ramble on about my research even though I'm sure it sounded like another language sometimes.

Table of Contents

List of Figures

Figure 4.2. Electropherogram of 150 μM norepinephrine (NE), 150 μM hydroquinone (HQ), and 100 μM ascorbic acid (AA) in normal polarity with and without the presence of a decoupler. The table on the right displays the peak heights for each analyte peak as well as the amplitude of the noise with and without a decoupler.

Figure 4.3. A graph of the noise amplitude as a function of separation field strength for a microchip with and without a decoupler.

Figure 4.4. Electropherogram of the separation of 100 μM NO_2^-, 100 μM ascorbic acid, and 200 μM hydrogen peroxide in reverse polarity with a cellulose acetate decoupler.

Figure 5.1. Reaction of MitoHE with $O_2^{\bullet-}$ and other ROS (adapted by permission from Macmillan Publishers Ltd: Nature Protocols, 2008.).

Figure 5.2. Calibration curve for 2-OH-MitoE^+ obtained from the reaction between MitoHE and NDS. $R^2 = 0.97$. $y=8.6\times10^{-4} + (4.0\times10^{-5})\,x$

Figure 5.3. MitoHE reaction with NDS prepared using (a) 3.6 mg of potassium NDS (NDS limited reaction) and (b) using 4.0 mg of potassium NDS (stoichiometric amount) from a 67.5% pure Fremy's salt. Laser alignment at 2.3 cm

Figure 5.4. Electropherograms for the injection of XA/XO reaction media + MitoHE with and without SOD.

Figure 5.5. SIN-1 decomposition in presence of OH^-. The reaction generates NO and $O_2^{\bullet-}$ that will react to form $ONOO^-$. Once inside a cell, esterases can also trigger a similar reaction pathway, producing SIN-1C and the byproducts NO, $O_2^{\bullet-}$ and $ONOO^-$. Reprinted with permission from Hulvey, M.K.; Frankenfeld, C.N.; Lunte, S.M. *Anal Chem*. **2010**, *82*, 1608-11. Copyright 2010 American Chemical Society.

Figure 5.6. Monitoring of $O_2^{\bullet-}$ release during SIN-1 conversion to SIN-1C as a function of time.

Figure 5.7. Electropherogram obtained for native and SIN-1 incubated RAW 264.7 macrophage cells. (a) Native RAW 264.7 macrophage cells; (b) SIN-1 incubated RAW 264.7 macrophage cells; (c) Native RAW 264.7 macrophage cells in presence of DDC; (d) SIN-1 incubated RAW 264.7 macrophage cells in presence of DDC. Detection point = 4.5 cm from T intersection

Figure 5.8. Stimulation optimization. RAW 264.7 macrophage cells were stimulated with 2 ng/mL PMA for 12 hours and then incubated with 6 uL of 5mM MitoHE for 10 minutes. (a) Fluorescence image of stimulated cells and (b) fluorescence image of native/control cells after stimulation protocol. (c) Electropherogram for (I) stimulated RAW 264.7 in comparison to (II) standard containing MitoE^+ and 2-OH-MitoE^+. Detection point = 2.5 cm from T intersection.

Figure 5.9. Electropherograms for RAW 264.7 lysate samples. Samples were prepared and diluted by a factor of 10 prior to injection. n = 5. (a) Lysate from 24 h PMA stimulated cells in

List of Tables

Chapter 1:

Introduction

Parts of this chapter were published in the following book chapter:

Joseph M. Siegel, Richard P. S. de Campos, Dulan B. Gunasekara, José A. F. da Silva, Susan M. Lunte. "Chapter 7: Electrophoretic Methods for Separation of Peroxynitrite and Related Compounds" in *Peroxynitrite Detection in Biological Media: Challenges and Advances*. The Royal Society of Chemistry, 2015.

1.1. Intracellular Nitrosative and Oxidative Stress

Nitrosative and oxidative stress are caused by an overproduction of reactive nitrogen species (RNS) and reactive oxygen species (ROS), respectively. Both of these forms of stress have been linked to the development of neurodegenerative diseases, such as Alzheimer's, Parkinson's, and Huntington's disease, cardiovascular disorders, and cancer [1-5]. Reactive nitrogen and oxygen species (RNOS) are capable of reacting with crucial biomolecules (proteins, DNA, lipids, etc.). Specifically, RNS and ROS cause the nitration and nitrosylation or oxidation and peroxidation of biomolecules, respectively [1-3]. Modifications of these substances disrupt intracellular biological processes and ultimately lead to apoptosis and cytotoxicity [6]. The primary sources of RNS and ROS are the production of nitric oxide (NO) and superoxide ($O_2^{\bullet-}$), respectively.

1.1.1. Cellular Production of RNOS

NO is produced via the nitric oxide synthase (NOS) enzyme that catalyzes the conversion of L-arginine into L-citrulline [7]. There are three forms of the enzyme present in mammals: endothelial NOS (eNOS), neuronal NOS (nNOS), and inducible NOS (iNOS). As the name implies, eNOS and nNOS are primarily found in endothelial and neuronal cells, respectively, whereas iNOS is present in immune cells [7, 8]. The activation of eNOS and nNOS is dependent on the intracellular calcium concentration [7]. iNOS is independent of calcium and is activated during the immune response [7].

The production of $O_2^{\bullet-}$ primarily occurs within the mitochondria during the electron transport chain (ETC). The ETC is comprised of five protein complexes (I, II, III, IV, and V). Protein complexes I and III are the sites in which O_2 is reduced to $O_2^{\bullet-}$ (Figure 1.1) [9-11].

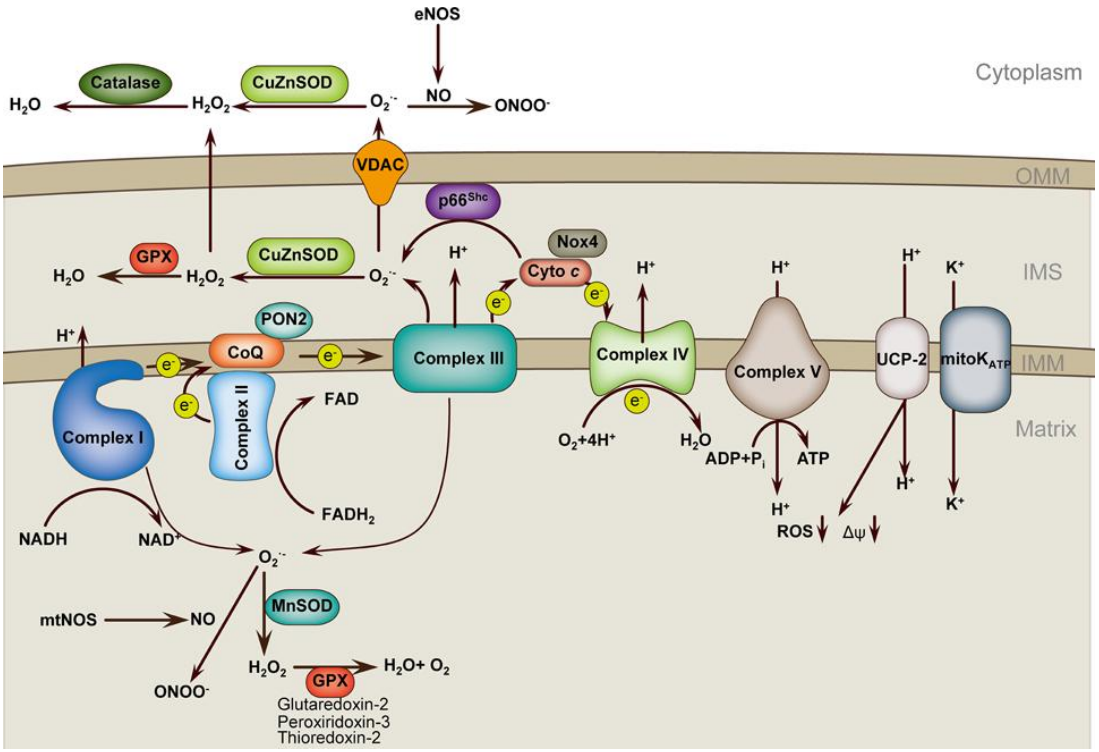

Figure 1.1. Production of $O_2^{\bullet-}$ inside the mitochondria during the electron transport chain (reproduced from Tang, X.; Lou, Y.; Chen, H.; Liu, D. *Front Physiol*. **2014**, *5*.).

Additionally, the $O_2^{\bullet-}$ production at protein complex I is significantly increased when the electron transport mechanism is reversed [9]. Production of $O_2^{\bullet-}$ can also occur in the cytosol of the cell during certain enzymatic reactions, such as the oxidation of NADPH to $NADP^+$ by the NOX2 enzyme [12].

The presence of NO and $O_2^{\bullet-}$ can lead to the production of a variety of other RNOS (Figure 1.2). Specifically, the simultaneous overproduction of NO and $O_2^{\bullet-}$ can lead to the production of peroxynitrite ($ONOO^-$) [1, 13]. $ONOO^-$ is a powerful oxidant that is cytotoxic due to its high reactivity with biomolecules and ability to travel across cell membranes when converted into the neutral species, peroxynitrous acid (ONOOH) [1, 13].

1.1.2. Biological Relevance of RNOS

$O_2^{\bullet-}$ is produced as a by-product of the ETC and is toxic to the cell. Superoxide dismutase (SOD) is present in both the mitochondria (Mn-SOD) and cytosol (Cu/Zn-SOD) of the cell and scavenges $O_2^{\bullet-}$ by converting it to hydrogen peroxide (H_2O_2) [14]. Catalase or glutathione peroxidase then reacts with H_2O_2 to produce O_2 and water. $O_2^{\bullet-}$ and H_2O_2 that are not properly scavenged can result in the production of other ROS, such as $^{\bullet}OH$ through the Fenton reaction, to cause additional intracellular oxidative damage.

NO production is very important to maintain biological homeostasis. NO produced from eNOS can diffuse into adjacent smooth muscle cells to stimulate the formation of cyclic guanosine monophosphate (cGMP), which is responsible for vasodilation [15, 16]. Additionally, NO also prevents the aggregation and adhesion of platelets within the vascular system [15]. In the brain, nNOS produces NO to once again cause the formation of cGMP, which modulates neurotransmitter release [17]. iNOS is capable of producing high concentrations of NO during

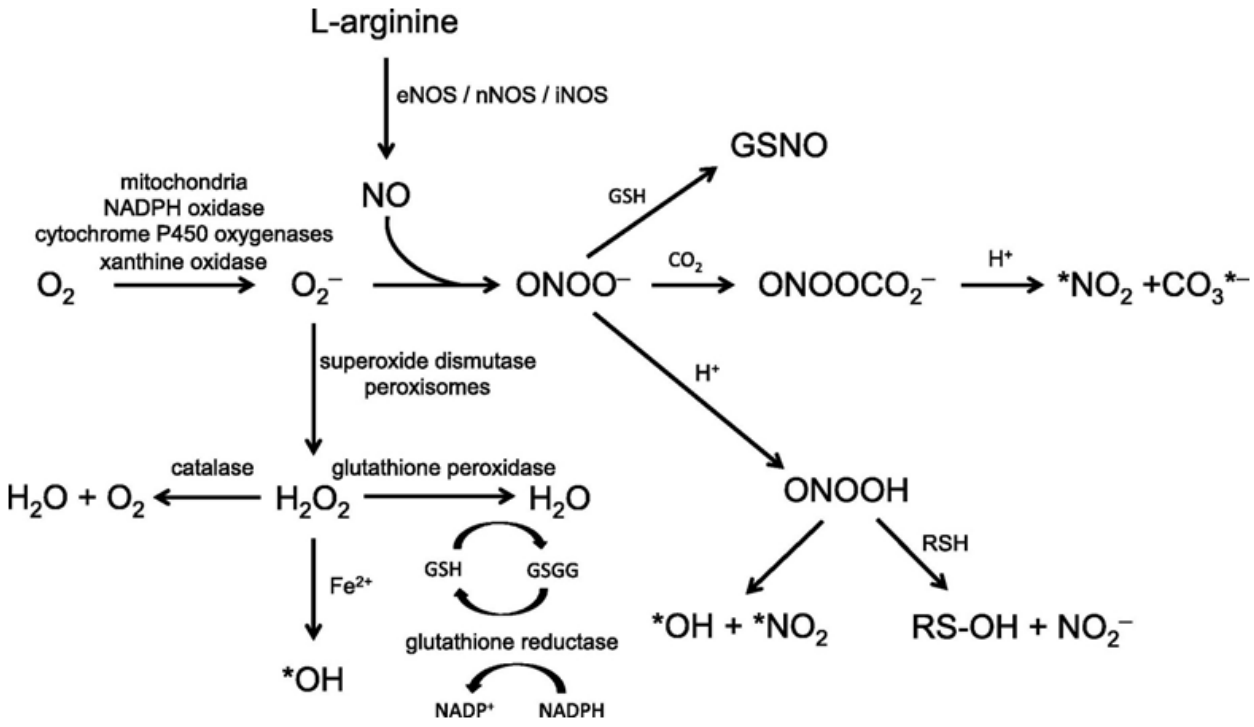

Figure 1.2. Diagram of RNOS production in a cellular environment (reprinted from Activation of intracellular matrix metalloproteinase-2 by reactive oxygen-nitrogen species: Consequences and therapeutic strategies in the heart, 540, Jacob-Ferreira, A. L. and Schulz, R., 82-93, 2013 with permission from Elsevier.).

the immune response. NO can react with a variety of small molecules to produce RNS like $ONOO^-$, $^{\bullet}NO_2$, and N_2O_3, which are able to react with and kill harmful microbes in the body such as bacteria, pathogens, and cancer cells.

Immune cells primarily express iNOS to protect tissues within the body. Macrophages are the most common type of immune cell. Macrophages that are unique to specific organs in the body can have different names based on their location. Examples include microglia (brain), aveolar (lungs), and Kupffer cells (liver) [18]. Furthermore, monocytes can be differentiated into macrophages in response to macrophage colony-stimulating factor (M-CSF) [19].

Macrophages are known to be heterogeneous and can be activated into different phenotypes based on the cytokines and endotoxins present in the cellular environment. The two primary phenotypes into which macrophages are activated are M1 and M2 (Figure 1.3). The M1 phenotype is activated with endotoxins, such as lipopolysaccharide, and interferon-γ. This activation is called "classical activation" and produces pro-inflammatory macrophages, which produce large amounts of RNOS through the expression of iNOS to eliminate threats to the body [20-23]. During this process, other molecules are also produced, such as tumor necrosis factor α and chemokines. Macrophages that undergo an alternative activation pathway are known as M2 cells. M2 cells are activated by interleukin 4, interleukin 10, or interleukin 13. M2 cells are anti-inflammatory and support tissue healing through the expression of arginase to produce vascular endothelial and epidermal growth factors [20-23]. These two phenotypes must stay balanced if a organism is to stay in homeostasis. If there is an overabundance of M1 cells, excessive tissue damage occurs, which can lead to cardiovascular disease and neurodegeneration [23-25]. On the other hand, an overabundance of M2 cells can lead to cancer due to unregulated cellular growth and proliferation [26].

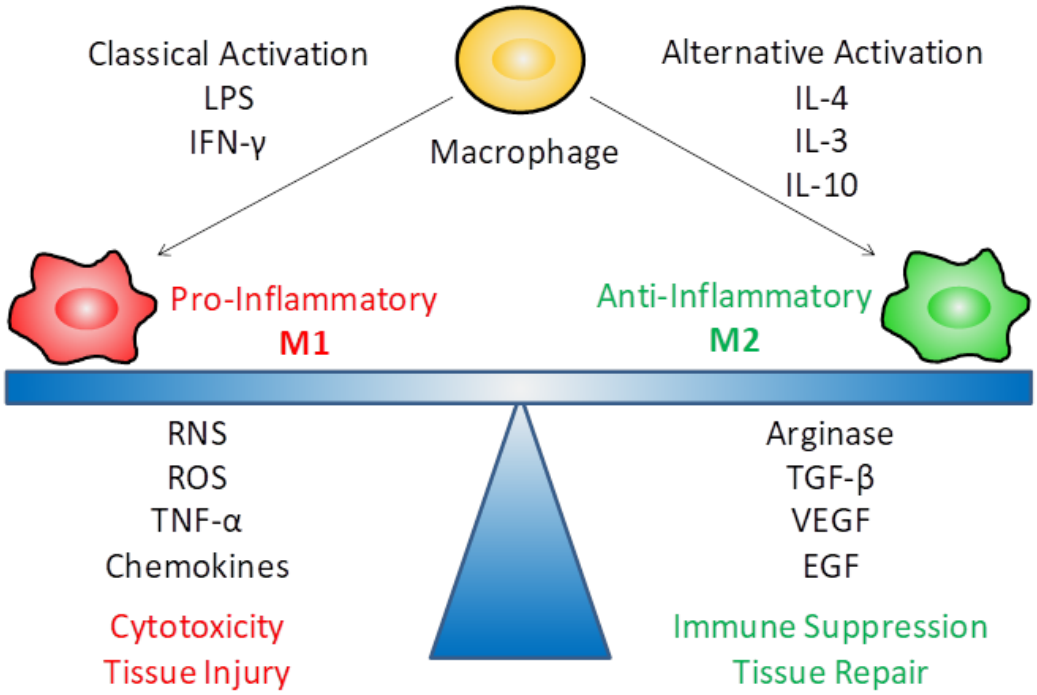

Figure 1.3. Illustration of the balance between the M1 and M2 macrophage phenotypes (adapted with permission from Laskin, D. L.; *Chem. Res. Toxicol*. **2009**, *22*, 1376-1385. Copyright 2009 American Chemical Society.).

1.1.3. RNOS Implications in Neurodegenerative Diseases

Neurodegenerative diseases, such as Alzheimer's and Parkinson's disease, are characterized by the deterioration of specific neuronal cell populations in the brain. The reason for this neuronal death is still unclear, but proposed causes include mislocalized nucleic acids, misfolded proteins, aggregated proteins, and overproduction of RNOS [27-30]. Alzheimer's disease is also associated with elevated amounts of amyloid-β (Aβ) aggregation in the extracellular space [28, 31]. The presence of Aβ activates the microglia in the local microenvironment to produce a pro-inflammatory response [32]. Parkinson's disease is caused by the death of dopaminergic neurons and is linked to the formation of intracellular α-synuclein deposits, which have also been shown to provoke an immune response [28, 29, 33]. Additionally, these protein aggregates have been shown to contain sites of amino acid nitration and oxidation implying a significant role for RNOS in these diseases [34].

1.2. Methods to Detect NO

Due to the involvement of NO in numerous important biological processes, a variety of methods to detect it have been developed. The techniques employed include electron paramagnetic resonance spectroscopy (EPR), chemiluminescence, fluorescence, and electrochemical detection [35-37]. Additionally, NO can be monitored indirectly by detecting nitrite (NO_2^-), which is the product of the natural reaction between NO and O_2 [35-39].

EPR has been shown to be a very useful NO detection method in complex matrices. EPR works by adding radical species, such as NO, into a magnetic field. When in the magnetic field, the unpaired electrons in different spin states form an energy difference. In EPR, the absorption of the electromagnetic radiation in the microwave region resulting from this difference is observed [40, 41]. Due to the instability of NO, a spin trap reagent must be added to the sample

that reacts with NO [40, 41]. The most common spin traps for NO are hemoglobin, myoglobin, and iron-dithiocarbamates. EPR is advantageous for NO detection because common potential interferents such as NO_2^-, NO_3^-, and CO are all diamagnetic and therefore are not affected in the magnetic field.

The detection of NO using chemiluminescence is commonly achieved through the reaction of NO with ozone (O_3). This reaction results in the formation of excited-state nitrogen dioxide (NO_2^*), which releases a photon during relaxation to the ground state. The light emitted from this process is greater than 600 nm. The most common problem with this approach is due to the reaction of O_3 with other species, such as carbonyls, ethylenes, and a number of sulfur compounds, that also produce excited-state products. However, most of these products emit light at wavelengths shorter than 600 nm, so wavelength filters can be used to eliminate the response from these potential interferences [42]. A catalytic coverter can be employed prior to the reaction chamber to reduce NO_2 (gaseous product of NO degradation) back to NO. Furthermore, the presence of NO_2^- and NO_3^- in the sample, which can both also be reduced to NO, can be removed by employing a carrier gas that only carries the NO and NO_2 to the converter and then the reaction chamber. Since the addition of the carrier gas only allows the detection of gaseous NO, this method is incompatible for many biological applications [42].

The other method of NO detection via chemiluminescence is using H_2O_2 and luminol. NO can react with the H_2O_2 to form $ONOO^-$, which then reacts with the luminol to produce a chemiluminescent signal. This method provides a low LOD (100 fmol/L), but this system cannot be used in biological environments because of the toxic effects of high H_2O_2 concentrations [37].

In order to detect NO using fluorescence detection, NO must react with a probe to produce that generates a fluorescent product. Many types of fluorescent probes have been

developed for NO detection including diaminofluoresceins (DAFs), diaminorhodamines (DARs), boron dipyrromethene (BODIPY)-based, and diaminocyanides (DACs), with the most popular being the DAF family [43-46]. Specifically, the probe 4-amino-5-methylamino-2',7'-difluorofluorescein (DAF-FM) has been used for a wide variety of biological applications [45, 46]. DAF-FM has been shown to be advantageous compared to other DAFs because it has been shown to be less susceptible to photobleaching and provides increased sensitivity. Additionally, DAF-FM is very selective towards NO, and these molecules react to form DAF-FM T, a highly fluorescent product (Figure 1.4). The main interferent with this reaction has been found to be dehydroascorbate (DHA), which produces a different fluorescent product (DAF-FM DHA) with the same excitation and emission wavelengths [47-49]. The use of fluorescence for NO detection provides LODs in the nM and pM range [35, 37].

NO can also be detected electrochemically via oxidation at an electrode. The use of electrochemical detection allows for real-time results while also providing the option to improve the selectivity and sensitivity through electrode modification and/or judicious selection of an applied potential. Many sensors have been developed to monitor NO directly using a variety of electrode materials [35, 50-53]. The most common microelectrode material used for electrochemical detection is carbon; however, metal microelectrodes (e.g. Pt or Pd) facilitate better oxidation of NO and $ONOO^-$. Since there are many electrochemially active molecules in biological samples that can interfere with the signal for NO, such as NO_2^-, ascorbic acid, glutathione, H_2O_2, CO, and uric acid, electrodes can be coated with a membrane made of materials such as cellulose acetate, Nafion, PTFE, or xerogel to increase selectivity toward NO [35, 50, 54]. These membranes are selective for NO by taking advantage of its hydrophobic

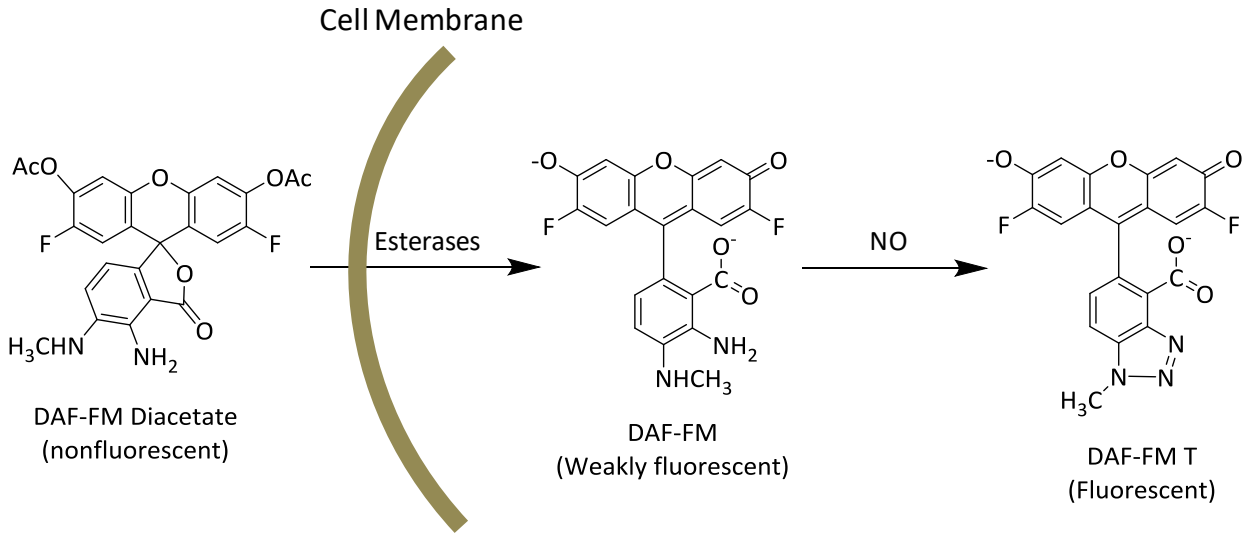

Figure 1.4. Reaction scheme of DAF-FM DA to react with intracellular NO.

nature and neutral charge. The sensitivity of a carbon or metal electrode for NO can be enhanced through the platinization of the electrode to produce platinum black [35].

There are many ways to detect NO indirectly. The most widely used approach is the detection of NO_2^- using the Griess assay. This assay involves reacting NO_2^- with sulfanilamide in acidic conditions to produce a diazonium salt intermediate that is then then coupled with N-(1-naphthyl)ethylenediamine to form the azo dye. The absorbance of the azo dye is measured at 540 nm to determine the concentration of NO_2^- [55, 56]. The LOD of this method for NO_2^- is approximately 0.5 μM [35]. The main disadvantage of this assay is that NO_2^- naturally degrades into nitrate (NO_3^-); however, this occurs at a slower rate than the conversion of NO into NO_2^-. This can be avoided by reducing NO_3^- back to NO_2^- prior to analysis with chemical reductants such as cadmium, zinc, and vanadium chloride [35].

1.3. Methods to Detect $O_2^{\bullet-}$

To obtain a better understanding of oxidative stress and oxidative damage in biological system, many detection methods have been developed to monitor $O_2^{\bullet-}$. These methods include chemiluminescence, fluorescence, and electrochemical detection [57-59]. Unfortunately, many of these methods suffer from low selectivity due to the presence of other ROS with similar oxidizing capabilities such as hydroxyl radicals, H_2O_2, and hypochlorite. The most reliable methods for $O_2^{\bullet-}$ detection are fluorescence following reaction with hydroethidium (HE) or 2-chloro-1,3-dibenzothiazolinecyclohexane (DBZTC) and electrochemical detection.

The use of HE has provided a good means of accurately detecting $O_2^{\bullet-}$ in biological systems because of its selectively. The commercially available HE derivative, MitoSOX Red, is currently the primarily form utilized. MitoSOX Red is HE with a triphenylphosphonium cation (TPP^+) congugated to it, which directs the probe away from the nucleus of the cell and toward

the mitochondria [60, 61]. $O_2^{\bullet-}$ reacts with MitoSOX Red to form the product 2-OH-MitoE^+. The disadvantage of this probe is that other ROS can react with the probe to form a different fluorescent product [60, 61]. Therefore, a separation is necessary to distinguish the fluorescent signal originating from each product. More information about this probe and its reactions with ROS can be found in Chapter 5.

DBZTC is a relatively new fluorescent probe for $O_2^{\bullet-}$ detection. It has shown very high selectivity for $O_2^{\bullet-}$. In fact, it has been shown that even a 1000-fold higher concentration of H_2O_2, as compared with the $O_2^{\bullet-}$, does not interfere with the reaction [62, 63]. The disadvantage of this probe is that, unlike MitoSOX Red, it is not commercially available.

$O_2^{\bullet-}$ can be reduced directly at a carbon or gold electrode, but this approach suffers from lower selectivity and high noise due to the reduction of water at a similar potential [57, 59, 64]. Therefore, electrochemical sensors for $O_2^{\bullet-}$ generally rely on electrodes that have been modified with enzymes that generate products from $O_2^{\bullet-}$, such as H_2O_2 or iron, that can be detected at an oxidatizing potential. The two most common enzymes used are SOD or cytochrome c (cyt c) [59, 64]. SOD converts the $O_2^{\bullet-}$ into H_2O_2, which can be easily oxidized. Cyt c is a small heme protein that has its iron center reduced by $O_2^{\bullet-}$. The reduced iron (Fe^{2+}) can then be oxidized back to Fe^{3+} to generate an electrochemical signal that is proportional to the $O_2^{\bullet-}$ concentration. To remove the interference from other ROS (mainly H_2O_2), these enzyme-coated electrodes are generally coated with a membrane, such as Teflon or polypyrrole [65]. In the case of SOD-based sensors, these membranes allow through $O_2^{\bullet-}$ but not H_2O_2, thereby allowing $O_2^{\bullet-}$ to go through enzymatic conversion to H_2O_2, which can then be oxidized and the signal can be related back to the presence of $O_2^{\bullet-}$.

1.4. Methods to Detect $ONOO^-$

UV detection is one of the simplest methods for $ONOO^-$ detection. The anionic form of $ONOO^-$ exhibits a maximum absorbance at λ = 302 nm (ε = 1670 M^{-1} cm^{-1}) [66]. This differs from that of the protonated form of $ONOO^-$ (ONOOH), which has a λ_{max} of 240 nm and NO_2^- and NO_3^- at λ_{max} of 214 nm [66]. Therefore, $ONOO^-$ can be distinguished from NO_2^- and NO_3^- based on its unique absorbance at 302 nm [67].

There are also fluorescent probes that have been developed to detect $ONOO^-$, such as HKGreen-3. HKGreen-3 is a $ONOO^-$-selective fluorescent probe reported by Peng et al. [68]. However, the use of this probe requires a separation step because the probe itself is fluorescent and has similar excitation and emission wavelengths as the $ONOO^-$-specific product. More information about this probe for the detection of $ONOO^-$ can be found in Chapter 7.

Electrochemical detection of $ONOO^-$ is also possible, but not as widely used [65]. Similar to electrochemical measurements of NO, there are number of electrochemically-active molecules in biological samples, making it impossible to distinguish the $ONOO^-$ signal. Peteu *et al*. have recently developed a $ONOO^-$-selective sensor [69]. This sensor consists of a boron-doped diamond microelectrode with an electropolymerized film of hemin and polyethylenedioxythiophene (hemin-PEDOT). When $ONOO^-$ comes into contact with the sensor the Fe^{4+} in the hemin is reduced to Fe^{3+}. The Fe^{3+} is then electrochemically oxidized to give a signal proportional to the $ONOO^-$ concentration [69]. This study only looked at serotonin, uric acid, and norepinephrine as interferents, so to ensure the selectivity of this sensor, more studies need to be completed with a wider variety of interferents.

$ONOO^-$ metabolites and products from reactions with biomolecules tend to have higher stability and can therefore be used to indirectly monitor $ONOO^-$ production. $ONOO^-$ degrades

into NO_2^- and NO_3^-, which can be detected using a variety of methods [70-75]. However, since there are two degradation products, it is difficult to obtain an accurate concentration of $ONOO^-$ with this method. The more commonly used marker for $ONOO^-$ production in biological systems is nitrotyrosine. ONOOH readily nitrates tyrosine residues in biological conditions to produce nitrotyrosine. Methods to detect nitrotyrosine have been developed using direct UV absorbance and laser induced fluorescence using various dyes such as fluorescein isothiocyanate (FITC) and 7-fluoro-4-nitro-2,1,3-benzoxadiazole (NBD-F) [76-78].

1.5. Electrophoretic Separations

During electrophoretic separations, molecules are separated based on the ratio of their charge-to-hydrodynamic radius. Once the separation channel or capillary is filled with run buffer, the sample is injected at one end and then a voltage is applied across the separation region. Following the application of an electric field, anions migrate toward the positive electrode (anode) and cations migrate toward the negative electrode (cathode). Neutral molecules will not move because they are unaffected by the electric field [79]. The velocity at which the ion will migrate toward its respective electrode (v) is defined as:

$$v = \mu E \qquad (1)$$

where E is the strength of the electric field and μ is the ion's electrophoretic mobility [79]. Since each ion has a unique electrophoretic mobility, it is possible to separate multiple ions simultaneously in an electric field. The electrophoretic mobility is defined as:

$$\mu = \frac{q}{6\pi\eta r} \qquad (2)$$

where q, η, and r are the net charge of the molecule, viscosity of the run buffer, and solvated ionic radius of the molecule, respectively [79].

In capillary electrophoresis (CE), a bulk flow called the electroosmotic flow (EOF) is generated due to the presence of an electric double layer (EDL) caused by the ionized silanol groups on the wall of the fused silica capillary. As the pH increases, more silanol groups are deprotonated, resulting in a more negatively charged wall and thicker EDL. It is the attraction of the solvated cations present in the background electrolyte (BGE) to the capillary wall that forms the EDL. The EDL consists two parts: (1) a compact layer of solvated cations that are strongly attracted to the negatively charged wall and (2) a diffuse layer of solvated cations that have a weaker attraction to the wall [79]. In normal polarity, when a positive voltage is applied from the anode at the inlet of the capillary to the cathode at the outlet, the solvated cations in the diffuse layer migrate toward the cathode and drag the bulk solution with them, causing the EOF. This bulk flow will force all the analytes to flow in one direction. So, in the case of normal polarity, the molecules will migrate past the detector in the order: positive, neutral, and lastly negative molecules (Figure 1.5). In the presence of this EOF, the apparent (experimental) mobility of a molecule (μ_{app}) in the capillary will be the vectorial sum of the molecule's actual electrophoretic mobility (μ_{ep}) and the mobility of the EOF (μ_{eof}) [79].

$$\mu_{app} = \mu_{ep} + \mu_{eof} \quad (3)$$

Surfactants can be added to the run buffer to dynamically modify the EOF within the capillary. A cationic surfactant, consisting of a positivity charged headgroup and a nonpolar tail, can be added to the run buffer to reverse the EOF. These surfactants adsorb to the walls of the capillary and form a bilayer that creates a positively charged wall. When using reverse polarity (applying a negative electric field across the capillary), the EOF will flow toward the anode, and the order in which the molecules migrate will be reversed [79]. This approach is ideal for the separation of small, negatively-charged molecules such as RNOS.

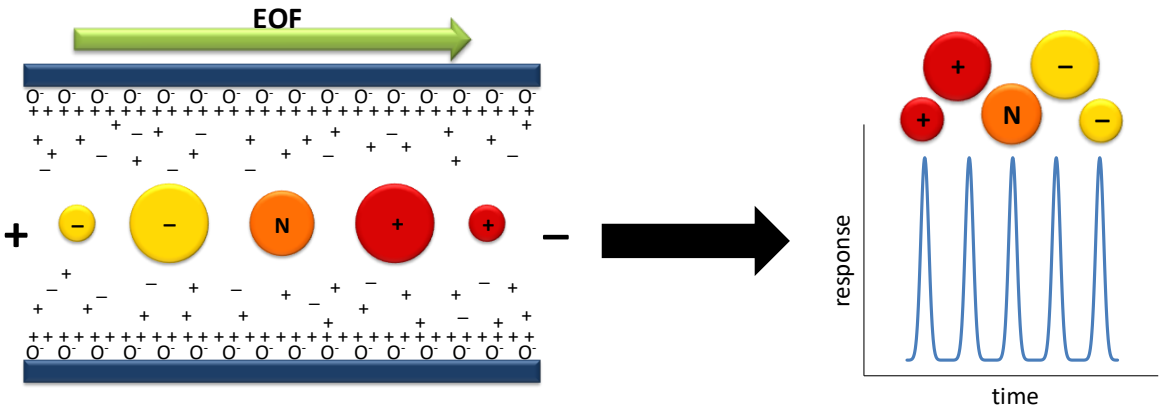

Figure 1.5. Illustration of an electrophoretic separation in normal polarity where the detector is near the cathode. The molecule migration order on an electropherogram can be seen on the right.

The magnitude of the EOF is dependent on a number of factors. In particular, the ionic strength of the run buffer used for the separation will change the magnitude of the EOF because it directly influences the zeta potential of the EDL [79]. The zeta potential is defined as the potential at the shear plane between the adsorbed and mobile layer of the EDL. Therefore, it describes the strength of electrical attraction between the buffer ions and the charged wall. A decrease in the ionic strength will cause an increase in the zeta potential, thus increasing the magnitude of the EOF [79]. This faster EOF will lead to shorter migration times; however, it could also lead to decreased resolution. Additionally, high ionic strengths can lead to Joule heating within the capillary, causing convection and a reduction in the separation efficiency [79]. In extreme cases, the temperature increase can cause the buffer to outgas and form bubbles, which will interrupt the electrical current through the separation channel. Therefore, the run buffer must be optimized to produce the ideal EOF strength and provide the best separation possible.

1.5.1. Microchip Electrophoresis

The separation channels used in microchip electrophoresis (ME) are normally much shorter than capillaries used in CE. Typical channel lengths are 5–15 cm compared to the 20–100 cm capillaries needed for CE. However, the electric field applied across the separation channel is still comparable to that of a CE system, making it possible to perform sub-minute separations on these devices [79]. This makes it an ideal approach for the separation of unstable or highly reactive species, such as NO and $ONOO^-$. A simple-t microchip design, as shown in Figure 1.6, is commonly used for ME. Typically, the separation and sampling channels and reservoirs are filled with run buffer and sample, respectively, and a high voltage is applied across

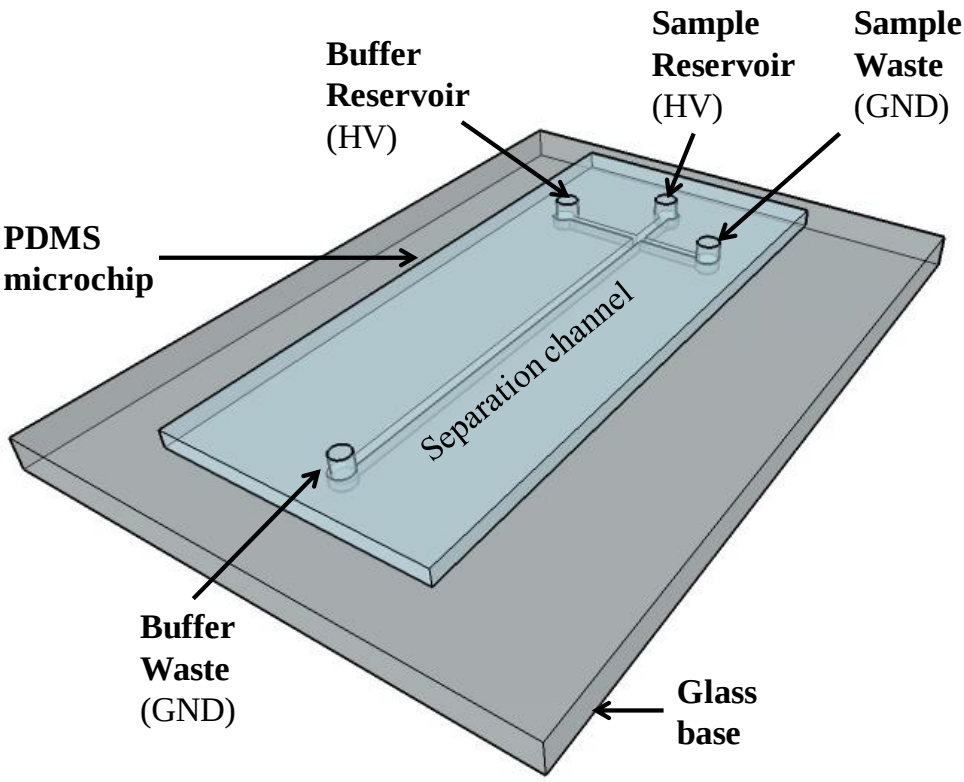

Figure 1.6. Schematic of a ME system that utilizes a simple-t design with a gated injection system.

the sample and separation channels using a high voltage power supply by placing platinum electrodes in reservoirs at both ends of the channels [80].

Microchips can be fabricated from glass, silicon, low temperature co-fired ceramics (LTCC), and polymer materials, such as poly(dimethylsiloxane) (PDMS), poly(methyl methacrylate) (PMMA), cyclic olefin copolymers (COC), and polyesters, among other polymers [81]. Conventional microfluidic devices made of glass or polymers are commercially available and can be fabricated in-house using photolithography or, for some polymeric substrates, hot embossing techniques.

The major advantage of glass-based microchips is that the surface chemistry of the separation channel is similar to that of a fused silica capillary. This makes transferring methods from CE to ME easier; also in addition, the presence of the free silanols leads to a generally reproducible EOF. However, the fabrication process for these microchips is time-consuming and costly [81]. Additionally, depending on the nature of the analytes, the microchannels can become clogged during experiments; this blockage can be hard to remove on irreversibly bonded devices.

For these reasons, polymeric substrates are usually chosen for method development. Of all the polymeric substrates available, PDMS is most commonly used due to its elastomeric properties, optical transparency, biocompatibility, low cost, and ease of fabrication [82, 83]. These combined properties make PDMS ideal for device prototyping and analytical method development. The major disadvantage of PDMS for ME systems is that the polymer surface is hydrophobic and contains relatively few silanol groups. The absence of a uniformly charged surface causes the EOF to be unstable and leads to changes in the migration times of analytes over the lifetime of the chip [84, 85]. Thus, to improve the stability of the EOF on a PDMS

device, ionic surfactants, such as sodium dodecyl sulfate (SDS), are often added to the running buffer as a dynamic surface modification method [86, 87]. The hydrophobic tail of the surfactant interacts with the hydrophobic walls of the channel, generating a charged surface.

ME systems most commonly use either a gated or pinched injection for sample introduction. The gated injection is considered an electrokinetic injection. To perform this type of injection, a high voltage is applied to both the buffer and sample reservoir, which establishes a "gate" at the intersection of the two voltages. The high voltage in the buffer reservoir is then floated for a short time to open the gate and permit a small amount of sample to enter the separation channel (Figure 1.7A) [88]. With a pinched injection, a high voltage is first applied to the sample reservoir, and then sample is injected by applying a voltage in a perpendicular direction across the sample (Figure 1.7B) [88]. The volume of the sample plug injected is based on the size of the intersection [88]. The advantage of using a pinched injection over a gated injection is that only one high voltage power supply is necessary instead of two. However, gated injections are more reproducible.

1.6. Amperometric Detection

Electrochemical detection in the amperometric mode (referred to as EC in this chapter) is a technique that detects molecules based on their oxidation or reduction at the surface of a working electrode. In amperometric detection, the working electrode is usually composed of metal or carbon and is held at a constant potential versus a reference electrode. A change in the faradaic current, which is proportional to analyte concentration, is observed when there is an oxidation or reduction at the electrode surface [89, 90]. Only electrochemically active species can be monitored with this technique but most biological samples contain many interfering

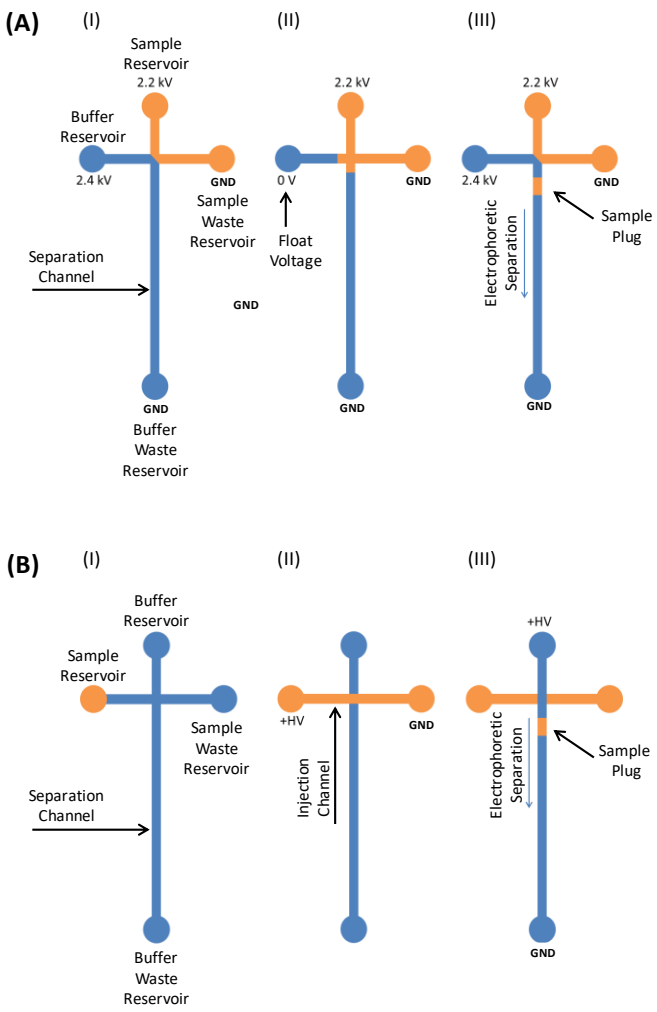

Figure 1.7. (A) ME schematic for the gated injection process. (I) A gate is established upon application of an external voltage to both the buffer and sample reservoirs. (II) The potential at the buffer reservoir is floated to allow the sample to enter the separation channel. (III) The gate is reestablished, thereby injecting the sample plug and starting the separation. (B) ME layout for pinched injection. (I) Sample is loaded into sample reservoir. (II) The injection channel is filled upon application of an electric field between the sample and sample waste reservoirs. (III) The injection occurs after switching the applied electric field to between the buffer and buffer waste reservoirs.

electrochemically active species [91]. EC can be coupled to ME to increase the selectivity by separating the analytes of interest from interferences.

1.6.1. Coupling EC to ME

Microelectrodes are the most commonly employed working electrodes for ME [92, 93]. They provide high signal-to-noise ratios and are compatible with the dimensions of the capillary or separation channel [89, 90, 94]. Microelectrodes can be incorporated into ME more easily than CE due to the planar format of ME devices. Even though carbon-based electrodes are the most popular electrode type for EC, metal electrodes are better for the oxidation of small RNS, such as NO and $ONOO^-$. Metal electrodes can be fabricated either on top of or into a trench etched in a glass substrate and then a PDMS microchip containing the separation channel is aligned on top to complete the device.

Metal sputtering is the most commonly employed protocol for the fabrication of metal electrodes on a glass substrate. Even though this fabrication method is commonly used, the microelectrodes produced are very thin (approximately 100–200 nm) and can be easily destroyed. When using these microelectrodes during the reversible sealing and subsequent removal of the PDMS layer from a glass substrate, the microelectrodes can peel off the glass. This limits the number of times the electrode plates can be used. More recently, the Lunte group developed an alternative fabrication method that consists of controlled etching of a trench in the glass prior to metal deposition [95]. This method provides electrodes that are more rugged and can therefore be reused numerous times with new PDMS substrates.

1.6.2. Electrode Alignments

There are three formats that can be employed when aligning a working electrode in a ME separation channel: end-channel, in-channel, and off-channel (Figure 1.8). End-channel

alignment allows the working electrode to be decoupled from the electrophoretic field, which provides decreased noise. However, upon exiting the separation channel, the analytes can diffuse into the waste reservoir, which leads to band broadening and decreased resolution [96]. With the in-channel alignment, the working electrode is placed in the separation channel. This alignment allows for the detection of analytes prior to reaching the waste reservoir, reducing (or eliminating) band broadening while still maintaining the detector sensitivity [96, 97]. However, since the working electrode that is placed in the channel is not decoupled from the electric field, an electrically isolated potentiostat must be employed or the electronics will be destroyed [97].

Off-channel alignment allows for the working electrode to be placed in the separation channel by adding a decoupler prior to the working electrode. This provides low noise measurements while still maintaining decent resolution. One disadvantage is that once the separation field is removed, analyte diffusion can occur, leading to band broadening [80]. However, these effects can be reduced by decreasing the distance between the decoupler and working electrode, thereby limiting the amount of time the analytes have to diffuse [98]. The most common type of decoupler in microchips is a metal (usually Pd) band electrode. These decoupler electrodes have been shown to work in electric fields up to 1200 V/cm [98]. However, they can only be operated in normal polarity separations because Pd can absorb H_2 gas, which is produced during the reduction of water in a positive separation field, but not O_2 gas, which is produced during the oxidation of water in a negative separation field. For CE-EC, Osbourn, D. M. et al. developed a decoupler that involved cutting slits into a CE capillary and covering them with a cellulose acetate membrane [99]. This membrane allowed charge to pass through it but not analytes. This decoupler was also applied to the ME format, and very low LODs for

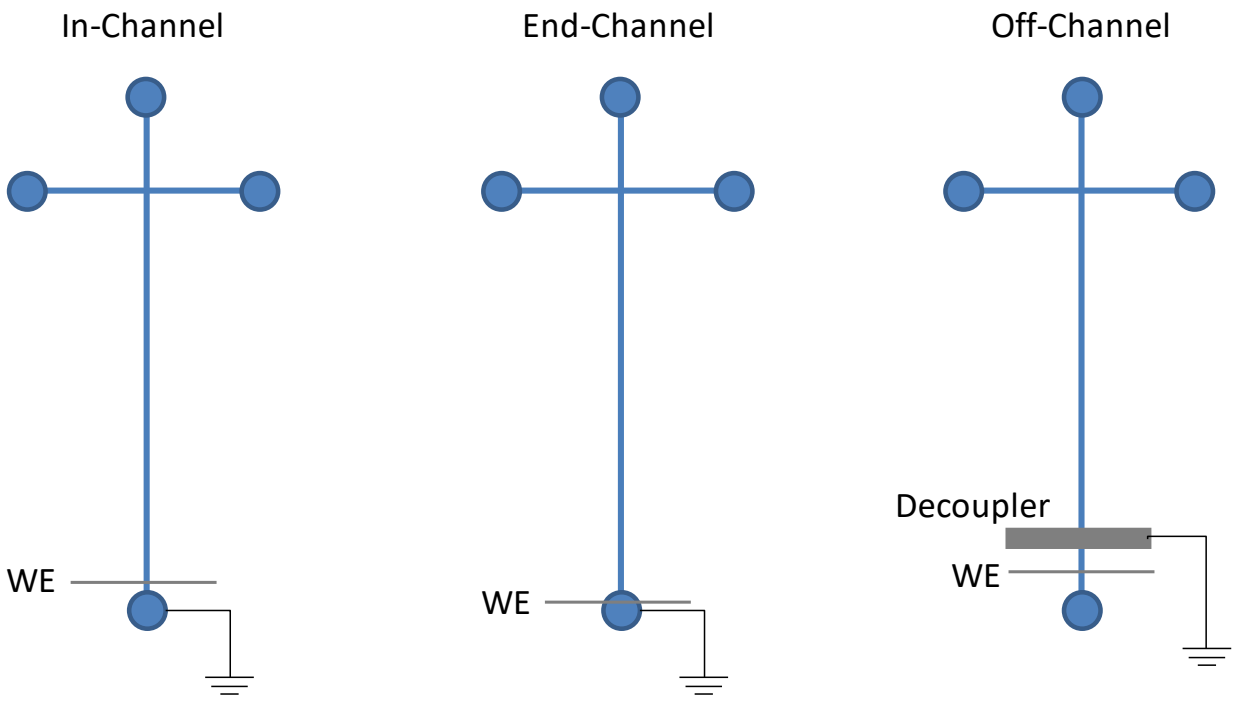

Figure 1.8. Working electrode alignments for coupling ME to EC.

dopamine (25 nM) were observed [100].

1.7. Conclusions and Thesis Goals

In order to properly understand the causes and effects of nitrosative and oxidative stress in biological systems, methods to monitor RNOS must be developed. The methods previously developed to detect RNOS are only capable of detecting a single analyte at a time. However, in order to gain an understanding of how intracellular RNOS interact as well as their implication in disease states, multiple RNOS must be detected simultaneously. Therefore, a separation step is necessary. ME provides very fast separations, which are ideal for short-lived molecules like NO, $O_2^{\bullet-}$, and $ONOO^-$. Additionally, ME can be easily coupled with laser-induced fluorescence (LIF) and EC detection. Therefore, the goal of this dissertation is to develop separation-based microfluidic platforms to monitor intracellular RNOS under nitrosative and oxidative stress conditions with ME-LIF or ME-EC.

1.8. Summary of Thesis Chapters

1.8.1. Chapter 1: Introduction

Part of this chapter has been previously published:

Joseph M. Siegel, Richard P. S. de Campos, Dulan B. Gunasekara, José A. F. da Silva, Susan M. Lunte. "Chapter 7: Electrophoretic Methods for Separation of Peroxynitrite and Related Compounds" in *Peroxynitrite Detection in Biological Media: Challenges and Advances*. The Royal Society of Chemistry, 2015.

This chapter describes the causes of intracellular nitrosative and oxidative stress as well as their implication in neurodegenerative disease. Additionally, the production and biological significance of RNOS is discussed. Analytical methods to detect NO, $O_2^{\bullet-}$, and $ONOO^-$ are also

described. A description of electrophoretic separations on microchips and their advantage for studying nitrosative stress is provided. Finally, this chapter also discusses electrochemical detection as a means of detecting RNOS.

1.8.2. Chapter 2: Development of a Method to Monitor Nitrosative Stress in RAW 264.7 Macrophage Cells

This work has been published in the following journal:

Dulan B. Gunasekara, **Joseph M. Siegel**, Giuseppe Caruso, Matthew K. Hulvey, Susan M. Lunte. "Microchip electrophoresis with amperometric detection method for profiling cellular nitrosative stress markers." Analyst. 2014, 139, 3265-3273.

This chapter describes a ME-EC method for the separation of intracellular nitrosative stress markers in macrophage cells. The separation of NO_2^-, azide (interference), iodide (internal standard), tyrosine, glutathione, and H_2O_2 (neutral marker) was achieved in under 40 s. Initially, NO production was monitored by the detection of NO_2^- in native and lipopolysaccharide (LPS)-stimulated cell lysates. ME-EC was then used for the direct detection of NO and glutathione in stimulated and native macrophage cell lysates. NO was identified in these studies based on its migration time and rapid degradation kinetics. The intracellular concentrations of glutathione in native and stimulated macrophages were also compared and no significant difference was observed between the two conditions.

1.8.3. Chapter 3: Indirect Detection of NO with Transient Isotachophoresis and Platinum Black Modified Working Electrodes

In this chapter, the ME-EC method to detect NO_2^- in cell lystes described in the previous chapter is improved upon with the implementation of transient isotachophoresis and a Pt black modified working electrode. The addition of 10 mM NaCl to the run buffer caused stacking of

the NO_2^- peak and improved limits of detection. To improve the electrochemical response for NO_2^-, the platinum working electrode was modified with Pt black using a combination of cyclic voltammetry followed by activation with alternating pulse voltammetry. The optimized ME-EC method using a platinum black modified Pt electrode was used to observe the NO_2^- in native and LPS-stimulated RAW 264.7 macrophage cells.

1.8.4. Chapter 4: Construction of a Cellulose Acetate-Based Decoupler for ME-EC

The fabrication and evaluation of a cellulose acetate decoupler for ME-EC is described in this chapter. This decoupler is shown to operate in both normal and reverse polarity while using a carbon ink and Pt electrode, respectively. During the normal polarity separation, a standard solution of norepinephrine, hydroquinone, and ascorbic acid was successfully separated and detected. However, the decoupler resulted in decreased peak-to-peak resolution compared to detection with an in-channel aligned working elctrode. Under reverse polarity conditions, the amplitude of the noise as a function of the separation field strength was determined in both the in-channel and off-channel alignments. Furthermore, a standard solution of NO_2^-, ascorbic acid, and H_2O_2 was detected after a cellulose acetate decoupler while using reverse polarity.

1.8.5. Chapter 5: Detection of Intracellular $O_2^{\bullet-}$ with MitoSOX Red

This work has been published in the following journal:

Richard P. S. de Campos, **Joseph M. Siegel**, Claudia G. Fresta, Giuseppe Caruso, José A. F. da Silva, Susan M. Lunte. "Indirect detection of superoxide in RAW 264.7 macrophage cells using microchip electrophoresis coupled to laser-induced fluorescence." Analytical and Bioanalytical Chemistry. 2015, 407, 7003-7012.

In this chapter, MitoSOX Red, a fluorescent probe that specifically reacts with $O_2^{\bullet-}$, was used in conjunction with ME-LIF to investigate changes in $O_2^{\bullet-}$ production by RAW 264.7

macrophage cells following stimulation with phorbol 12-myristate 13-acetate (PMA). The use of ME is necessary to separate the $O_2^{\bullet-}$-specific fluorescent product from the fluorescent molecule produced from the reaction of MitoSOX Red with other ROS. A calibration curve to quantify the intracellular $O_2^{\bullet-}$ concentration was made by reacting MitoSOX Red with potassium nitrosodisulfonate (Fremy's salt) to produce known quantities of the $O_2^{\bullet-}$-specific fluorescent product. The PMA stimulation protocol was performed in the presence and absence of the SOD inhibitors diethyldithiocarbamate (DDC) and 2-methoxyestradiol (2-ME). Furthermore, the effect of 3-morpholino-sydnonimine (SIN-1) incubation on $O_2^{\bullet-}$ production was investigated using the same probe and analytical system.

1.8.6. Chapter 6: Simultaneous Detection of NO and $O_2^{\bullet-}$ in RAW 264.7 Macrophage Cells

This work has been published in the following journal:

Giuseppe Caruso, Claudia G. Fresta, **Joseph M. Siegel**, Manjula B. Wijesinghe, Susan M. Lunte. "Microchip electrophoresis with laser-induced fluorescence detection for the determination of the ratio of nitric oxide to superoxide production in macrophages during inflammation." Analytical and Bioanalytical Chemistry. 2017, *Accepted*.

This chapter describes the use of 4-amino-5-methylamino-2',7'-difluorofluorescein diacetate (DAF-FM DA) and MitoSOX Red in conjunction with ME-LIF for the simultaneous detection of NO and $O_2^{\bullet-}$ in RAW 264.7 macrophage cell lysates following different stimulation procedures. Cell stimulations were performed in the presence and absence of cytosolic (DDC) and mitochondrial (2-ME) SOD inhibitors. The NO/$O_2^{\bullet-}$ ratios in macrophage cell lysates under physiological and pro-inflammatory conditions were determined. The effect of carnosine (antioxidant) or Ca^{2+} (intracellular messenger) on the NO/$O_2^{\bullet-}$ ratio was also investigated.

1.8.7. Chapter 7: Conclusions and Future Directions

This chapter describes the main conclusions of the dissertation. These conclusions include the ME-EC and ME-LIF methods that were developed to study intracellular nitrosative and oxidative stress and their applications in the future. The immediate future directions are to optimize the cellulose acetate decoupler and couple it to a single cell analysis microfluidic device. Additionally, a method to measure intracellular $ONOO^-$ using the fluorescent probe HKGreen-3 will be developed and used in conjunction with the method described in Chapter 6 to simultaneously monitor NO, $O_2^{\bullet-}$, and $ONOO^-$. Long term goals include applying the ME-EC methods to study nitrosative stress to the single cell analysis format, which will allow for the detection of intracellular RNOS with respect to cell heterogeneity.

1.9. References

1. Pacher, P.; Beckman, J.S.; Liaudet, L. Nitric Oxide and Peroxynitrite in Health and Disease. *Physiol Rev*. **2007**, *87*, 315-424.

2. Espey, M.G.; Miranda, K.M.; Thomas, D.D.; Xavier, S.; Citrin, D.; Vitek, M.P.; Wink, D.A. A Chemical Perspective on the Interplay between NO, Reactive Oxygen Species, and Reactive Nitrogen Oxide Species. *Ann NY Acad Sci*. **2002**, *962*, 195-206.

3. Sies, H.; Berndt, C.; Jones, D.P. Oxidative Stress. *Annu Rev Biochem*. **2017**, *86*.

4. Torreilles, F.; Salman-Tabcheh, S.D.; Guérin, M.-C.; Torreilles, J. Neurodegenerative Disorders: The Role of Peroxynitrite. *Brain Res Rev*. **1999**, *30*, 153-63.

5. Szabó, C.; Ischiropoulos, H.; Radi, R. Peroxynitrite: Biochemistry, Pathophysiology and Development of Therapeutics. *Nat Rev Drug Discov*. **2007**, *6*, 662-80.

6. Miranda, K.M.; Espey, M.G.; Wink, D.A. A Discussion of the Chemistry of Oxidative and Nitrosative Stress in Cytotoxicity. *J Inorg Biochem*. **2000**, *79*, 237-40.

7. Alderton, W.K.; Cooper, C.E.; Knowles, R.G. Nitric Oxide Synthases: Structure, Function and Inhibition. *Biochem J*. **2001**, *357*, 593-615.

8. Macmicking, J.; Xie, Q.-W.; Nathan, C. Nitric Oxide and Macrophage Function. *Annu Rev Immunol*. **1997**, *15*, 323-50.

9. Murphy, M.P. How Mitochondria Produce Reactive Oxygen Species. *Biochem J*. **2009**, *417*, 1-13.

10. Liu, Y.; Fiskum, G.; Schubert, D. Generation of Reactive Oxygen Species by the Mitochondrial Electron Transport Chain. *J Neurochem*. **2002**, *80*, 780-7.

11. Tang, X.; Luo, Y.-X.; Chen, H.-Z.; Liu, D.-P. Mitochondria, Endothelial Cell Function, and Vascular Diseases. *Front Physiol*. **2014**, *5*.

12. Judkins, C.P.; Diep, H.; Broughton, B.R.S.; Mast, A.E.; Hooker, E.U.; Miller, A.A.; Selemidis, S.; Dusting, G.J.; Sobey, C.G.; Drummond, G.R. Direct Evidence of a Role for Nox2 in Superoxide Production, Reduced Nitric Oxide Bioavailability, and Early Atherosclerotic Plaque Formation in ApoE$^{-/-}$ Mice. *Am J Physiol Heart Circ Physiol*. **2010**, *298*, H24-H32.

13. Ferrer-Sueta, G.; Radi, R. Chemical Biology of Peroxynitrite: Kinetics, Diffusion, and Radicals. *ACS Chem Biol*. **2009**, *4*, 161-77.

14. Brand, M.D.; Affourtit, C.; Esteves, T.C.; Green, K.; Lambert, A.J.; Miwa, S.; Pakay, J.L.; Parker, N. Mitochondrial Superoxide: Production, Biological Effects, and Activation of Uncoupling Proteins. *Free Radical Biol Med*. **2004**, *37*, 755-67.

15. D S Bredt, A.; Snyder, S.H. Nitric Oxide: A Physiologic Messenger Molecule. *Annu Rev Biochem*. **1994**, *63*, 175-95.

16. Naseem, K.M. The Role of Nitric Oxide in Cardiovascular Diseases. *Mol Aspects Med*. **2005**, *26*, 33-65.

17. Prast, H.; Philippu, A. Nitric Oxide as Modulator of Neuronal Function. *Prog Neurobiol*. **2001**, *64*, 51-68.

18. Hume, D.A. The Biology of Macrophages. *Science Progress*. **1985**, *69*, 485-94.

19. Becker, S.; Warren, M.K.; Haskill, S. Colony-Stimulating Factor-Induced Monocyte Survival and Differentiation into Macrophages in Serum-Free Cultures. *J Immunol*. **1987**, *139*, 3703-9.

20. Laskin, D.L. Macrophages and Inflammatory Mediators in Chemical Toxicity: A Battle of Forces. *Chem Res Toxicol*. **2009**, *22*, 1376-85.

21. Varin, A.; Gordon, S. Alternative Activation of Macrophages: Immune Function and Cellular Biology. *Immunobiology*. **2009**, *214*, 630-41.

22. Wilson, H.M. Macrophages Heterogeneity in Atherosclerosis – Implications for Therapy. *J Cell Mol Med*. **2010**, *14*, 2055-65.

23. Tang, Y.; Le, W. Differential Roles of M1 and M2 Microglia in Neurodegenerative Diseases. *Mol Neurobiol*. **2016**, *53*, 1181-94.

24. Hoozemans, J.J.M.; Veerhuis, R.; Rozemuller, J.M.; Eikelenboom, P. Neuroinflammation and Regeneration in the Early Stages of Alzheimer's Disease Pathology. *Int J Dev Neurosci*. **2006**, *24*, 157-65.

25. Manabe, I. Chronic Inflammation Links Cardiovascular, Metabolic and Renal Diseases. *Circ J*. **2011**, *75*, 2739-48.

26. Mantovani, A.; Sozzani, S.; Locati, M.; Allavena, P.; Sica, A. Macrophage Polarization: Tumor-Associated Macrophages as a Paradigm for Polarized M2 Mononuclear Phagocytes. *Trends Immunol*. **2002**, *23*, 549-55.

27. Barnham, K.J.; Masters, C.L.; Bush, A.I. Neurodegenerative Diseases and Oxidative Stress. *Nat Rev Drug Discov*. **2004**, *3*, 205-14.

28. Heneka, M.T.; Kummer, M.P.; Latz, E. Innate Immune Activation in Neurodegenerative Disease. *Nat Rev Immunol*. **2014**, *14*, 463-77.

29. Perry, V.H.; Nicoll, J.a.R.; Holmes, C. Microglia in Neurodegenerative Disease. *Nat Rev Neurol*. **2010**, *6*, 193-201.

30. Wyss-Coray, T.; Mucke, L. Inflammation in Neurodegenerative Disease—a Double-Edged Sword. *Neuron*. **2002**, *35*, 419-32.

31. Palop, J.J.; Mucke, L. Amyloid-β-Induced Neuronal Dysfunction in Alzheimer's Disease: From Synapses toward Neural Networks. *Nat Neurosci*. **2010**, *13*, 812-8.

32. Goodwin, J.L.; Uemura, E.; Cunnick, J.E. Microglial Release of Nitric Oxide by the Synergistic Action of β-Amyloid and Ifn-γ. *Brain Res*. **1995**, *692*, 207-14.

33. Hirsch, E.C.; Hunot, S. Neuroinflammation in Parkinson's Disease: A Target for Neuroprotection? *Lancet Neurol*. **2009**, *8*, 382-97.

34. Ischiropoulos, H.; Beckman, J.S. Oxidative Stress and Nitration in Neurodegeneration: Cause, Effect, or Association? *J Clin Invest*. **2003**, *111*, 163-9.

35. Hetrick, E.M.; Schoenfisch, M.H. Analytical Chemistry of Nitric Oxide. *Annu Rev Anal Chem*. **2009**, *2*, 409-33.

36. Bryan, N.S.; Grisham, M.B. Methods to Detect Nitric Oxide and Its Metabolites in Biological Samples. *Free Rad Biol Med*. **2007**, *43*, 645-57.

37. Nagano, T. Practical Methods for Detection of Nitric Oxide. *Luminescence*. **1999**, *14*, 283-90.

38. Tsikas, D. A Critical Review and Discussion of Analytical Methods in the L-Arginine/Nitric Oxide Area of Basic and Clinical Research. *Anal Biochem*. **2008**, *379*, 139-63.

39. Tsikas, D. Reviewmethods of Quantitative Analysis of the Nitric Oxide Metabolites Nitrite and Nitrate in Human Biological Fluids. *Free Radical Res*. **2005**, *39*, 797-815.

40. Kleschyov, A.L.; Wenzel, P.; Munzel, T. Electron Paramagnetic Resonance (EPR) Spin Trapping of Biological Nitric Oxide. *J Chromatogr B*. **2007**, *851*, 12-20.

41. Hogg, N. Detection of Nitric Oxide by Electron Paramagnetic Resonance Spectroscopy. *Free Radical Biol Med*. **2010**, *49*, 122-9.

42. Bates, J.N. Nitric Oxide Measurement by Chemiluminescence Detection. *Neuroprotocols*. **1992**, *1*, 141-9.

43. Miller, E.W.; Chang, C.J. Fluorescent Probes for Nitric Oxide and Hydrogen Peroxide in Cell Signaling. *Curr Opin Chem Biol*. **2007**, *11*, 620-5.

44. Kojima, H.; Nakatsubo, N.; Kikuchi, K.; Kawahara, S.; Kirino, Y.; Nagoshi, H.; Hirata, Y.; Nagano, T. Detection and Imaging of Nitric Oxide with Novel Fluorescent Indicators: Diaminofluoresceins. *Anal Chem*. **1998**, *70*, 2446-53.

45. Nagano, T. Bioimaging Probes for Reactive Oxygen Species and Reactive Nitrogen Species. *J Clin Biochem Nutr*. **2009**, *45*, 111-24.

46. Gomes, A.; Fernandes, E.; Lima, J.L.F.C. Use of Fluorescence Probes for Detection of Reactive Nitrogen Species: A Review. *J Fluoresc*. **2006**, *16*, 119-39.

47. Balcerczyk, A.; Soszynski, M.; Bartosz, G. On the Specificity of 4-Amino-5-Methylamino-2′,7′-Difluorofluorescein as a Probe for Nitric Oxide. *Free Radical Biol Med*. **2005**, *39*, 327-35.

48. Zhang, X.; Kim, W.-S.; Hatcher, N.; Potgieter, K.; Moroz, L.L.; Gillette, R.; Sweedler, J.V. Interfering with Nitric Oxide Measurements: 4,5-Diaminofluorescein Reacts with Dehydroascorbic Acid and Ascorbic Acid. *J Biol Chem*. **2002**, *277*, 48472-8.

49. Kim, W.-S.; Ye, X.; Rubakhin, S.S.; Sweedler, J.V. Measuring Nitric Oxide in Single Neurons by Capillary Electrophoresis with Laser-Induced Fluorescence: Use of Ascorbate Oxidase in Diaminofluorescein Measurements. *Anal Chem*. **2006**, *78*, 1859-65.

50. Bedioui, F.; Griveau, S. Electrochemical Detection of Nitric Oxide: Assessement of Twenty Years of Strategies. *Electroanalysis*. **2013**, *25*, 587-600.

51. Privett, B.J.; Shin, J.H.; Schoenfisch, M.H. Electrochemical Nitric Oxide Sensors for Physiological Measurements. *Chem Soc Rev*. **2010**, *39*, 1925-35.

52. Pontié, M.; Gobin, C.; Pauporté, T.; Bedioui, F.; Devynck, J. Electrochemical Nitric Oxide Microsensors: Sensitivity and Selectivity Characterisation. *Anal Chim Acta*. **2000**, *411*, 175-85.

53. Bedioui, F.; Villeneuve, N. Electrochemical Nitric Oxide Sensors for Biological Samples – Principle, Selected Examples and Applications. *Electroanalysis*. **2003**, *15*, 5-18.

54. Shin, J.H.; Weinman, S.W.; Schoenfisch, M.H. Sol−Gel Derived Amperometric Nitric Oxide Microsensor. *Anal Chem*. **2005**, *77*, 3494-501.

55. Sun, J.; Zhang, X.; Broderick, M.; Fein, H. Measurement of Nitric Oxide Production in Biological Systems by Using Griess Reaction Assay. *Sensors*. **2003**, *3*, 276-84.

56. Tsikas, D. Analysis of Nitrite and Nitrate in Biological Fluids by Assays Based on the Griess Reaction: Appraisal of the Griess Reaction in the L-Arginine/Nitric Oxide Area of Research. *J Chromatogr B*. **2007**, *851*, 51-70.

57. Burns, J.M.; Cooper, W.J.; Ferry, J.L.; King, D.W.; Dimento, B.P.; Mcneill, K.; Miller, C.J.; Miller, W.L.; Peake, B.M.; Rusak, S.A.; Rose, A.L.; Waite, T.D. Methods for Reactive Oxygen Species (ROS) Detection in Aqueous Environments. *Aquat Sci*. **2012**, *74*, 683-734.

58. Chen, X.; Tian, X.; Shin, I.; Yoon, J. Fluorescent and Luminescent Probes for Detection of Reactive Oxygen and Nitrogen Species. *Chem Soc Rev*. **2011**, *40*, 4783-804.

59. Calas-Blanchard, C.; Catanante, G.; Noguer, T. Electrochemical Sensor and Biosensor Strategies for Ros/Rns Detection in Biological Systems. *Electroanalysis*. **2014**, *26*, 1277-86.

60. Dickinson, B.C.; Srikun, D.; Chang, C.J. Mitochondrial-Targeted Fluorescent Probes for Reactive Oxygen Species. *Curr Opin Chem Biol*. **2010**, *14*, 50-6.

61. Kalyanaraman, B.; Darley-Usmar, V.; Davies, K.J.A.; Dennery, P.A.; Forman, H.J.; Grisham, M.B.; Mann, G.E.; Moore, K.; Roberts Ii, L.J.; Ischiropoulos, H. Measuring

Reactive Oxygen and Nitrogen Species with Fluorescent Probes: Challenges and Limitations. *Free Radical Biol Med*. **2012**, *52*, 1-6.

62. Gao, J.J.; Xu, K.H.; Tang, B.; Yin, L.L.; Yang, G.W.; An, L.G. Selective Detection of Superoxide Anion Radicals Generated from Macrophages by Using a Novel Fluorescent Probe. *FEBS J*. **2007**, *274*, 1725-33.

63. Liu, X.; Li, Q.; Gong, X.; Li, H.; Chen, Z.; Tong, L.; Tang, B. Rapid Determination of Superoxide Free Radical in Hepatocellular Carcinoma Cells by MCE with LIF. *Electrophoresis*. **2009**, *30*, 1077-83.

64. Borgmann, S. Electrochemical Quantification of Reactive Oxygen and Nitrogen: Challenges and Opportunities. *Anal Bioanal Chem*. **2009**, *394*, 95-105.

65. Bedioui, F.; Quinton, D.; Griveau, S.; Nyokong, T. Designing Molecular Materials and Strategies for the Electrochemical Detection of Nitric Oxide, Superoxide and Peroxynitrite in Biological Systems. *Phys Chem Chem Phys*. **2010**, *12*, 9976-88.

66. Yagil, G.; Anbar, M. The Formation of Peroxynitrite by Oxidation of Chloramine, Hydroxylamine and Nitrohydroxamate. *J Inorg Nucl Chem*. **1964**, *26*, 453-60.

67. Frankenfeld, C.N.; Rosenbaugh, M.R.; Fogarty, B.A.; Lunte, S.M. Separation and Detection of Peroxynitrite and Its Metabolites by Capillary Electrophoresis with UV Detection. *J Chromatogr A*. **2006**, *1111*, 147-52.

68. Peng, T.; Yang, D. Hkgreen-3: A Rhodol-Based Fluorescent Probe for Peroxynitrite. *Organic Letters*. **2010**, *12*, 4932-5.

69. Peteu, S.F.; Whitman, B.W.; Galligan, J.J.; Swain, G.M. Electrochemical Detection of Peroxynitrite Using Hemin-Pedot Functionalized Boron-Doped Diamond Microelectrode. *Analyst*. **2016**, *141*, 1796-806.

70. Miyado, T.; Tanaka, Y.; Nagai, H.; Takeda, S.; Saito, K.; Fukushi, K.; Yoshida, Y.; Wakida, S.-I.; Niki, E. Simultaneous Determination of Nitrate and Nitrite in Biological Fluids by Capillary Electrophoresis and Preliminary Study on Their Determination by Microchip Capillary Electrophoresis. *J Chromatogr A*. **2004**, *1051*, 185-91.

71. Miyado, T.; Nagai, H.; Takeda, S.; Saito, K.; Fukushi, K.; Yoshida, Y.; Wakida, S.-I.; Niki, E. Development of a Novel Running Buffer for the Simultaneous Determination of Nitrate and Nitrite in Human Serum by Capillary Zone Electrophoresis. *J Chromatogr A*. **2003**, *1014*, 197-202.

72. Szökő, É.; Tábi, T.; Halász, A.S.; Pálfi, M.; Magyar, K. High Sensitivity Analysis of Nitrite and Nitrate in Biological Samples by Capillary Zone Electrophoresis with Transient Isotachophoretic Sample Stacking. *J Chromatogr A*. **2004**, *1051*, 177-83.

73. Gao, L.; Barber-Singh, J.; Kottegoda, S.; Wirtshafter, D.; Shippy, S.A. Determination of Nitrate and Nitrite in Rat Brain Perfusates by Capillary Electrophoresis. *Electrophoresis*. **2004**, *25*, 1264-9.

74. Kikura-Hanajiri, R.; Martin, R.S.; Lunte, S.M. Indirect Measurement of Nitric Oxide Production by Monitoring Nitrate and Nitrite Using Microchip Electrophoresis with Electrochemical Detection. *Anal Chem*. **2002**, *74*, 6370-7.

75. Troška, P.; Chudoba, R.; Danč, L.; Bodor, R.; Horčičiak, M.; Tesařová, E.; Masár, M. Determination of Nitrite and Nitrate in Cerebrospinal Fluid by Microchip Electrophoresis with Microsolid Phase Extraction Pre-Treatment. *J Chromatogr B*. **2013**, *930*, 41-7.

76. Massip, C.; Riollet, P.; Quemener, E.; Bayle, C.; Salvayre, R.; Couderc, F.; Causse, E. Choice of Different Dyes to Label Tyrosine and Nitrotyrosine. *J Chromatogr A*. **2002**, *979*, 209-15.

77. Maeso, N.; Cifuentes, A.; Barbas, C. Large-Volume Sample Stacking-Capillary Electrophoresis Used for the Determination of 3-Nitrotyrosine in Rat Urine. *J Chromatogr B*. **2004**, *809*, 147-52.

78. Ren, H.; Wang, L.; Wang, X.; Liu, X.; Jiang, S. Measurement of Acid Dissociation Constants and Ionic Mobilities of 3-Nitro-Tyrosine and 3-Chloro-Tyrosine by Capillary Zone Electrophoresis. *J Pharm Biomed Anal*. **2013**, *77*, 83-7.

79. Weinberger, R. Practical Capillary Electrophoresis. 2 ed. San Diego, CA: Academic Press; 2000.

80. Lacher, N.A.; Garrison, K.E.; Martin, R.S.; Lunte, S.M. Microchip Capillary Electrophoresis/Electrochemistry. *Electrophoresis*. **2001**, *22*, 2526-36.

81. Culbertson, C.T.; Mickleburgh, T.G.; Stewart-James, S.A.; Sellens, K.A.; Pressnall, M. Micro Total Analysis Systems: Fundamental Advances and Biological Applications. *Anal Chem*. **2014**, *86*, 95-118.

82. De Campos, R.P.S.; Yoshida, I.V.P.; Da Silva, J.a.F. Surface Modification of PDMS Microchips with Poly (Ethylene Glycol) Derivatives for Mtas Applications. *Electrophoresis*. **2014**, *35*, 2346-52.

83. Mcdonald, J.C.; Duffy, D.C.; Anderson, J.R.; Chiu, D.T.; Wu, H.; Schueller, O.J.A.; Whitesides, G.M. Fabrication of Microfluidic Systems in Poly(Dimethylsiloxane). *Electrophoresis*. **2000**, *21*, 27-40.

84. Lacher, N.A.; De Rooij, N.F.; Verpoorte, E.; Lunte, S.M. Comparison of the Performance Characteristics of Poly (Dimethylsiloxane) and Pyrex Microchip Electrophoresis Devices for Peptide Separations. *J Chromatogr A*. **2003**, *1004*, 225-35.

85. Coltro, W.K.T.; Lunte, S.M.; Carrilho, E. Comparison of the Analytical Performance of Electrophoresis Microchannels Fabricated in Pdms, Glass, and Polyester-Toner. *Electrophoresis*. **2008**, *29*, 4928-37.

86. Makamba, H.; Kim, J.H.; Lim, K.; Park, N.; Hahn, J.H. Surface Modification of Poly (Dimethylsiloxane) Microchannels. *Electrophoresis*. **2003**, *24*, 3607-19.

87. Roman, G.T.; Mcdaniel, K.; Culbertson, C.T. High Efficiency Micellar Electrokinetic Chromatography of Hydrophobic Analytes on Poly (Dimethylsiloxane) Microchips. *Analyst*. **2006**, *131*, 194-201.

88. Karlinsey, J.M. Sample Introduction Techniques for Microchip Electrophoresis: A Review. *Anal Chim Acta*. **2012**, *725*, 1-13.

89. Bard, A.J.; Faulkner, L.R. Electrochemical Methods: Fundamentals and Applications. 2 ed. Hoboken, NJ: John Wiley & Sons, Inc.; 2001.

90. Kissinger, P.T.; Heineman, W.R. Laboratory Techniques in Electroanalytical Chemistry. 2 ed. New York, NY: Marcel Dekker, Inc.; 1996.

91. Amatore, C.; Arbault, S. Oxidative Stress at the Single Cell Level. In: Michael AC, Borland LM, editors. Electrochemical Methods for Neuroscience. Boca Raton, FL: CRC Press; 2007. p. 261-84.

92. Vandaveer, W.R.; Pasas-Farmer, S.A.; Fischer, D.J.; Frankenfeld, C.N.; Lunte, S.M. Recent Developments in Electrochemical Detection for Microchip Capillary Electrophoresis. *Electrophoresis*. **2004**, *25*, 3528-49.

93. Gunasekara, D.B.; Wijesinghe, M.B.; Saylor, R.A.; Lunte, S.M. Fundamental Principles and Strategies for Microchip Electrophoresis with Amperometric Detection. In: Arrigan DWM, editor. Electrochemical Strategies in Detection Science. Cambridge, UK: The Royal Society of Chemistry; 2014.

94. Wightman, R.M. Probing Cellular Chemistry in Biological Systems with Microelectrodes. *Science*. **2006**, *311*, 1570-4.

95. Scott, D.E.; Grigsby, R.J.; Lunte, S.M. Microdialysis Sampling Coupled to Microchip Electrophoresis with Integrated Amperometric Detection on an All-Glass Substrate. *ChemPhysChem*. **2013**, *14*, 2288-94.

96. Fischer, D.J.; Hulvey, M.K.; Regel, A.R.; Lunte, S.M. Amperometric Detection in Microchip Electrophoresis Devices: Effect of Electrode Material and Alignment on Analytical Performance. *Electrophoresis*. **2009**, *30*, 3324-33.

97. Martin, R.S.; Ratzlaff, K.L.; Huynh, B.H.; Lunte, S.M. In-Channel Electrochemical Detection for Microchip Capillary Electrophoresis Using an Electrically Isolated Potentiostat. *Anal Chem*. **2002**, *74*, 1136-43.

98. Lacher, N.A.; Lunte, S.M.; Martin, R.S. Development of a Microfabricated Palladium Decoupler/Electrochemical Detector for Microchip Capillary Electrophoresis Using a Hybrid Glass/Poly(Dimethylsiloxane) Device. *Anal Chem*. **2004**, *76*, 2482-91.

99. Osbourn, D.M.; Lunte, C.E. Cellulose Acetate Decoupler for on-Column Electrochemical Detection in Capillary Electrophoresis. *Anal Chem.* **2001**, *73*, 5961-4.

100. Osbourn, D.M.; Lunte, C.E. On-Column Electrochemical Detection for Microchip Capillary Electrophoresis. *Anal Chem*. **2003**, *75*, 2710-4.

Chapter 2:

Development of a Method to Monitor Nitrosative Stress in RAW 264.7 Macrophage Cells

This work has been published in the following journal publication:

Dulan B. Gunasekara, **Joseph M. Siegel**, Giuseppe Caruso, Matthew K. Hulvey, Susan M. Lunte. "Microchip electrophoresis with amperometric detection method for profiling cellular nitrosative stress markers." Analyst. 2014, 139, 3265-3273.

2.1. Introduction

There are many different types of immune cells in the human body, and macrophages are the primary cell type that is activated as part of an immune response [1, 2]. It is also well known that monocytes can be differentiated into macrophages, and it has been shown that monocytes in blood can migrate into the intima of a blood vessel and can be differentiated into macrophages during atherosclerosis [3, 4]. Macrophages produce NO primarily through the activation of iNOS; however, an uncontrolled or large NO production in these cell types results in cellular nitrosative stress, which has been implicated in many neurodegenerative and cardiovascular diseases [5, 6]. The toxic effects of cellular pro-oxidants produced from NO can be mitigated by the presence of antioxidant molecules in the cell [7, 8]. Glutathione (GSH) is an antioxidant produced by the cells that can scavenge NO and produce nitrosoglutathione. Also, GSH can react with hydrogen peroxide to form glutathione disulfide. This reaction is catalyzed in the cell by glutathione peroxidase [7, 8]. The balance between pro- and antioxidants is important for regulating cellular nitrosative stress [9].

More recently, microfluidic devices have been employed to detect the production of cellular NO and its metabolites [10-15]. These devices have many advantages over classical methods for the study of NO, including the possibility of performing on-chip cell culture, simulating the cellular response in constricted blood vessels, modeling *in vivo* environments by immobilizing cells on a microchannel, and single cell analysis that can be difficult to achieve using classical methods [10-15]. Spectroscopic detection is predominantly used in these devices, and methods for monitoring NO production from erythrocytes [15], endothelial [16], and macrophage cells [13] have been reported. Separations with microfluidic devices are most commonly performed using electrophoresis. The use of high field strengths with short channels

in the planar format makes it possible to routinely perform subminute separations using this technique. Therefore, this method is especially useful for the detection of chemically labile species since they can be separated and detected before significant degradation occurs [17].

In this report, a method that allows the direct detection of NO and its metabolites simultaneously in macrophage cells using ME-EC is described. The electrophoretic method permits subminute separation of NO, NO_2^-, and cellular antioxidants as well as potential interferences and other electrochemically active intracellular components (e.g. tyrosine and nitrotyrosine). This approach makes it possible to gather information regarding the overall redox status of the macrophage cells along with NO production. The method was used to investigate NO and intracellular GSH levels in macrophages under native and stimulated conditions. The ME-EC method reported here will be adapted in the future for single cell analysis studies.

2.2. Materials and Methods

2.2.1. Materials and Reagents

The following chemicals and materials were used as received: SU-8 10 photoresist and SU-8 developer (MicroChem Corp., Newton, MA, USA); AZ 1518 photoresist and 300 MIF developer (Mays Chemical Co., Indianapolis, IN, USA); photolithography film mask (50,000 dpi; Infinite Graphics Inc., Minneapolis, MN, USA); N(100) 100 mm (4”) silicon (Si) wafers (Silicon, Inc., Boise, ID, USA); chrome and AZ1518 positive photoresist coated soda lime glass substrate (4" × 4" × 0.090", Nanofilm, Westlake, CA, USA); Pt film-coated glass substrates (2000 Å Pt layer over 200 Å Ti) (The Stanford Nanofabrication Facility, Stanford, CA, USA); Sylgard 184 Silicone Elastomer Kit: Polydimethylsiloxane (Ellsworth Adhesives, Germantown, WI, USA); Titanium (Ti) etchant (TFTN; Transene Co., Danvers, MA, USA); epoxy and 22 gauge Cu wire (Westlake Hardware, Lawrence, KS, USA); silver colloidal paste (Ted Pella,

Inc., Redding, CA, USA); acetone, 2-propanol (isopropyl alcohol, IPA), 30% H_2O_2, H_2SO_4, HNO_3, NaOH, HCl, and Trypan blue (Fisher Scientific, Fair Lawn, NJ, USA); sodium nitrite, boric acid, tetradecyltrimethylammonium bromide (TTAB), tetradecyltrimethylammonium chloride (TTAC), ascorbic acid (AA), tyrosine, reduced glutathione, sodium azide, potassium iodide, NaCl, Lipopolysaccharides from Escherichia coli 0111:B4, and Griess reagent (modified) (Sigma, St. Louis, MO, USA) and buffered oxide etchant (JT Baker, Austin, TX, USA). All water used was ultrapure (18.3 MΩ·cm) (Milli-Q Synthesis A10, Millipore, Burlington, MA, USA).

2.2.2. PDMS Fabrication

The fabrication of PDMS-based microfluidic devices has been described previously [18]. Briefly, SU-8 10 negative photoresist (for electrophoresis channels) was spin-coated on a 4 in diameter Si wafer to a thickness of 15 ± 1 µm using a Cee 100 spincoater (Brewer Science Inc., Rolla, MO, USA). The wafer was then transferred to a programmable hotplate (Thermo Scientific, Asheville, NC, USA) for a soft bake at 65°C for 2 min and then 95°C for 5 min. Microfluidic channel designs were created using AutoCad LT 2004 (Autodesk, Inc., San Rafael, CA, USA) and printed onto a transparency film at a resolution of 50,000 dpi (Infinite Graphics Inc., Minneapolis, MN, USA). The coated wafer was covered with the transparency film mask and exposed (344 mJ/cm^2 using an i-line UV flood source (ABM Inc., San Jose, CA, USA)). Following the UV exposure, the wafer was post-baked at 65°C for 2 min and 95°C for 10 min. The wafer was then developed in SU-8 developer, rinsed with IPA, and dried under nitrogen. A final "hard-bake" was performed at 175°C for 2 h. The thickness of the raised photoresist, which corresponds to the depth of the PDMS channels, was measured with a profilometer (Alpha Step-200, Tencor Instruments, Mountain View, CA, USA). PDMS microstructures were made by

casting a 10:1 mixture of PDMS elastomer and curing agent, respectively, against the patterned Si master. A simple-T device containing a 5 cm separation channel (from the T intersection to the end of the separation channel) and 0.75 cm side arms was used for these studies. The width and depth of the electrophoresis microchannels were 40 μm and 14 μm, respectively. Holes for the reservoirs were created in the polymer using a 4 mm biopsy punch (Harris Uni-core, Ted Pella Inc., Redding, CA, USA).

2.2.3. Platinum Electrode Fabrication

All electrochemical measurements were obtained using 15 μm Pt working electrodes. Electrodes were either fabricated using an in-house magnetron sputtering system (AXXIS DC magnetron sputtering system, Kurt J. Lesker Co., Jefferson Hills, PA, USA) or received from the Stanford nanofabrication facility. Details of fabrication of Pt electrodes provided by the Stanford nanofabrication facility were reported previously [19]. In the Stanford plates, the Pt electrodes are deposited on top of the glass surface. To obtain better stability, Pt electrodes were fabricated in-house by making a 500–600 nm trench in the glass substrate using a procedure previously reported by our group [20]. Briefly, the electrode designs were created using AutoCad LT 2004 (Autodesk, San Rafael, CA, USA) and printed onto a transparency film at a resolution of 50,000 dpi (Infinite Graphics, Minneapolis MN, USA). Then the electrode design was patterned on a chrome and AZ1518 positive photoresist-coated soda lime glass plate. The plate was developed using an AZ®300 MIF (Capitol Scientific, Inc., Austin, TX, USA) solution for 30 s and then baked at 100ºC for 10 min on a programmable hotplate (Thermo Scientific, Asheville, NC, USA). Once the photoresist layer was developed, the exposed chrome layer was the shape of the electrode. This chrome layer was then etched using chrome etchant to expose the glass surface underneath. Next, the glass plate was etched for about 5 min using a 10:1 buffered oxide etchant

(JT Baker, Austin, TX, USA) to obtain a 500 to 600 nm trench. It has been observed that if the trench is not deep enough (below 400 nm), the Pt-deposited electrodes are not stable under high applied potentials (greater than 1200 mV) and the Pt electrode flakes off the trench during electrophoresis. The plate was washed thoroughly with $CaCO_3$ and water after buffered oxide etching, and the depth of the trench was measured using an Alpha-step 200 profilometer (Tencor Instruments). The plate was dried at 100ºC for 10 min and then exposed to an oxygen plasma for 1 min (March Plasmod, Concord, CA, USA). The glass plate was immediately transferred to an AXXIS DC magnetron sputtering system (Kurt J. Lesker Co.). After pumping down the vacuum chamber of the sputtering system to a pressure of 1.0×10^{-6} Torr, a 20-nm Ti layer was deposited (220 V deposition voltage, 40 s deposition time, and 5.0×10^{-3} Torr deposition pressure) and then a Pt layer was deposited (200 V deposition voltage, 17 to 20 min deposition time, and 5.0×10^{-3} Torr deposition pressure). After metal deposition, the glass plate was washed with acetone to remove the photoresist layer along with all excess Pt. The remaining chrome was then removed from the plate with chrome etchant. The width and height of the resulting Pt electrodes were measured again using an Alpha-step 200 profilometer.

2.2.4. Solution Preparation

All solutions were made using 18.3 MΩ ultrapure water from a Millipore A10 system. Stock solutions of nitrite (NO_2^-, 10 mM), hydrogen peroxide (H_2O_2, 10 mM), GSH (10 mM), KI (5 mM), NaN_3 (5 mM), and AA (10mM) were all prepared in ultrapure water using appropriate amounts and were stored at 4°C. To dissolve tyrosine (Tyr, 10 mM), the solution was acidified using 1–1.5 M HCl. Subsequent dilutions of each stock solution for use in the microchip system were made in the appropriate run buffer at the time of analysis. For separation and sampling buffer, a boric acid (20 mM) stock solution was prepared and the pH was adjusted to 11 using 10

M or 1 M NaOH solution. The pH-adjusted boric acid buffer was diluted with other buffer constituents in order to obtain a 10 mM boric acid solution. The buffer pH was measured after dilution and before adding surfactant. The buffer pH was 10.3–10.7. TTAC (100 mM) stock solution, NaCl (50 mM) stock solution, and ultrapure water were used for buffer dilution.

2.2.5. Chip Construction and Electrophoresis Procedure

PDMS microchips consisting of a simple-T design with a 5 cm separation channel were used for all studies. Amperometric signals were recorded using a 15 µm Pt working electrode against a Ag/AgCl reference electrode, which was placed in the buffer waste reservoir after the separation ground lead (Figure 2.1A). The chip containing the separation channel was aligned and reversibly sealed to the glass plate containing the Pt electrode. For in-channel detection, the electrode was placed exactly at the channel end of the separation channel as shown in Figure 2.1B.

Electrophoretic separations were carried out using reverse polarity with TTAC as the cationic surfactant to modify the channel walls. Two negative high voltage Pt leads (Pt wire) were placed in the sample and buffer reservoirs, while two earth ground Pt leads were placed in the sample waste and buffer waste reservoirs. For sampling, -2200 V was employed, while -2400 V was used for the separation. A gated injection was used to inject the sample, with an injection time between 0.5 and 1 s. Boric acid buffer conditions were evaluated for the separation of NO_2^-, azide (interference), iodide, tyrosine, GSH, AA, and H_2O_2. To balance the conductivity difference between the cell lysate and separation buffer, 7.5 to 10 mM NaCl was added to the run buffer. The cells were lysed in buffered solution containing surfactant (10 mM boric acid and 2 mM TTAC) without NaCl.

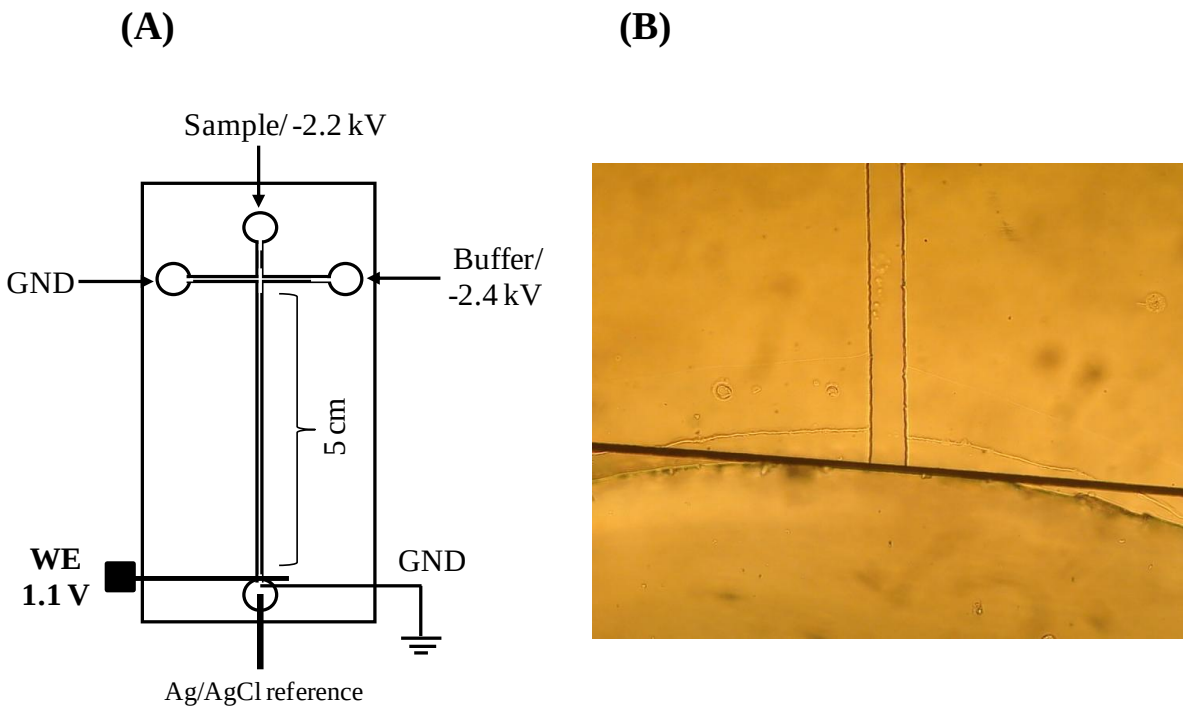

Figure 2.1. (A) Schematic of ME-EC setup with in-channel configuration. (B) Electrode alignment.

2.2.6. Electrochemical Detection

EC detection was accomplished using a modified model of an 8151BP, 8100-K6, or 9051 single- or dual-channel wireless, electrically isolated potentiostat (Pinnacle Technology Inc., Lawrence, KS, USA) operating in a two-electrode format (Pt working; Ag/AgCl reference: Bioanalytical Systems, West Lafayette, IN, USA). The model 8151P, 8100-K6, and 9051 potentiostats have a sampling rate of 5 Hz (Gain = 5,000,000 V/A, Resolution = 30 fA), 10 Hz (Gain = 5,000,000 V/A, Resolution = 27 fA), and 6.5 to 13 Hz (Gain = 5,000,000 V/A, Resolution = 47 fA), respectively. Pinnacle Acquisition Laboratory (PAL or Sirenia) software was used for all data acquisition. The data acquisition is performed via wireless data transmission or Bluetooth from the potentiostat to a computer. A working electrode potential of 1100 mV versus Ag/AgCl reference was used for all experiments.

2.2.7. Cell Culture and Preparation

RAW 264.7 cells were purchased from American Type Culture Collection (ATCC, Manassas, VA, USA) and cultured in Dulbecco's Modified Eagle's medium containing 10% (v/v) fetal bovine serum, L-glutamine (2 mM), penicillin (50 IU/mL), and streptomycin (50 µg/mL) (ATCC). The cells were maintained in a humidified environment at 37°C and 5% CO_2 and cultured in 25 mL polystyrene culture flasks (Fisher Scientific). Cells were passaged every 2–3 days to avoid overgrowth.

2.2.7.1. Cell Viability

Cell viability was measured using the Trypan blue (Fisher Scientific) exclusion assay and a hemocytometer cell count (C-Chip disposable hemocytometer, Bulldog Bio, Inc., Portsmouth, NH, USA). The RAW cell suspension was diluted using a 1:1 to 1:3 ratio (based on cell density) with a 0.4% Trypan blue solution. The number of viable cells and the cell density were

determined using a 4 mm^2 total area hemocytometer. Native RAW cells typically had densities of about 5 million cells in a 25 cm^2 flask prior to passaging.

2.2.7.2. Stimulation Protocol

Stimulation of NO production in cells was accomplished using purified LPS from the *Escherichia coli* line 0111:B4. A freshly prepared 50 µL aliquot of a 10 µg/mL LPS stock solution was added to healthy RAW 264.7 cells in a 25 cm^2 cell culture flask to obtain a 100 ng/mL final LPS concentration and then incubated for 24 h. An unstimulated RAW macrophage cell flask from the same population was incubated under identical conditions and used as a control (native) for each stimulation experiment.

2.2.7.3. Sample Preparation

The protocol used for cell analysis is shown in the Figure 2.2A. Cells were grown in 25 cm^2 polystyrene flasks until they reached approximately 80% confluence. At 80% confluence level, there are around 5 million RAW cells in the flask. These cells were stimulated using LPS and, after the stimulation period (24 h with a 100 ng/mL final LPS concentration, Figure 2.2B), cells were harvested using a scraper and centrifuged at 3500 rpm for 2.5 min to make a live cell pellet. Before centrifugation, 250 µL of the cell solution was taken out for cell counting. The supernatant medium was then removed, leaving only the cell pellet. Then the cell pellet was washed with 10 mM phosphate buffered saline at pH 7.4. Next the cell pellet was lysed using a lysis buffer containing 10 mM boric acid and 2 mM TTAC at pH 10.3 to 10.7. Both the high pH and surfactant assisted with the immediate lysis of cells. Higher molecular weight compounds such as proteins and cell membranes were removed by centrifugation of the lysate for 2–7 min using a 3 kDa molecular weight cut-off filter (VWR International, West Chester, PA, USA). The filtered lysate was then loaded into the sample reservoir of the microchip.

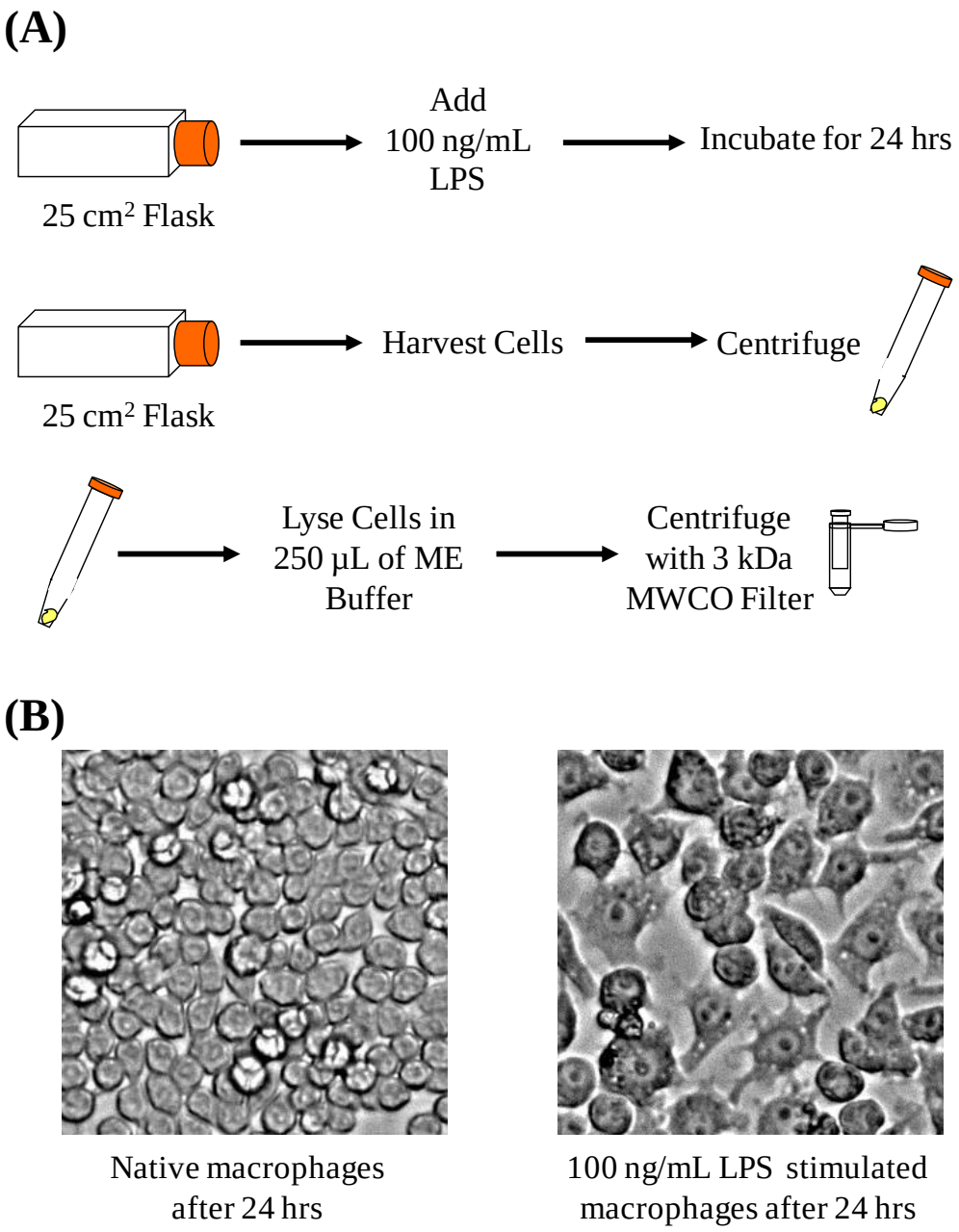

Figure 2.2. (A) Diagram of the stimulation and sample preparation protocol for RAW 264.7 macrophage cells prior to ME-EC and Griess assay analyses. (B) Images of RAW 264.7 macrophage cells after 24 h without stimulation (left) and with LPS stimulation (right).

For the standard addition studies, four 25 cm^2 cell flasks with the same passage number were harvested and lysed using 1 mL of 10 mM boric acid with 2 mM TTAC at pH 10.3 (for 1 cell flask, 250 µl of buffer was used). The lysate was divided into five portions, and the internal standard was appropriately added to ensure a final concentration of 10 µM. Standard addition concentrations of 15, 30, 60, and 120 µM NO_2^- were chosen and the required NO_2^- volume from a 1 mM NO_2^- standard was added to the cell lysates. Before adding iodide and NO_2^-, an equal volume of iodide and NO_2^- was removed from the cell lysate.

2.2.7.4. Griess Assay Protocol

The Griess assay was performed using 96-well plates and a plate reader (Molecular Devices, Spectra Max M5, Sunnyvale, CA, USA). To perform the assay, 100 µL of the filtered cell lysate was added into 100 µL of Griess reagent, left to react for 15 min, after which the absorbance at 540 nm was recorded using the plate reader. A buffer background was always employed for these measurements. For NO_2^- quantitation, a calibration curve was prepared using NO_2^- standards from 1 to 50 µM. Cell counts were taken before lysing the cells, and the final NO_2^- concentration was calculated, taking into account the cell counts.

2.3. Results and Discussion

2.3.1. Microchip Electrophoresis with Electrochemical Detection

There are two primary electrode configurations that are used for ME under reverse polarity conditions. The electrode can be placed either slightly inside the channel (in-channel) or outside the channel (end-channel). The advantage of the in-channel configuration is it allows higher resolution between closely migrating species, which cannot be separated by end-channel configuration due to band broadening [19]. Therefore, faster separations and shorter analysis times can be obtained using the in-channel configuration. Also, we have observed an increase in

peak height, better sensitivity, and a higher number of theoretical plates with the in-channel configuration compared to the end-channel configuration [19]. However, an important consideration with in-channel detection is that one must take into account the working electrode potential shift that occurs due to the separation voltage when an electrode is placed inside the channel. To minimize this effect in these experiments, the working electrode was placed exactly at the channel end, which still preserves the higher resolution and separation efficiencies characteristic of in-channel detection that are necessary for these studies, but minimizes the potential shift at the working electrode (Figure 2.1B) [19].

2.3.2. Separation Buffer Optimization

The analytes of interest in our studies of nitrosative stress included NO, NO_2^- (a metabolite of NO), GSH (cellular antioxidant), AA (cellular antioxidant), and tyrosine (amino acid, which is nitrated in the presence of $ONOO^-$). We have previously reported the separation and detection of several of these analytes (NO_2^-, ascorbic acid, tyrosine, glutathione, and H_2O_2) by ME-EC as compounds that could potentially interfere with the quantitation of NO and NO_2^- in macrophage cell lysates [19]. For the macrophage cell lysate studies described here, the same separation conditions (10 mM boric acid with 2 mM TTAB) with slight modifications were utilized.

2.3.2.1. Internal Standard, Surfactant, and Interferences

To quantitate the compounds in the cell lysates and increase the precision of the analytical method, iodide was incorporated as an internal standard and, therefore, had to be taken into consideration during the separation optimization procedures. In our previous studies, TTAB was used to reverse the EOF. In these studies, TTAB was replaced with TTAC, where the counter ion is Cl^- instead of Br^-. It was found that bromide can be oxidized to Br_2 at around 1200

mV versus Ag/AgCl, leading to an increase in background current at the EC detector. Bromide, chloride, and NO_2^- have similar electrophoretic mobilities and, hence, migrate closely. We observed a vacancy peak close to the NO_2^- peak during initial cell studies due to high Cl^- content. Another species that needed to be separated from the cell lysate components was azide. The molecular weight cut-off filters used for cell lysate filtration were found to contain a small amount of this compound, which is used as an anti-microbial agent. Under these separation conditions, azide migrated between NO_2^- and iodide but did not interfere with either measurement.

2.3.2.2. Conductivity Issues

During the initial analysis of the cell lysates, it was observed that the sampling current was always higher than the separation current and the high conductivity samples suppressed the NO_2^- peak due to destacking [21]. A similar suppression in the NO_2^- signal has been reported in CE when a high conductivity sample was analyzed [22]. To reduce the amount of salt and matrix components present in biological samples prior to CE analysis, solid-phase microextraction [23], acetonitrile addition (acetonitrile lowers the sample conductivity) [22], dialysis [24], and pre-electrophoresis separation [25] have been widely employed.

An alternative approach to avoid NO_2^- destacking is to increase the conductivity of the separation buffer by using sodium chloride. Figure 2.3A shows the NO_2^- peak suppression that occurs when standards are prepared in a high conductivity buffer (10 mM boric acid with 2 mM TTAC and 10 mM NaCl at pH 10.3) and the separation buffer consists of a low conducting buffer (10 mM boric acid with 2 mM TTAC at pH 10.3). In contrast, Figure 2.3B illustrates that the addition of 7.5 mM NaCl to the separation buffer causes an approximately 3-fold increase in

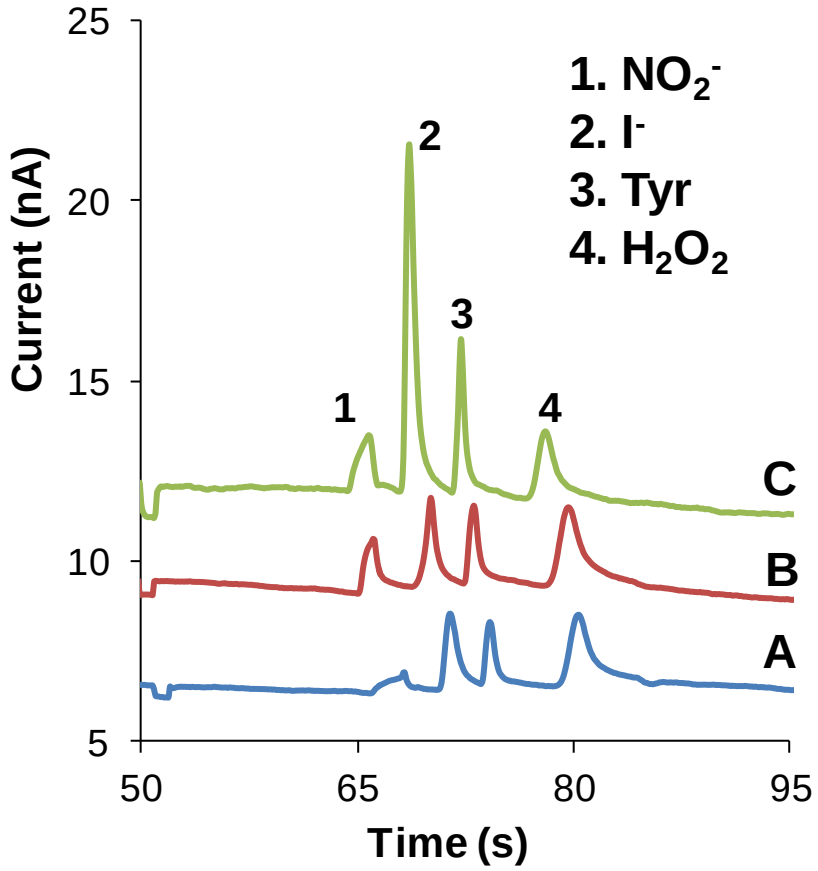

Figure 2.3. Electropherograms of a standard containing 100 μM NO_2^-, 10 μM iodide (internal standard), 50 μM tyrosine, and 200 μM hydrogen peroxide (neutral marker) using a 10 mM boric acid and 2 mM TTAC buffer at pH 10.3 while varying the sample and run buffer conductivities. (A) High conductivity sample buffer (10 mM NaCl) and normal separation buffer. (B) High conductivity sample buffer (10 mM NaCl) and high conductivity separation buffer (7.5 mM NaCl). (C) No change to the conductivity of the sample and separation buffer.

the NO_2^- signal. This can then be compared to a case where both the sample buffer and separation buffer are low conductivity buffers (10 mM boric acid with 2 mM TTAC at pH 10.3) (Figure 2.3C). In this last case, the NO_2^- signal is similar to that seen in Figure 2.3B. These experiments confirmed the destacking of NO_2^- in high conductivity samples. All three electropherograms used for the comparison studies were recorded with the same microchip, working electrode, and working electrode potential.

2.3.3. Detection of NO_2^- from Macrophage Cell Lysates

RAW 264.7 macrophage cells are known to produce large amounts of NO through the activation of iNOS. LPS, an endotoxin in negative gram bacteria and an external stimulant, can be used to activate iNOS [26, 27]. It has been reported that RAW 264.7 macrophage cells produce significantly higher amounts of NO in the presence of LPS [26, 27]. In these studies, a LPS concentration of 100 ng/mL over 24 h was used for cell stimulation (Figure 2.2A). A substantial difference in physical appearance between native and LPS-stimulated cells was observed, as can be seen in Figure 2.2B.

To compare intracellular NO_2^- produced in stimulated and native macrophage cells, bulk cell lysates were prepared as shown in Figure 2.2A, and analyzed by ME-EC. The Griess assay was also performed to compare with the results obtained with ME-EC. To confirm that NO production was due solely to an increase in iNOS activity, a separate set of cells was exposed to L-NAME, which is a known inhibitor of iNOS, before LPS stimulation and analyzed via Griess assay. These results were compared to those from native and LPS-stimulated cell lysate samples with the same passage number. Each flask contained around 5 million cells, which were lysed in 250 μL of borate buffer (10 mM boric acid with 2 mM TTAC at pH 10.3 to 10.7) in order to minimize the sample conductivity (Figure 2.3A).

Figure 2.4A shows the electropherograms obtained for native and LPS-stimulated cell lysates using our ME-EC device. The migration times for the first two peaks in the native cell electropherogram were similar to those for NO_2^- and iodide standards, and the peak identities were confirmed by spiking with standards. Azide was also spiked to further ensure that the NO_2^- peak does not comigrate with azide during cell studies.

2.3.4. Comparison of NO_2^- Production in Macrophage Cell Lysates using ME-EC and Griess Assay

Three different pairs of native and LPS-stimulated cell lysates were analyzed by ME-EC and the Griess assay, respectively, for the comparison of NO_2^- concentrations. Both methods were used to determine NO_2^- production increase in LPS-stimulated cells versus native cells (Figure 2.4B). A t-test was performed to compare the two sets of data (Griess versus ME-EC), and it was found that these two series showed no statistical difference at a 90% confidence level. This shows that the NO_2^- level detected with ME-EC is similar to that seen in the results of the Griess assay.

The NO_2^- concentration varied from one sample to another due to the samples having different cell counts. Therefore, the cell counts were taken into account in both the Griess assay and ME-EC studies when calculating the final NO_2^- concentrations. The NO_2^- production in a single cell was estimated by assuming that the volume of a macrophage is approximately 0.5 pL. The Griess assay results show that the average intracellular concentrations of NO_2^- in single unstimulated and LPS-stimulated macrophage cells are 0.63 ± 0.16 mM (0.31 ± 0.08 fmol/cell) and 1.69 ± 1.06 mM (0.84 ± 0.53 fmol/cell), respectively.

In the case of ME-EC analysis, an external calibration curve could not be used for the

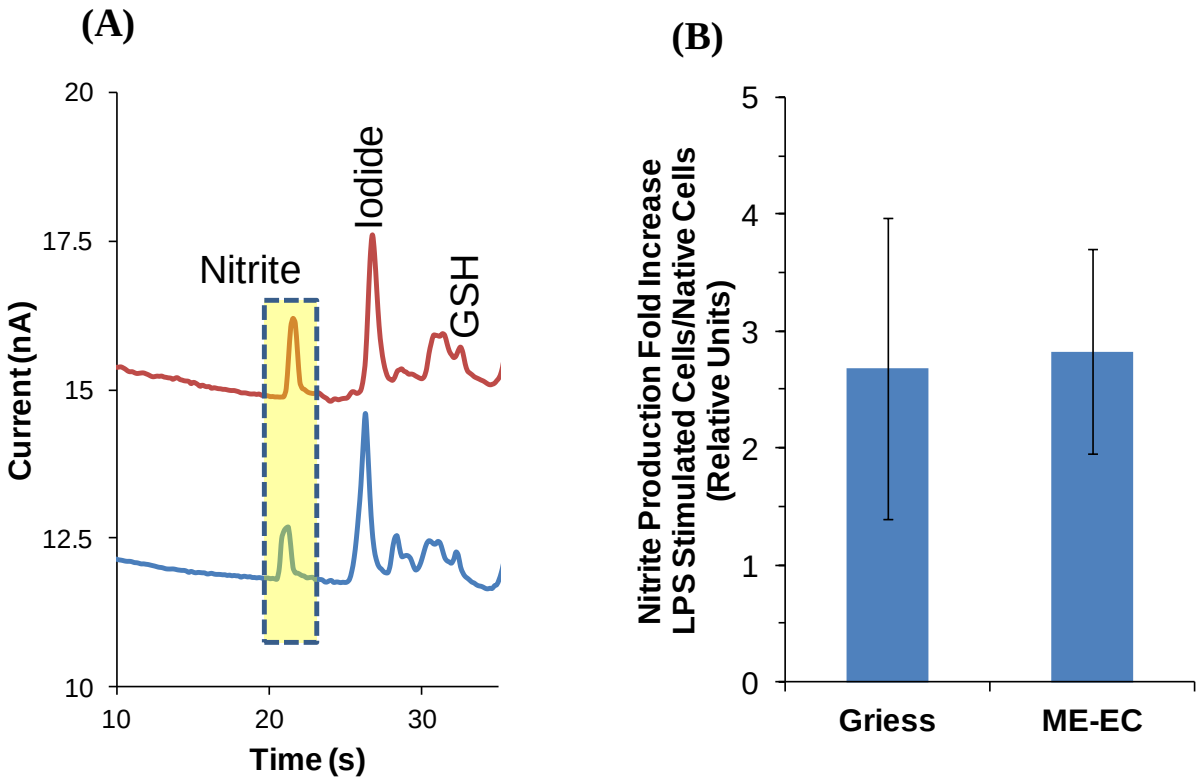

Figure 2.4. (A) Comparison of LPS-stimulated (top) and native (bottom) RAW 264.7 macrophage cell lysates using ME-EC. (B) Comparison of the ME-EC method and the Griess assay for determining the increase in NO_2^- concentration resulting from a 24 h LPS stimulation relative to the NO_2^- concentration produced from native cells. The sample was prepared in 10 mM boric acid and 2 mM TTAC buffer at pH 10.3 and the separation was achieved with a 10 mM boric acid, 7.5 mM NaCl and 2 mM TTAC buffer at pH 10.3.

quantitation of NO_2^- due to the NO_2^- peak suppression. Therefore, the method of standard additions was used, employing iodide as an internal standard. Two different ME-EC setups were used for the analysis of these samples, and two standard addition calibration curves of the NO_2^- /iodide response vs. standard addition concentration were plotted. These plots yielded a R^2 of 0.987 and 0.973 with values of 0.58 and 0.83 fmol/cell, respectively. An average native NO_2^- concentration of 1.41 mM (0.71 fmol/cell) for a single macrophage cell was calculated using these two standard addition curves. The average NO_2^- level in single LPS-stimulated cells was then estimated using the NO_2^- production increase in LPS-stimulated cells relative to that in native cells, which is a 2.83-fold increase (Figure 2.4B). Consequently, LPS-stimulated cells have a NO_2^- concentration of around 4.00 mM (1.99 fmol/cell). Goto *et al.* reported similar levels for extracellular NO_2^- production (1 fmol/cell) in single LPS-stimulated macrophage cells using the Griess reagent and a microfluidic device [13].

2.3.5. Direct Detection of NO and Other Electroactive Species in Macrophage Cells

2.3.5.1. NO Detection

The reason for employing ME-EC in these studies is the ability to directly detect NO, its metabolite NO_2^-, and other cellular electroactive species (*e.g.*, cellular antioxidants) simultaneously. The overall goal is to implement this in a single cell analysis system in the future. Detection of all these species cannot be achieved with the Griess assay or LIF detection alone.

When detecting NO in cell lysates, sample preparation steps were shortened to minimize NO degradation and evaporation. Cells were quickly lysed (10–20 s), and the lysate was centrifuged for only 2 min. Figure 2.5 shows electropherograms obtained for native and LPS-

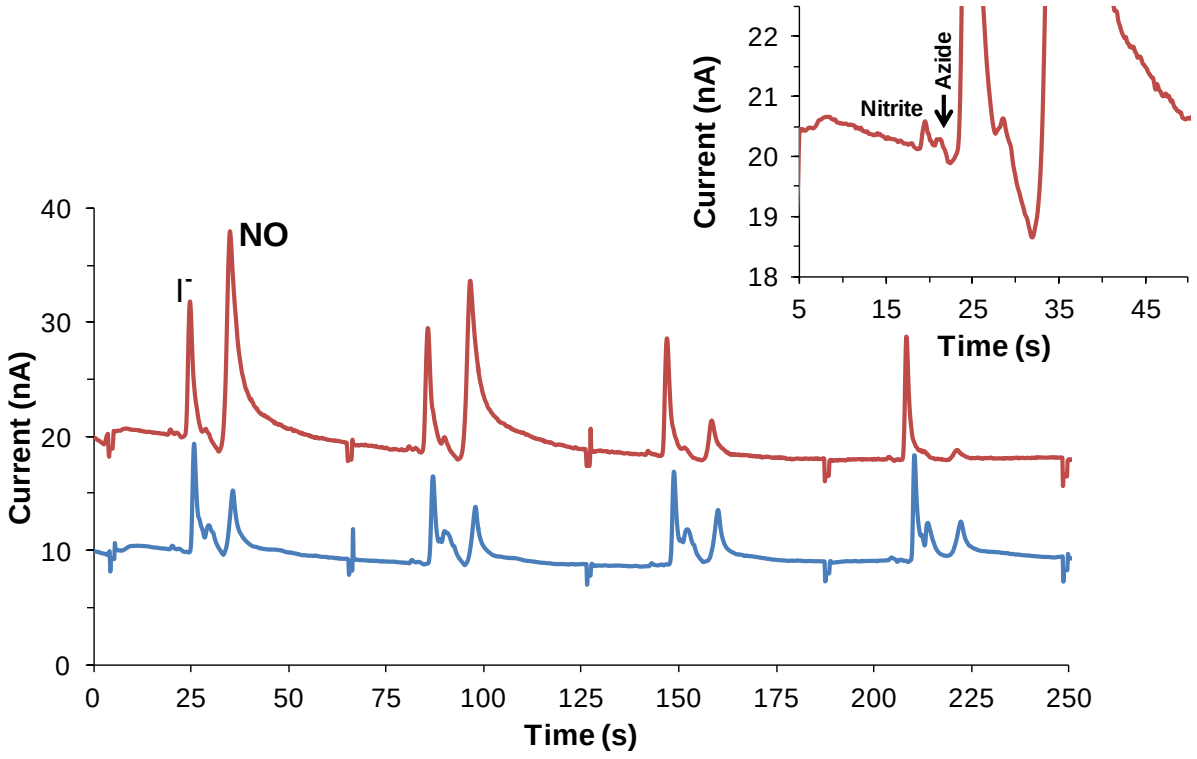

Figure 2.5. Detection of NO in cell lysate. LPS-stimulated cell lysate (top) and native cell lysate (bottom). Inset is a magnified portion of the LPS-stimulated cell lysate. The sample was prepared in 10 mM boric acid and 2 mM TTAC buffer at pH 10.3 and the separation was achieved with a 10 mM boric acid, 7.5 mM NaCl and 2 mM TTAC buffer at pH 10.3.

stimulated cell lysates following this procedure. It can be seen that the height of the peak that migrates at approximately 30 s decreases over time compared to the internal standard peak. The migration time of the decreasing peak is close to the neutral marker (32.3 ± 2.1 s), and the quick disappearance of this peak over several injections suggests that the compound is unstable. Since cells produce NO following LPS stimulation due to the induction of iNOS, this peak is most likely NO. The disappearance of this peak is probably due to loss of the gas through the open reservoirs on the microchip or permeation through the PDMS. NO_2^- was also detected during these studies, but the NO_2^- peak is very small compared to the NO peak (Figure 2.5 inset), which confirms that NO disappears from the wells quickly before degradation occurs. When the sample preparation time was lengthened, this peak disappeared.

We previously reported a ME method for the detection of NO generated using diethylamine NONOate (DEA/NO) and proline NONOate (PROLI/NO) salts [17]. The migration time of NO in those studies is comparable to the migration time of the decaying peak in the cell lysates considering the slight variation in chip-to-chip migration times that is expected in PDMS-based systems [17]. It can be seen in the native cell lysate that the last peak does not decay at the same rate as the unstable NO peak seen in LPS-stimulated cell lysate. This indicates that the peak observed in the native cell sample is contaminated with a more stable electroactive species. This species was found to be an interfering filter component that migrates close to the neutral marker (Figure 2.5). Therefore, the NO peak observed in these studies is contaminated.

Currently, the NO peak cannot be used for a quantitative comparison of native and stimulated cells due to the necessity for further peak identification, experimental variability, the presence of an interference due to the filters, and, most importantly, the fact that the peak decreases quickly over time due to evaporation and degradation. However, detection of NO will

be better accomplished using a single cell analysis microfluidic device where cells are lysed inside the device and the content is immediately analyzed. Since the cell lysis procedure is automated, a single cell cytometric device would provide better precision. Furthermore, a single cell cytometric device eliminates the cell lysate filtering step.

2.3.5.2. Comparison of Glutathione Levels in Native and Stimulated Cells

Other electroactive species such as tyrosine and GSH were also detected in macrophage cell lysates. However, electropherograms of native and LPS-stimulated cell lysates showed a very small peak or no peak for AA, which agreed with previous ME-LIF studies [28]. Macrophages do not naturally produce AA and an AA free media was used for cell culture. Previous studies reported undetectable levels of AA in RAW macrophage cells [29].

The relative GSH and NO_2^- levels for three separate LPS-stimulated cell lysates were compared to that of a native cell lysate with the same passage number using the same ME-EC conditions used for NO_2^- detection. As before, it was found that the NO_2^- level in LPS-stimulated cells was increased 5.74 ± 2.44 times relative to the native cell lysates. However, the GSH levels showed no significant change (1.30 ± 0.31) when the cells were stimulated with LPS (Figure 2.6). Hothersall *et al.* also observed that GSH levels were not changed when macrophage cells were stimulated with LPS alone. However, they have shown that the GSH level changed when the cells were stimulated with LPS and interferon gamma [30].

2.4. Conclusions

In this chapter, a ME-EC method was optimized for the detection of NO_2^-, NO, and other electroactive species within macrophage cell lysates. ME-EC makes it possible to obtain more information regarding the overall cellular redox state of the cell. It also provides a

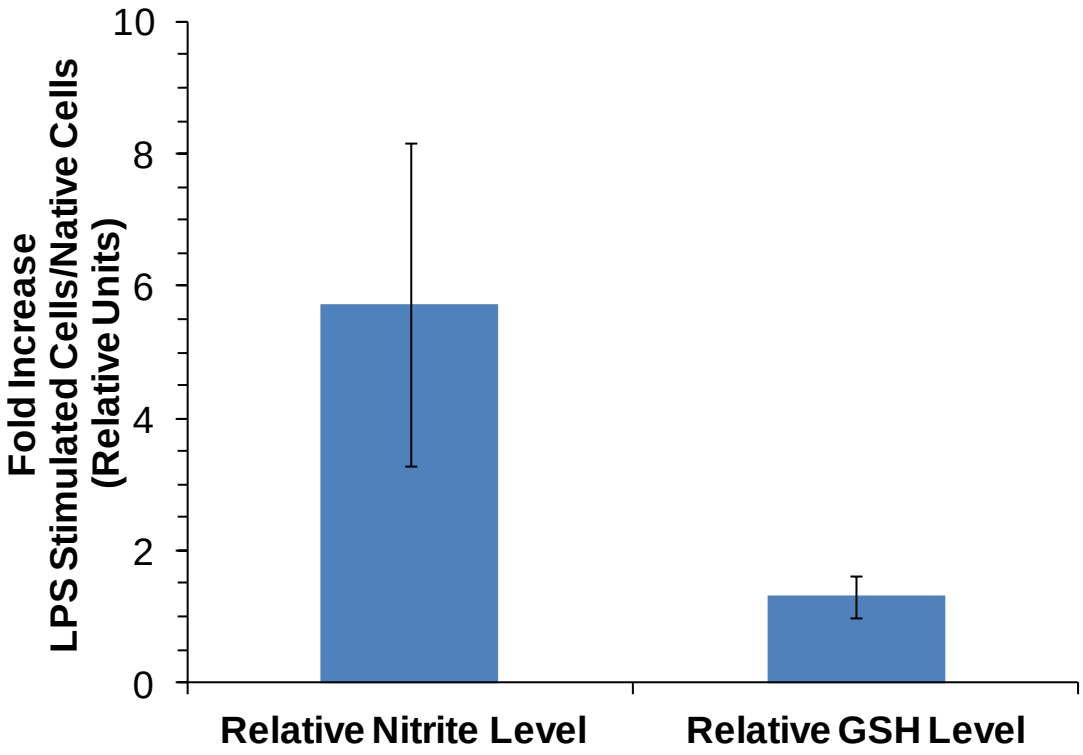

Figure 2.6. Comparison of the NO_2^- and glutathione (GSH) levels as a result of LPS stimulation relative to that of the native cell lysate. The sample was prepared in 10 mM boric acid and 2 mM TTAC buffer at pH 10.3 and the separation was achieved with a 10 mM boric acid, 10 mM NaCl and 2 mM TTAC buffer at pH 10.7.

separation of interfering species from the analytes of interest that cannot be achieved using classical methods such as the Griess assay and fluorescence imaging. Initially, NO production was detected through the detection of NO_2^- using a ME-EC device. The results obtained for NO_2^- production between LPS-stimulated and native cell lysates using ME-EC were compared to those from the Griess assay. Then this method was used for the direct detection of NO and other electroactive species in the cell lysate. An unstable species, which had many of the chemical and physical properties of NO, was detected during these studies. However, the NO peak cannot currently be used for a quantitative comparison of native and stimulated cells. The detection of NO will be better accomplished using a single cell analysis microfluidic device where cells are lysed inside the device and the contents are immediately analyzed. We have already reported a single cell chemical cytometric device for NO detection from Jurkat cells using a NO-selective fluorophore [11]. The ultimate goal is to use ME-EC to measure multiple redox-active species in a single cell as an indication of nitrosative stress.

2.5. References

1. Macmicking, J.; Xie, Q.-W.; Nathan, C. Nitric Oxide and Macrophage Function. *Annu Rev Immunol*. **1997**, *15*, 323-50.

2. Martinez, F.O.; Helming, L.; Gordon, S. Alternative Activation of Macrophages: An Immunologic Functional Perspective. *Annu Rev Immunol*. **2009**, *27*, 451-83.

3. Gordon, S.; Taylor, P.R. Monocyte and Macrophage Heterogeneity. *Nat Rev Immunol*. **2005**, *5*, 953-64.

4. Lilly, L.S. Pathophysiology of Heart Disease: A Collaborative Project of Medical Students and Faculty. Lippincott Williams & Wilkins; 2012.

5. Pacher, P.; Beckman, J.S.; Liaudet, L. Nitric Oxide and Peroxynitrite in Health and Disease. *Physiol Rev*. **2007**, *87*, 315-424.

6. Minghetti, L.; Levi, G. Microglia as Effector Cells in Brain Damage and Repair: Focus on Prostanoids and Nitric Oxide. *Prog Neurobiol*. **1998**, *54*, 99-125.

7. Valko, M.; Leibfritz, D.; Moncol, J.; Cronin, M.T.D.; Mazur, M.; Telser, J. Free Radicals and Antioxidants in Normal Physiological Functions and Human Disease. *Int J Biochem Cell Biol*. **2007**, *39*, 44-84.

8. Zhang, H.; Forman, H.J. Glutathione Synthesis and Its Role in Redox Signaling. *Semin Cell Dev Biol*. **2012**, *23*, 722-8.

9. Schulz, J.B.; Lindenau, J.; Seyfried, J.; Dichgans, J. Glutathione, Oxidative Stress and Neurodegeneration. *Eur J Biochem*. **2000**, *267*, 4904-11.

10. Hunter, R.A.; Privett, B.J.; Henley, W.H.; Breed, E.R.; Liang, Z.; Mittal, R.; Yoseph, B.P.; Mcdunn, J.E.; Burd, E.M.; Coopersmith, C.M.; Ramsey, J.M.; Schoenfisch, M.H. Microfluidic Amperometric Sensor for Analysis of Nitric Oxide in Whole Blood. *Anal Chem*. **2013**, *85*, 6066-72.

11. Metto, E.C.; Evans, K.; Barney, P.; Culbertson, A.H.; Gunasekara, D.B.; Caruso, G.; Hulvey, M.K.; Fracassi Da Silva, J.A.; Lunte, S.M.; Culbertson, C.T. An Integrated Microfluidic Device for Monitoring Changes in Nitric Oxide Production in Single T-Lymphocyte (Jurkat) Cells. *Anal Chem*. **2013**, *85*, 10188-95.

12. Vogel, P.A.; Halpin, S.T.; Martin, R.S.; Spence, D.M. Microfluidic Transendothelial Electrical Resistance Measurement Device That Enables Blood Flow and Postgrowth Experiments. *Anal Chem*. **2011**, *83*, 4296-301.

13. Goto, M.; Sato, K.; Murakami, A.; Tokeshi, M.; Kitamori, T. Development of a Microchip-Based Bioassay System Using Cultured Cells. *Anal Chem*. **2005**, *77*, 2125-31.

14. Hulvey, M.K.; Martin, R.S. A Microchip-Based Endothelium Mimic Utilizing Open Reservoirs for Cell Immobilization and Integrated Carbon Ink Microelectrodes for Detection. *Anal Bioanal Chem*. **2009**, *393*, 599-605.

15. Halpin, S.T.; Spence, D.M. Direct Plate-Reader Measurement of Nitric Oxide Released from Hypoxic Erythrocytes Flowing through a Microfluidic Device. *Anal Chem*. **2010**, *82*, 7492-7.

16. Letourneau, S.; Hernandez, L.; Faris, A.N.; Spence, D.M. Evaluating the Effects of Estradiol on Endothelial Nitric Oxide Stimulated by Erythrocyte-Derived ATP Using a Microfluidic Approach. *Anal Bioanal Chem*. **2010**, *397*, 3369-75.

17. Gunasekara, D.B.; Hulvey, M.K.; Lunte, S.M.; Da Silva, J.A.F. Microchip Electrophoresis with Amperometric Detection for the Study of the Generation of Nitric Oxide by Nonoate Salts. *Anal Bioanal Chem*. **2012**, *403*, 2377-84.

18. Hulvey, M.K.; Frankenfeld, C.N.; Lunte, S.M. Separation and Detection of Peroxynitrite Using Microchip Electrophoresis with Amperometric Detection. *Anal Chem*. **2010**, *82*, 1608-11.

19. Gunasekara, D.B.; Hulvey, M.K.; Lunte, S.M. In-Channel Amperometric Detection for Microchip Electrophoresis Using a Wireless Isolated Potentiostat. *Electrophoresis*. **2011**, *32*, 832-7.

20. Scott, D.E.; Grigsby, R.J.; Lunte, S.M. Microdialysis Sampling Coupled to Microchip Electrophoresis with Integrated Amperometric Detection on an All-Glass Substrate. *ChemPhysChem*. **2013**, *14*, 2288-94.

21. Boden, J.; Bächmann, K. Investigation of Matrix Effects in Capillary Zone Electrophoresis. *J Chromatogr A*. **1996**, *734*, 319-30.

22. Friedberg, M.A.; Hinsdale, M.E.; Shihabi, Z.K. Analysis of Nitrate in Biological Fluids by Capillary Electrophoresis. *J Chromatogr A*. **1997**, *781*, 491-6.

23. Boudko, D.Y. High-Resolution Capillary Electrophoresis of Nitrite and Nitrate in Biological Samples. In: Hassid A, editor. Nitric Oxide Protocols. Totowa, NJ: Humana Press; 2004. p. 9-19.

24. Haddad, P.R.; Doble, P.; Macka, M. Developments in Sample Preparation and Separation Techniques for the Determination of Inorganic Ions by Ion Chromatography and Capillary Electrophoresis. *J Chromatogr A*. **1999**, *856*, 145-77.

25. Timerbaev, A.R.; Fukushi, K.; Miyado, T.; Ishio, N.; Saito, K.; Motomizu, S. Analysis of Highly Saline Samples by Capillary Zone Electrophoresis: Enhanced Direct Uv Detection of Inorganic Anions Using on-Capillary Preconcentration and Clean-up Techniques. *J Chromatogr A*. **2000**, *888*, 309-19.

26. Lorsbach, R.B.; Murphy, W.J.; Lowenstein, C.J.; Snyder, S.H.; Russell, S.W. Expression of the Nitric Oxide Synthase Gene in Mouse Macrophages Activated for Tumor Cell Killing. Molecular Basis for the Synergy between Interferon-Gamma and Lipopolysaccharide. *J Biol Chem*. **1993**, *268*, 1908-13.

27. Held, T.K.; Weihua, X.; Yuan, L.; Kalvakolanu, D.V.; Cross, A.S. Gamma Interferon Augments Macrophage Activation by Lipopolysaccharide by Two Distinct Mechanisms, at the Signal Transduction Level and Via an Autocrine Mechanism Involving Tumor Necrosis Factor Alpha and Interleukin-1. *Infect Immun*. **1999**, *67*, 206-12.

28. Mainz, E.R.; Gunasekara, D.B.; Caruso, G.; Jensen, D.T.; Hulvey, M.K.; Fracassi Da Silva, J.A.; Metto, E.C.; Culbertson, A.H.; Culbertson, C.T.; Lunte, S.M. Monitoring

Intracellular Nitric Oxide Production Using Microchip Electrophoresis and Laser-Induced Fluorescence Detection. *Anal Methods*. **2012**, *4*, 414-20.

29. Badrakhan, C.-D.; Petrat, F.; Holzhauser, M.; Fuchs, A.; Lomonosova, E.E.; De Groot, H.; Kirsch, M. The Methanol Method for the Quantification of Ascorbic Acid and Dehydroascorbic Acid in Biological Samples. *J Biochem Bioph Methods*. **2004**, *58*, 207-18.

30. Hothersall, J.S.; Cunha, F.Q.; Neild, G.H.; Norohna-Dutra, A.A. Induction of Nitric Oxide Synthesis in J774 Cells Lowers Intracellular Glutathione: Effect of Modulated Glutathione Redox Status on Nitric Oxide Synthase Induction. *Biochem J*. **1997**, *322*, 477-81.

Chapter 3:

Indirect Detection of NO with Transient Isotachophoresis and Platinum Black Modified Working Electrodes

3.1. Introduction

While amperometric detection does have several distinct advantages over other detection methods such as LIF, electrochemical methods can suffer from lower sensitivity and higher limits of detection for monitoring NO production, especially at the single cell level. Therefore, efforts have been made to improve the sensitivity and detection limits of electrochemical sensors for NO and related species. One approach is to use platinum black to enhance the surface area and improve the electron transfer kinetics of an electrode for NO detection. Pt black may be deposited, also referred to as "platinization," on a variety of electrode materials (i.e. gold, carbon, platinum), resulting in an enhanced signal for NO and related compounds [1-6]. Pt black electrodes have been used for a variety of applications, including scanning electrochemical microscopy imaging of NO, microarrays for the detection of NO released from endothelial cells, amperometric sensors to measure NO generation from kidney slices, 3D printed microfluidic devices for the detection of dopamine and NO, and the detection of RNS released by single cells [1, 7-13]. While Pt black electrodes have been utilized for the detection of NO for several biological applications, the majority of these methods are limited to the specific detection of NO with interferences, such as NO_2^-, eliminated through the use of NO-selective membranes such as Nafion [8, 13].

In this chapter, a method is reported for the indirect detection of NO through its degradation product, NO_2^-, using ME-EC with a Pt black modified working electrode (WE). The signal enhancement obtained for NO_2^-, ascorbic acid (AA), and hydrogen peroxide resulting from the Pt black modification is reported. Additionally, a stacking method that is compatible with cell lysate samples was developed for improved detection of NO_2^-. The stacking method

was then combined with ME-EC using the Pt black modified electrode to determine NO_2^- in native and LPS stimulated RAW 264.7 macrophage cells as an indicator of NO production.

3.2. Materials and Methods

3.2.1. Materials and Reagents

The following materials and chemicals were used as received: boric acid, sodium chloride, tetradecyltrimethylammonium chloride (TTAC), sodium nitrite, ascorbic acid, lead (II) acetate trihydrate, and hydrogen hexachloroplatinate (IV) solution (Sigma-Aldrich, St. Louis, MO, USA); sodium hydroxide (NaOH), acetone, 2-propanol (IPA), phosphate buffered saline (PBS), 30% hydrogen peroxide (H_2O_2), lipopolysaccharide (LPS), and ethanol (Fisher Scientific, Pittsburgh, PA, USA); SU-8 photoresist, SU-8 developer, and MIF 300 developer (Micro-Chem, Newton, MA, USA); glass substrates (4" x 4" x 0.090") coated with chrome and AZ1518 photoresist (Nanofilm, Westlake, CA, USA); buffered oxide etchant (JT Baker, Austin, TX, USA); chrome etchant (Cyantek Corp., Freemont, CA, USA); Ti and Pt targets (Kurt J. Lesker Co., Jefferson Hills, PA, USA); polydimethylsiloxane (PDMS) and curing agent (Sylgard 184 elastomer kit, Ellsworth Adhesives, Germantown, WI, USA); 4" diameter silicon wafers (Silicon, Inc., Boise, ID, USA); epoxy and Cu wire (Westlake Hardware, Lawrence, KS, USA); silver colloidal (Ted Pella, Inc., Redding, CA, USA); RAW 264.7 cells, Delbecco's Modified Eagle's medium (DMEM), fetal bovine serum (FBS), and penicillin-streptomycin solution (ATCC, Manassas, VA, USA). All water was ultrapure (18.2 MΩ) and generated from a Milli-Q Synthesis A10 system (Millipore, Burlington, MA, USA).

3.2.2. PDMS Microchip Fabrication

The fabrication of PDMS microchips has been previously described [14]. Briefly, a 4" diameter silicon wafer was coated with SU-8 10 negative photoresist to a thickness of 15 μm

with a Cee 100 spincoater (Brewer Science Inc., Rolla, MO, USA). The wafer then underwent a soft bake at 65 °C for 2 min and then 95 °C for 5 min on a programmable hotplate (Thermo Scientific, Waltham, MA, USA). The designs for the microchip were drawn with AutoCad (Autodesk, San Rafael, CA, USA) and printed onto a transparency (Infinite Graphics, Minneapolis, MN, USA). The coated wafer was then covered with the negative transparency and exposed at 344 mJ cm-2 with a UV flood source (ABC Inc., San Jose, CA, USA). Next, the wafer was transferred to a programmable hotplate again for a postbake at 65 °C for 1 min and then 95 °C for 2 min. After the postbake, the wafer was developed in SU-8 developer, rinsed with IPA, and dried with nitrogen. Lastly, the wafer underwent a hard bake at 200 °C for 2 h. The final silicon master contained 15 μm thick and 40 μm wide microchannels, which were measured with an Alpha Step-200 surface profiler (KLA-Tencor Instruments, Milpitas, CA, USA). The microchip used for these studies consisted of a simple-t design with a 5 cm separation channel and 0.75 cm side arms. A PDMS microchip was made by pouring a degassed 10:1 mixture of PDMS and curing agent, respectively, over the silicon master and then curing the mixture overnight at 70 °C. The PDMS microchip was then peeled from the master and reservoirs were punched into the PDMS with a 4 mm biopsy punch (Harris Uni-Core, Ted Pella, Inc., Redding, CA, USA).

3.2.3. Electrode Fabrication

The method of fabricating in-house Pt electrodes has been previously described [15]. Briefly, electrode designs are drawn with AutoCad and printed onto a transparency with a resolution of 50,000 dpi. A borofloat glass substrate (4" x 4" x 0.090") pre-coated with a layer of chrome and then AZ1518 positive photoresist is covered by the transparency and exposed at 344 mJ cm^{-2} with a UV flood source for 4 s. Then the glass substrate is developed in MIF 300

developer for about 15 s and baked at 100 °C for 10 min on a programmable hotplate. At this point, the electrode pattern is imprinted in the photoresist, thereby exposing the chrome layer below. The exposed chrome is removed with chrome etchant. Trenches in the pattern of the electrodes are then created with the use of buffered oxide etchant to a depth of about 300 nm. After thoroughly washing the substrate with $CaCO_3$ solution and water, the trench depth is measured with an Alpha Step-200 surface profiler. Next, the glass substrate is exposed to an oxygen plasma for 1 min (March Plasmod, Concord, CA, USA) and immediately placed into an AXXIS DC magnetron sputtering system (Kurt J. Lesker Co., Jefferson Hills, PA, USA). After allowing the sputterer chamber to reach a pressure of 1.0×10^{-6} Torr, Ti was deposited on to the substrate for 40 s at 220 V and 5.0×10^{-3} Torr to produce a 20 nm Ti layer. Then Pt was deposited for 15 min at 200 V and 5.0×10^{-3} Torr. Next, the substrate was washed with acetone and then chrome etchant. The final width and height of the fabricated Pt electrodes were measured with an Alpha Step-200 surface profiler.

3.2.4. Electrophoresis Procedure

Microchips were constructed by reversibly bonding a layer of PDMS containing the simple-t design to the glass substrate containing the embedded Pt electrode. The Pt electrode was aligned at the intersection of the separation channel and the waste reservoir. Pt leads were inserted into each reservoir. Two Spellman CZE 1000R high voltage power supplies (Spellman, Hauppauge, NY, USA) controlled with a LabView (National Instruments, Austin, TX, USA) program written in-house were used for all electrophoresis procedures. Samples were injected using a gated injection protocol. A gate was established by applying -2400 V and -2200 V to the buffer and sample reservoirs, respectively, while both the buffer waste and sample waste reservoirs were grounded. Sample injection occurred by floating the voltage in the buffer

reservoir for 1 s. The run buffer used in these experiments was 10 mM boric acid pH adjusted to 10 with NaOH with 5.5 mM TTAC and 10 mM NaCl.

3.2.5. Electrochemical Detection and Data Analysis

Electrochemical detection was accomplished with a two-channel wireless isolated potentiostat (Pinnacle Technology, Inc., Lawrence, KS, USA). The potentiostat used had a sampling rate of 6.5 to 13 Hz (gain = 5,000,000 V/A, resolution = 47 fA). Sirenia software (Pinnacle Technology, Inc., Lawrence, KS, USA) was used for all data acquisition. Electrochemical measurements were taken at a WE potential of +1.100 V vs. Ag/AgCl reference electrode (BASi, West Layfayette, IN, USA). All data analysis was performed with Origin 8.6 software (OriginLab, Northhampton, MA, USA).

3.2.6. Pt Black Deposition

A 10 mM lead (II) acetate trihydrate stock solution was prepared. The Pt black deposition solution was then prepared by adding 1 mL of 8% w/v hydrogen hexachloroplatinate solution and 0.42 mL of 10 mM lead (II) acetate trihydrate stock solution to 5.94 mL of PBS. Pt black deposition was achieved by running a cyclic voltammogram on the Pt WE in the presence of the deposition solution, from +0.6 V to -0.35 V vs. Ag/AgCl reference at a scan rate of 0.02 V/s. The potential was controlled using a CHI electrochemical analyzer (CH Instruments, Inc., Austin, TX, USA) controlled by CHI software. After deposition, the area around the electrode was thoroughly washed with water to remove salt crystals formed during the deposition. Next, the modified electrode area was activated while in 10 mM boric acid at pH 10 by applying alternating pulses of +0.2 V and -0.5 V for 1 s each for 30 cycles.

3.2.7. Cell Culture and Sample Preparation

RAW 264.7 cells were cultured, stimulated, and tested for viability as previously reported [16]. To prepare the cell lysate samples, the stimulated cells were first harvested with a scraper and centrifuged at 3500 rpm for 3 min. Then the supernatant media was removed, leaving behind a cell pellet. This cell pellet was washed once with cold 10 mM PBS and then once with sterile water. The cell pellet was then lysed in 150 μL of buffer consisting of 10 mM boric acid at pH 10 and 5.5 mM TTAC. After lysis, the lysate was centrifuged through a 3 kDa molecular weight cut-off filter (VWR International, West Chester, PA, USA) for 8 min to remove large compounds, such as membranes and proteins. The filtered lysate was run on the ME-EC device for analysis.

3.3. Results and Discussion

3.3.1. Separation Optimization and Transient Isotachophoresis

Initial experiments used a background electrolyte consisting of 10 mM boric acid with 2 mM TTAC at pH 10 for the ME-EC separation. However, when cell lysate samples were analyzed, NO_2^- comigrated with an interferent peak coming from azide on the filters used for sample preparation. To enhance the separation of these two components, the concentration of TTAC in the BGE was varied from 2 mM to 9 mM. The optimal TTAC concentration was determined to be 5.5 mM. At this concentration, all the peaks were baseline resolved in less than 30 seconds (Figure 3.1).

In previous studies of cell lysates, destacking of the NO_2^- peak was observed due to the high conductivity of the sample matrix [16]. The addition of NaCl to the BGE was shown to reduce the destacking effect [16]. In these studies, the standard solutions were diluted in the

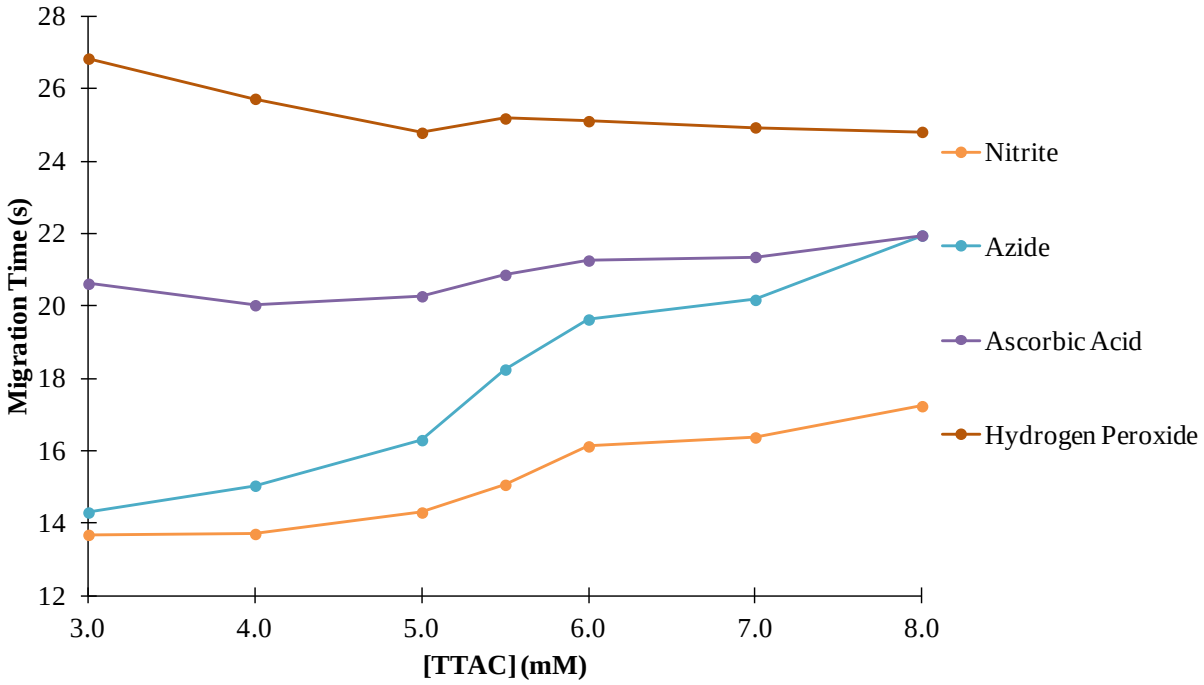

Figure 3.1. Migration times of NO_2^-, azide, ascorbic acid, and hydrogen peroxide by ME-EC with a BGE consisting of 10 mM boric acid at pH 10 with varying concentrations of TTAC.

BGE without NaCl (only 10 mM boric and 5.5 mM TTAC at pH 10) while the rest of the microchip was filled with BGE containing 10 mM NaCl. This resulted in a greatly enhanced NO_2^- peak due to transient isotachophoretic stacking without affecting the response or resolution of the other analytes in the solution (Figure 3.2).

In a transient isotachophoresis separation, the zone of the analyte of interest (NO_2^-) is stacked between a leading and a tailing electrolyte, which have faster and slower electrophoretic mobilites than the analyte of interest, respectively. In this transient isotachophoresis system, the leading electrolyte is the chloride ion because its electrophoretic mobility is slightly faster than that of NO_2^- under these separation conditions [17]. It is hypothesized that the boric ion is the tailing electrolyte in this system. Furthermore, it was found that the concentration of NaCl must be in excess compared to the NO_2^- concentration in order for stacking to occur (Figure 3.3) [18]. A concentration of 10 mM NaCl was chosen in these studies because it provided optimal stacking without adding unnecessary conductivity to the system. Even though the addition of 15 mM NaCl to the run buffer sometimes caused better stacking of the NO_2^- peak, there was more variability in the NO_2^- peak height, which is believed to be due to the higher conductivity buffer leading to joule heating. Using transient isotachophoresis and a bare Pt electrode, the LOD for NO_2^- was reduced approximately 5-fold from 2.6 μM, as previously reported by our group [19], to 500 nM.

3.3.2. Platinum Black Deposition Optimization

Initial attempts to deposit Pt black on the Pt electrode on the glass plate were performed in bulk. The deposition area was defined by punching a 4 mm hole in a featureless PDMS substrate and aligning the hole over the WE to create a reservoir, which was filled

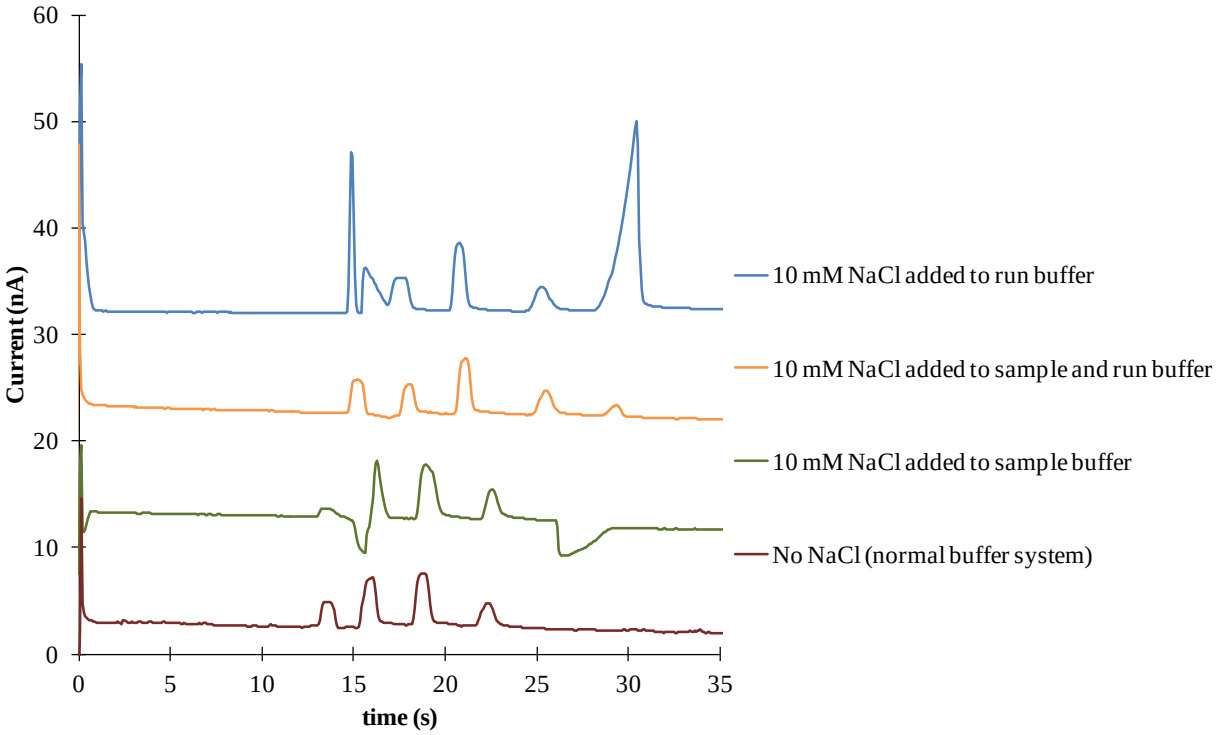

Figure 3.2. Electropherograms illustrating a standard solution of 50 µM NO_2^-, 20 µM azide, 40 µM ascorbic acid, and 100 µM hydrogen peroxide using a run buffer and sample buffer consisting of 10 mM boric acid and 5.5 mM TTAC at pH 10, the effect of adding 10 mM NaCl to both the run buffer and sample buffer, and only adding 10 mM NaCl to the run buffer.

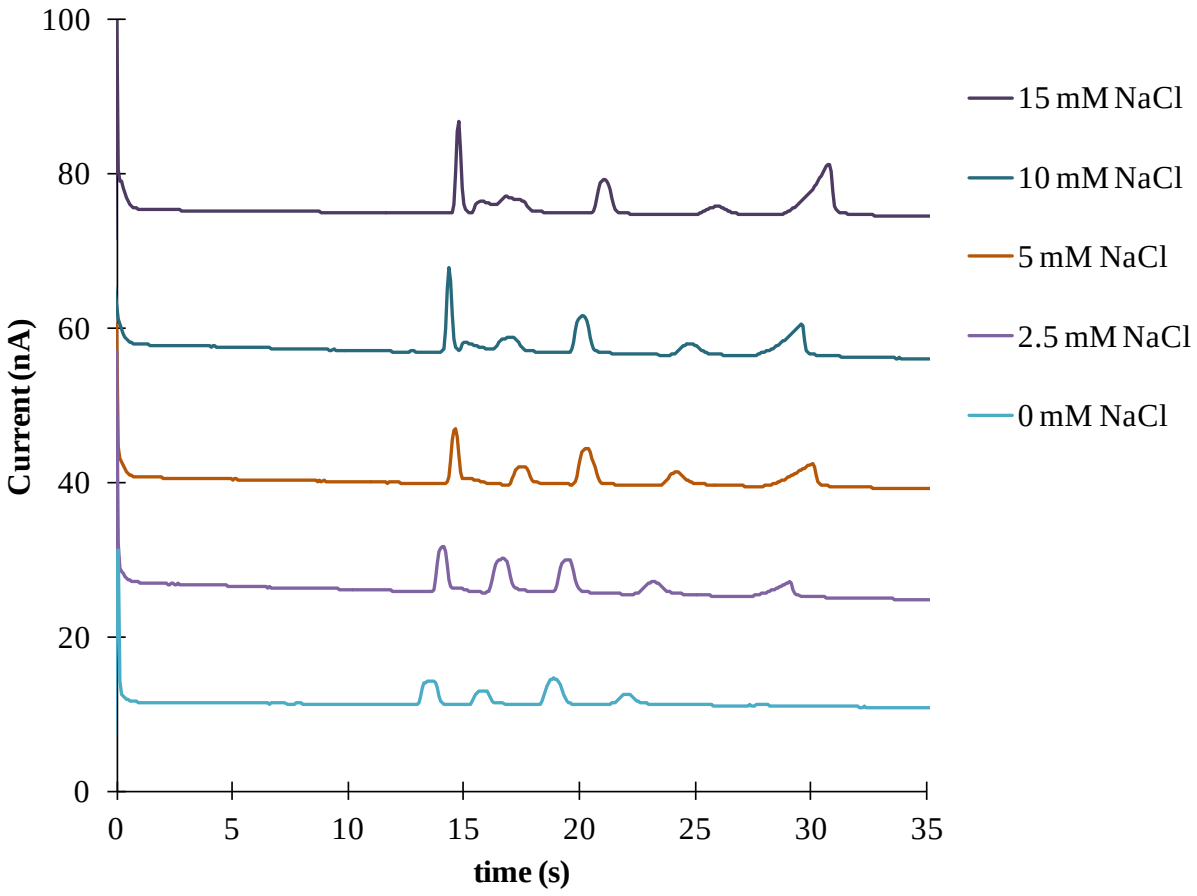

Figure 3.3. Electropherograms depicting the change in NO_2^- stacking due to transient isotachophoresis as a result of adding increasing concentrations of NaCl to the run buffer consisting of 10 mM boric acid at pH 10 and 5.5 mM TTAC.

with deposition solution. Pt black was then deposited on the WE using cyclic voltammetry. During these experiments, there was a physical change in the color of the electrode area contained within the reservoir (turned black), indicating that the modification was successful. However, a deposition wider than the separation channel made it difficult to seal the PDMS to the glass substrate. Normally, if the electrode height is less than about 200 nm, a reversible seal can be achieved. However, it was observed that this deposition procedure resulted in electrode heights greater than 200 nm. To remedy this problem, the deposition was performed after the PDMS substrate with channels was already aligned on the WE and sealed to the glass substrate. Deposition solution added to the bottom waste reservoir and was pulled through the separation channel with an aspirator, thereby covering the exposed section of the WE used for detection. During the deposition, flow was stopped, which allowed the deposition to occur in stationary deposition solution. Defining the deposition area with the actual microchip design prevented the deposition onto the portion of the electrode that was underneath the PDMS substrate and kept the seal intact.

It was found that using cyclic voltammetry to deposit the Pt black onto the surface of the WE resulted in an unstable modification. When a separation was performed and a voltage was applied through the separation channel, large drops in the background current at the WE was observed, which implied that the Pt black was detaching from the WE. Therefore, the electrode modified via cyclic voltammetry was activated using differential pulse voltammetry as previously described by Li *et al*. [12]. The activation process has been reported to increase the stability of the Pt black modification [12]. SEM images of activated and non-activated modified electrodes show a drastic difference in the physical properties due to the modification (Figure 3.4).

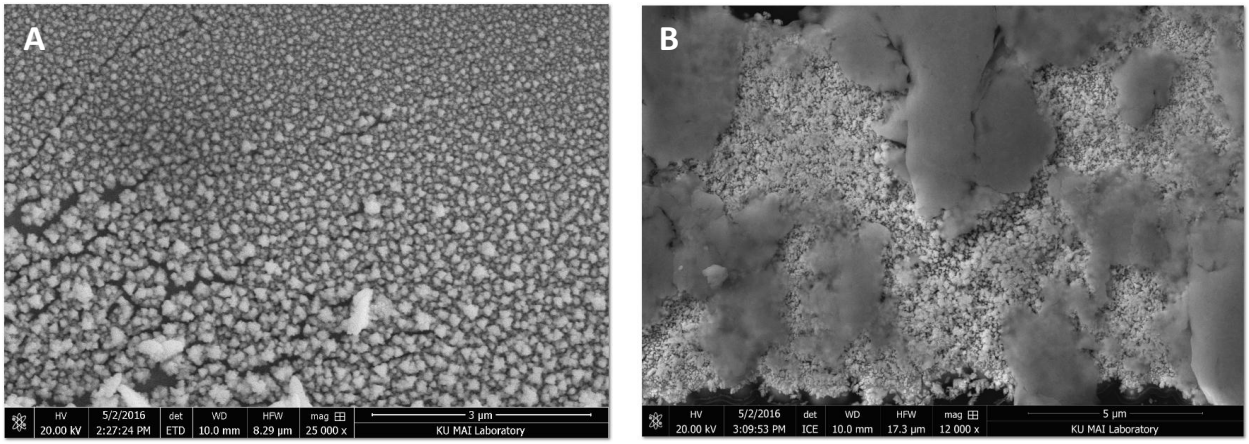

Figure 3.4. SEM images of a (A) non-activated and (B) activated Pt black modified WE.

The deposition process resulted in the formation of salt crystals both in the buffer waste reservoir and in the separation channel, so the chip had to be washed with water after this process and inspected to ensure no crystals were present. The presence of crystals can lead to irreproducible signal measurements due to irregular flows throughout the microchip channels.

3.3.3. Signal Enhancement

In order to accurately determine the degree of signal enhancement produced by the Pt black modification, compared to a bare Pt WE, the response for a standard mixture of NO_2^-, AA, and hydrogen peroxide was measured before and after the deposition with the same microchip and electrode alignment. This was important because variations in electrode alignment can cause changes in both the amplitude of the noise and signal. While using the same microchip for these enhancement measurements, the channels of the microchip were thoroughly washed with water to ensure no run buffer remained in the channel during deposition. Figure 3.5 shows electropherograms of a mixture of NO_2^-, AA, and hydrogen peroxide standards before and after a Pt WE was modified. The modified electrode generated a significant increase in signal, but also exhibited a higher background current. This increase in background current was expected since the geometric area of the electrode was increased. Average signal enhancements of 2.5 ± 0.2, 1.7 ± 0.2, and 7.2 ± 0.2 were observed for NO_2^-, AA, and hydrogen peroxide, respectively with the Pt black modified electrode.

An external calibration curve was generated to determine the effect of the Pt black deposition and activation on the sensitivity of NO_2^- measurements (Figure 3.6). The sensitivity for the detection of NO_2^- with a bare Pt and Pt black modified WE were 0.245 ± 0.001 and 0.580 ± 0.008 nA μM^{-1}, respectively. The modification of the WE resulted in a 2.36 ± 0.03-fold

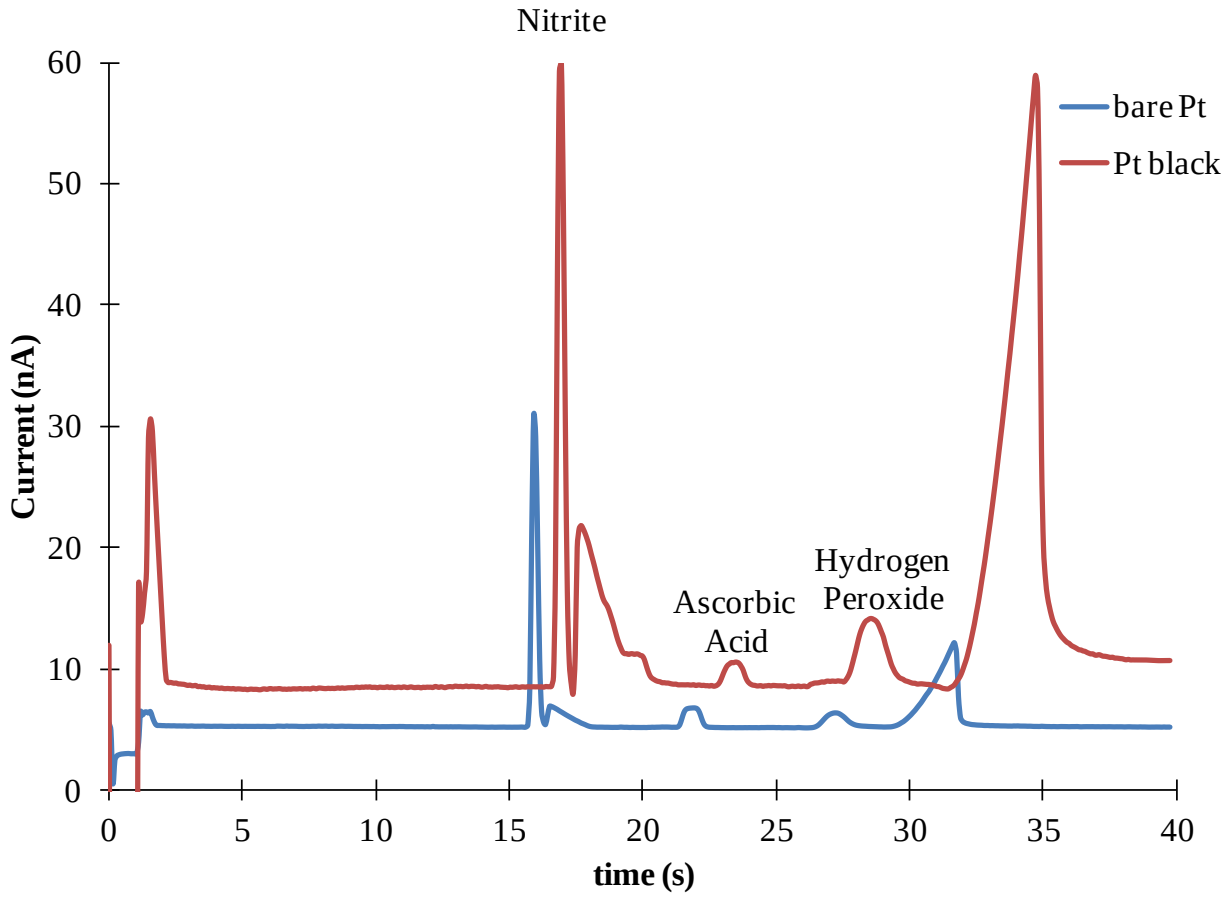

Figure 3.5. Electropherograms of 100 µM NO_2^-, 40 µM AA, and 100 µM hydrogen peroxide standards before and after Pt black modification.

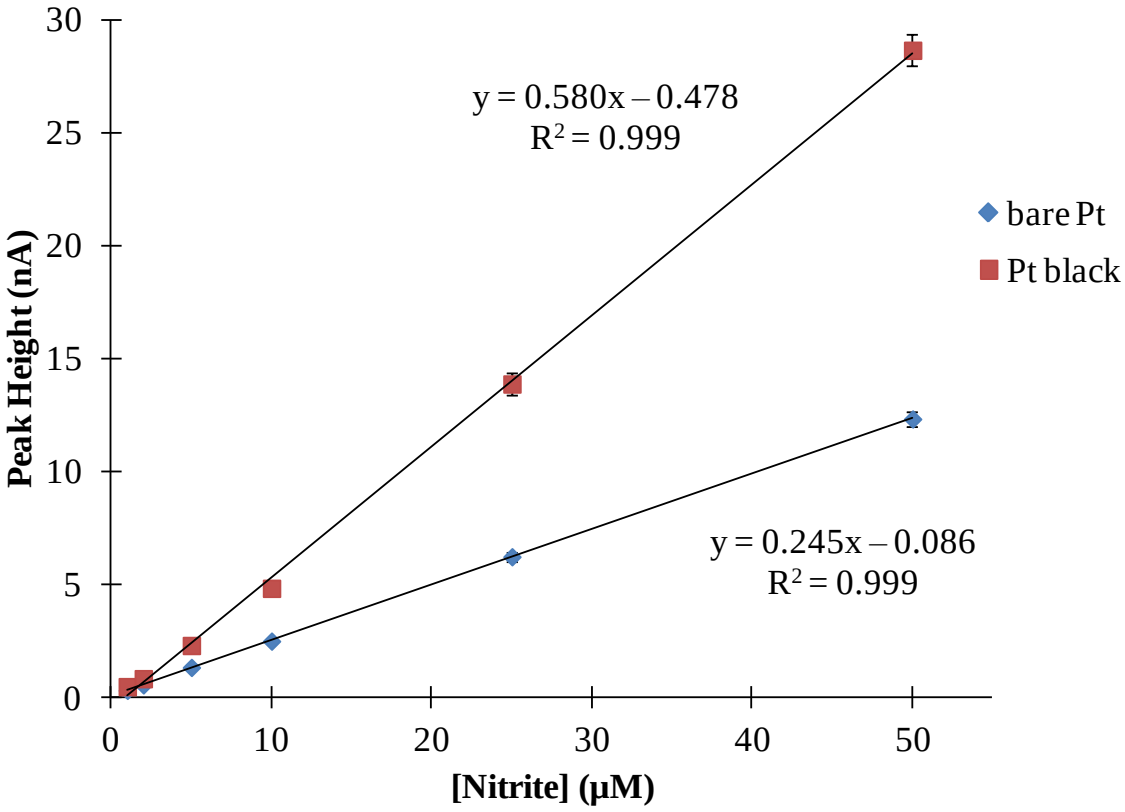

Figure 3.6. External calibration curve of NO_2^- obtained with bare Pt and Pt black.

enhancement in the sensitivity toward NO_2^-. These results are comparable with those obtained by Shim *et al*., where a sensitivity enhancement for NO was observed when a Pt WE underwent platinization [7]. This increase in sensitivity is the result of the increase in the electroactive surface area of the electrode [7]. Unfortunately, electrode modification also resulted in an enhancement of the noise. The comparable signal and noise enhancement resulted in an unchanged S/N ratio and therefore the LOD of the system did not change.

3.3.4. NO_2^- in Biological Sample

Cell lysate samples with high conductivities have been previously reported to suppress the NO_2^- peak due to destacking effects [16]. To avoid these effects, the cell pellet was washed first with PBS followed by deionized water to eliminate the high salt concentrations from the PBS wash prior to lysing with run buffer. The addition of the water wash step in the cell prep resulted in samples that had much lower conductivities (similar to normal standard solutions in run buffer). The lower conductivity cell lysates allowed for stacking of the NO_2^- peak with the tITP system, which provided additional signal enhancement and peak consistency.

It is known that LPS stimulated RAW 264.7 macrophages produce high amounts of NO [20]. LPS is an endotoxin found on the outer membrane of gram-negative bacteria and causes the activation of the iNOS pathway in macrophages, resulting in the overproduction of NO. In this study, macrophage cells were stimulated with 100 ng mL^{-1} of LPS for 24 hours.

The effect of the signal enhancement obtained with the Pt black modified electrodes combined with tITP on the determination of intracellular NO_2^- was investigated on both native and LPS stimulated bulk cell lysate samples. Figure 3.7A shows electropherograms obtained for a LPS stimulated cell lysate sample obtained with the same electrode and microchip before and

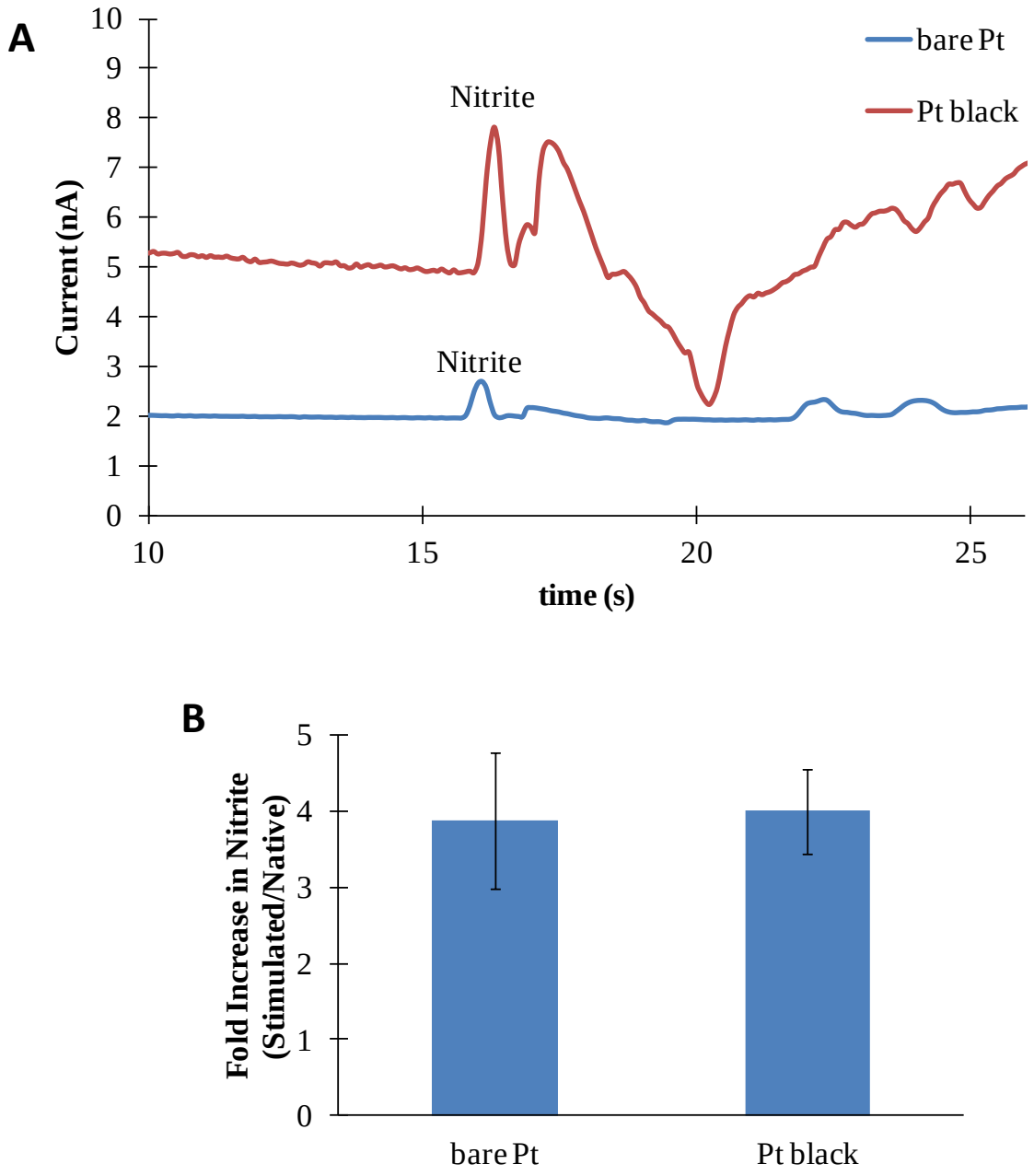

Figure 3.7. (A) Electropherograms of a LPS stimulated RAW 264.7 macrophage cell lysate sample obtained using bare Pt and Pt black. (B) A comparison of the change in the intracellular NO_2^- concentration due to LPS stimulation of a bare Pt electrode and a Pt electrode modified with Pt black.

after the WE had been modified with Pt black. The identity of the NO_2^- peak was determined through spiking and comparison of the migration order with a method previously developed by our group [16]. The electrode modification resulted in an average 4.31 ± 0.33-fold enhancement in the NO_2^- signal, which was averaged over both native and stimulated (n=3 for both sets) cell lysates. Due to the differing number of cells in each sample, the results were corrected based on their respective cell count.

The fold increase in NO_2^- due to the presence of LPS was also calculated to ensure that the same result was achieved with an unmodified and modified WE (Figure 3.7B). A t-test was performed to compare this data, and it was determined that at 95% confidence there is no statistically significant difference between the two sets of data. Furthermore, this fold increase in NO_2^- agrees with results previously reported by Gunasekara *et al* [16].

3.4. Conclusions

A ME-EC method that uses transient isotachophoresis and a Pt black modified WE to enhance the signal and detect NO_2^- as well as other electrochemically active species was reported. The ability to monitor multiple species involved in oxidative and nitrosative stress will make it possible to better understand the underlying mechanisms of various disease states, such as neurodegeneration. First, a stacking method to enhance the signal of NO_2^- through the addition of NaCl to the run buffer was developed. Then a procedure to modify a Pt WE with Pt black was optimized. This electrode modification was then coupled with a ME-EC method and a signal enhancement in NO_2^-, hydrogen peroxide, and ascorbic acid was obtained. Additionally, the use of a Pt black modified WE resulted in an increased sensitivity for NO_2^-. This method was also used to indirectly detect NO in bulk cell lysate samples by detecting NO_2^-. It was found that a WE modified with Pt black enhances the signal of NO_2^- in biological samples. The

incorporation of the tITP system and Pt black modified WE improved the method previously reported by our group by providing increased sensitivity and decreasing the LOD. In the future, this method can be expanded to monitor multiple species in bulk and single cell studies. Additionally, other cell lines can be studied. The incorporation of this method into a single cell analysis device will make it possible to monitor short-lived species, such as NO and peroxynitrite, in real time.

3.5. References

1. Li, Y.; Sella, C.; Lemaître, F.; Guille Collignon, M.; Thouin, L.; Amatore, C. Highly Sensitive Platinum-Black Coated Platinum Electrodes for Electrochemical Detection of Hydrogen Peroxide and Nitrite in Microchannel. *Electroanalysis*. **2013**, *25*, 895-902.

2. Li, Y.; Meunier, A.; Fulcrand, R.; Sella, C.; Amatore, C.; Thouin, L.; Lemaître, F.; Guille-Collignon, M. Multi-Chambers Microsystem for Simultaneous and Direct Electrochemical Detection of Reactive Oxygen and Nitrogen Species Released by Cell Populations. *Electroanalysis*. **2016**, *28*, 1865-72.

3. Fagan-Murphy, A.; Hachoumi, L.; Yeoman, M.; Patel, B. Electrochemical Sensor for the Detection of Multiple Reactive Oxygen and Nitrogen Species from Ageing Central Nervous System Homogenates. *Mech Ageing Dev*. **2016**, *160*, 28-31.

4. Teshima, N.; Genfa, Z.; Dasgupta, P.K. Catalytic Decomposition of Hydrogen Peroxide by a Flow-through Self-Regulating Platinum Black Heater. *Anal Chim Acta*. **2004**, *510*, 9-13.

5. Ikariyama, Y.; Yamauchi, S.; Yukiashi, T.; Ushioda, H. Surface Control of Platinized Platinum as a Transducer Matrix for Micro-Enzyme Electrodes. *J Electroanal Chem Interfacial Electrochem*. **1988**, *251*, 267-74.

6. Casella, I.G.; Salvi, A.M. Voltammetric Behavior and Ion Chromatographic Detection of Nitrite at a Dispersed Platinum Glassy Carbon Electrode. *Electroanalysis*. **1997**, *9*, 596-601.

7. Shim, J.H.; Lee, Y. Amperometric Nitric Oxide Microsensor Based on Nanopore-Platinized Platinum: The Application for Imaging NO Concentrations. *Anal Chem*. **2009**, *81*, 8571-6.

8. Selimovic, A.; Martin, R.S. Encapsulated Electrodes for Microchip Devices: Microarrays and Platinized Electrodes for Signal Enhancement. *Electrophoresis*. **2013**, *34*, 2092-100.

9. Lee, Y.; Yang, J.; Rudich, S.M.; Schreiner, R.J.; Meyerhoff, M.E. Improved Planar Amperometric Nitric Oxide Sensor Based on Platinized Platinum Anode. 2. Direct Real-Time Measurement of No Generated from Porcine Kidney Slices in the Presence of L-Arginine, L-Arginine Polymers, and Protamine. *Anal Chem*. **2004**, *76*, 545-51.

10. Lee, Y.; Kim, J. Simultaneous Electrochemical Detection of Nitric Oxide and Carbon Monoxide Generated from Mouse Kidney Organ Tissues. *Anal Chem*. **2007**, *79*, 7669-75.

11. Park, S.S.; Tatum, C.E.; Lee, Y. Dual Electrochemical Microsensor for Simultaneous Measurements of Nitric Oxide and Oxygen: Fabrication and Characterization. *Electrochem Commun*. **2009**, *11*, 2040-3.

12. Li, Y.; Sella, C.; Lemaître, F.; Guille-Collignon, M.; Thouin, L.; Amatore, C. Electrochemical Detection of Nitric Oxide and Peroxynitrite Anion in Microchannels at Highly Sensitive Platinum-Black Coated Electrodes. Application to ROS and RNS Mixtures Prior to Biological Investigations. *Electrochim Acta*. **2014**, *144*, 111-8.

13. Erkal, J.L.; Selimovic, A.; Gross, B.C.; Lockwood, S.Y.; Walton, E.L.; Mcnamara, S.; Martin, R.S.; Spence, D.M. 3D Printed Microfluidic Devices with Integrated Versatile and Reusable Electrodes. *Lab Chip*. **2014**, *14*, 2023-32.

14. Duffy, D.C.; Mcdonald, J.C.; Schueller, O.J.A.; Whitesides, G.M. Rapid Prototyping of Microfluidic Systems in Poly(Dimethylsiloxane). *Anal Chem*. **1998**, *70*, 4974-84.

15. Scott, D.E.; Grigsby, R.J.; Lunte, S.M. Microdialysis Sampling Coupled to Microchip Electrophoresis with Integrated Amperometric Detection on an All-Glass Substrate. *ChemPhysChem*. **2013**, *14*, 2288-94.

16. Gunasekara, D.B.; Siegel, J.M.; Caruso, G.; Hulvey, M.K.; Lunte, S.M. Microchip Electrophoresis with Amperometric Detection Method for Profiling Cellular Nitrosative Stress Markers. *Analyst*. **2014**, *139*, 3265-73.

17. Timerbaev, A.R.; Hirokawa, T. Recent Advances of Transient Isotachophoresis-Capillary Electrophoresis in the Analysis of Small Ions from High-Conductivity Matrices. *Electrophoresis*. **2006**, *27*, 323-40.

18. Szökő, É.; Tábi, T.; Halász, A.S.; Pálfi, M.; Magyar, K. High Sensitivity Analysis of Nitrite and Nitrate in Biological Samples by Capillary Zone Electrophoresis with Transient Isotachophoretic Sample Stacking. *J Chromatogr A*. **2004**, *1051*, 177-83.

19. Gunasekara, D.B.; Hulvey, M.K.; Lunte, S.M. In-Channel Amperometric Detection for Microchip Electrophoresis Using a Wireless Isolated Potentiostat. *Electrophoresis*. **2011**, *32*, 832-7.

20. Lorsbach, R.B.; Murphy, W.J.; Lowenstein, C.J.; Snyder, S.H.; Russell, S.W. Expression of the Nitric Oxide Synthase Gene in Mouse Macrophages Activated for Tumor Cell Killing. Molecular Basis for the Synergy between Interferon-Gamma and Lipopolysaccharide. *J Biol Chem*. **1993**, *268*, 1908-13.

Chapter 4:

Construction of a Cellulose Acetate-Based Decoupler for Microchip Electrophoresis with Electrochemical Detection

4.1. Introduction

The majority of decouplers used in ME-EC utilize large (500 to 1000 μm) metal electrodes, usually made of platinum or palladium, to decouple the separation field from the electrochemical detector [1-5]. Metal decouplers made of Pt or Pd are capable of adsorbing the H_2 gas produced during normal polarity separations; however, their weakness is the inability to adsorb O_2 gas to function in reverse polarity separation fields [6]. Furthermore, these metal electrodes are difficult to fabricate and can delaminate or fracture in the presence of high electric fields [6]. Therefore, other methods have been investigated to decouple amperometric detectors from the high electric fields used for the separation.

The first alternative to a metal decoupler for ME-EC was described by Rossier *et al*. [7]. In this study, the decoupler consisted of an array of 10 μm holes that was fabricated in a layer of polyethylene with a separation channel positioned across the array [7]. This method did successfully decouple the separation voltage from the working electrode but, because there was no barrier to stop analytes from leaving the separation channel, analyte LODs were high. Then, Osbourn *et al.* developed a cellulose acetate-based decoupler [8]. The addition of a cellulose acetate membrane over a series of laser etched slits prevented analytes from leaving the separation channel but still allowed charge transfer. An additional advantage of this design, that was not mentioned in the report, is that the decoupling process occured outside of the separation space, so any gas produced by the decoupler does not interfere with the separation. Therefore, this system could theoretically be applied to both normal and reverse polarity separations.

In this chapter, a cellulose acetate membrane-based decoupler for use with ME-EC was developed. This platform uses thicker glass than previously reported (500 μm as compared to 250 μm), and the method used to drill decoupler reservoirs in this thicker glass is described. To

evaluate the decoupler performance, a separation of norepinephrine, hydroquinone, and ascorbic acid was run in normal polarity with a carbon ink working electrode for detection. To demonstrate this platform's applicability to reverse polarity separations, the effect of the separation field on the noise amplitude with and without a decoupler, was determined. Finally, NO_2^-, ascorbic acid, and hydrogen peroxide were separated in reverse polarity and detected after a decoupler with a platinum working electrode.

4.2. Materials and Methods

4.2.1. Materials and Reagents

The following materials and chemicals were used as received: boric acid, tetradecyltrimethylammonium chloride (TTAC), sodium nitrite, ascorbic acid, cellulose acetate, hydroquinone, norepinephrine, sodium phosphate monobasic, and sodium phosphate dibasic (Sigma-Aldrich, St. Louis, MO, USA); sodium dodecyl sulfate (SDS), dioxane, sodium hydroxide (NaOH), acetone, 2-propanol (IPA), and 30% hydrogen peroxide (H_2O_2) (Fisher Scientific, Pittsburgh, PA, USA); carbon ink and solvent thinner (Ercon Inc., Wareham, MA, USA); SU-8 photoresist, SU-8 developer, and MIF 300 developer (Micro-Chem, Newton, MA, USA); glass substrates (4" x 4" x 0.5 mm) coated with chrome and AZ1518 photoresist (Nanofilm, Westlake, CA, USA); buffered oxide etchant (JT Baker, Austin, TX, USA); chrome etchant (Cyantek Corp., Freemont, CA, USA); Ti and Pt targets (Kurt J. Lesker Co., Jefferson Hills, PA, USA); polydimethylsiloxane (PDMS) and curing agent (Sylgard 184 elastomer kit, Ellsworth Adhesives, Germantown, WI, USA); 4" diameter silicon wafers (Silicon, Inc., Boise, ID, USA); epoxy and Cu wire (Westlake Hardware, Lawrence, KS, USA); silver colloidal (Ted Pella, Inc., Redding, CA, USA). All water was ultrapure (18.2 MΩ) and generated from a Milli-Q Synthesis A10 system (Millipore, Burlington, MA, USA).

4.2.2. PDMS Microchip Fabrication

A 4" diameter silicon wafer was coated with SU-8 10 negative photoresist to a thickness of 25 μm with a Cee 100 spincoater (Brewer Science Inc., Rolla, MO, USA). The wafer then underwent a soft bake at 65 °C for 2 min and then 95 °C for 6 min on a programmable hotplate (Thermo Scientific, Waltham, MA, USA). The design for the microchip was drawn with AutoCad (Autodesk, San Rafael, CA, USA) and printed onto a transparency (Infinite Graphics, Minneapolis, MN, USA). The coated wafer was then covered with the negative transparency and exposed at 344 mJ cm^{-2} with a UV flood source (ABC Inc., San Jose, CA, USA). Next, the wafer was transferred to a programmable hotplate again for a postbake at 65 °C for 1 min and then 95 °C for 2 min. After the postbake, the wafer was developed in SU-8 developer, rinsed with IPA, and dried with nitrogen. Lastly, the wafer underwent a hard bake at 200 °C for 2 h. The final silicon master contained 25 μm thick and 40 μm wide microchannels, which were measured with an Alpha Step-200 surface profiler (KLA-Tencor Instruments, Milpitas, CA, USA). The microchip used for these studies consisted of a simple-t design with a 5 cm separation channel and 0.75 cm side arms. A PDMS microchip was made by pouring a degassed 20:1 mixture of PDMS and curing agent, respectively, over the silicon master and then curing the mixture overnight at 70 °C. The PDMS microchip was then peeled from the master.

4.2.3. Carbon Ink Electrode Fabrication

Carbon ink working electrodes were for the normal polarity separations. First, a trench was etched into a piece of borofloat glass coated with chrome and AZ1518 positive photoresist as described in Chapter 3. The AZ1518 coating was then removed by thoroughly washing the glass substrate in acetone and the chrome layer was removed with chrome etchant. The trench had a final width and depth of approximately 15 and 10 μm, respectively, which were measured

with an Alpha-step 200 profilometer. The electrode was made by covering the trench with 20 μL of a solution of 0.2% (w/v) carbon ink in solvent thinner and heating the glass substrate at 95 °C in an oven for 30 min. After heating, the excess carbon around the trench was removed by running a razor blade across the surface of the glass.

4.2.4. Platinum Electrode Fabrication

Platinum electrodes were used as working electrodes for the reverse polarity separations. These electrodes were fabricated as described in Chapter 3.

4.2.5. Glass Drilling Procedure

Marks were made with a Sharpie on a glass substrate already containing a working electrode for amperometric detection to denote the location of the four reservoirs on a microchip with a simple-t design. Additionally, a mark was made approximately 500 μm up-channel from the electrode for a decoupler reservoir. Holes were then cut into a blank piece of PDMS that matched the marks on the glass with a 3 mm biopsy punch (Harris Uni-core, Ted Pella Inc., Redding, CA, USA). The holes in the PDMS were aligned with the marks on the glass and the PDMS was reversibly sealed to the top of the glass (the side with exposed electrodes). The PDMS must cover the electrode to prevent electrode damage during sand blasting. Next, holes were drilled in the glass where each mark was made on the glass with a sand blaster (Airbrasive Jet Technologies, LLC., Piscataway, NJ, USA). Holes were drilled from the back of the glass (no exposed electrode) to the front because the entrance holes were much rougher than the exit holes during drilling. After drilling, the PDMS was removed and excess sand was removed by washing with water.

4.2.6. Cellulose Acetate Membrane Fabrication

First, a piece of PDMS was placed on the top of the glass substrate to cover the decoupler reservoir. Then, the reservoir was filled with 5 μL of a solution of 5% (w/v) cellulose acetate in dioxane. Next, the glass substrate was heated in an oven at 95 °C for 20 min. The process of filling the reservoir with solution and heating was repeated 3 times to make a thicker membrane with more structural integrity. After the last layer was complete, the PDMS was removed, leaving behind a smooth cellulose acetate membrane that was flush with the surface of the glass.

4.2.7. Electrophoresis Procedure

Microchips were constructed by aligning a PDMS substrate containing a simple-t design over the holes drilled in the glass substrate and then reversibly bonding the two substrates (Figure 4.1). Pt leads for electrophoresis were placed in the buffer, sample, sample waste, and decoupler reservoirs. Two Spellman CZE 1000R high voltage power supplies (Spellman, Hauppauge, NY, USA) controlled with a LabView (National Instruments, Austin, TX, USA) program written in-house were used for all electrophoresis procedures. Samples were injected using a gated injection protocol. While using normal polarity, a gate was established by applying +2400 V and +2200 V to the buffer and sample reservoirs, respectively, whereas -2400 V and -2200 V were used in reverse polarity. The sample waste and decoupler reservoirs were grounded. Sample was injected into the separation channel by floating the buffer voltage for 1 s. The run buffer used during normal polarity separations was 10 mM phosphate buffer at pH 7.4 with 2 mM SDS. The run buffer used during reverse polarity separations was 10 mM boric acid adjusted to pH 10 with NaOH and 5.5 mM TTAC.

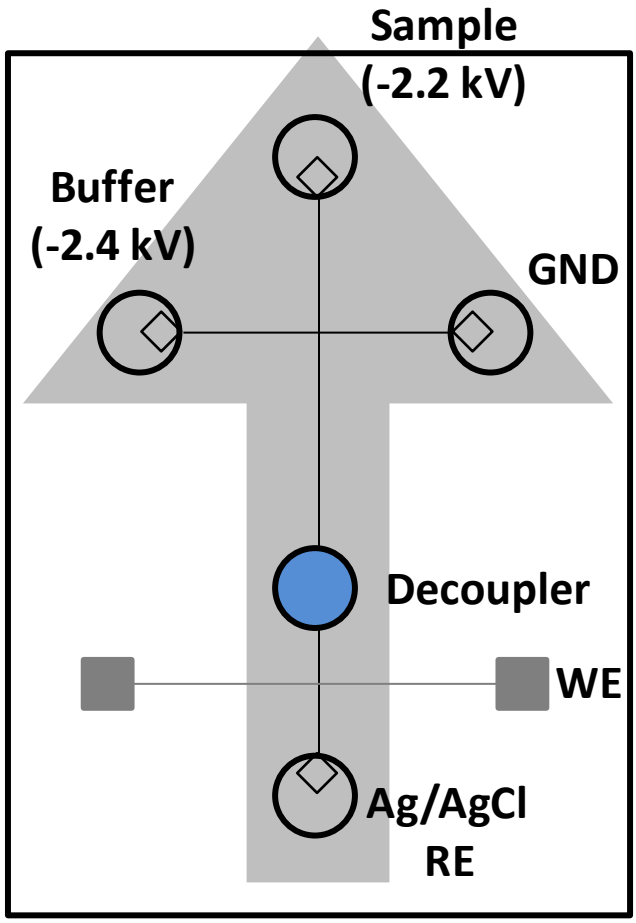

Figure 4.1. Illustration of a microchip with a simple-t design and a decoupler reservoir (image not to scale).

4.2.8. Electrochemical Detection and Data Analysis

Electrochemical detection was accomplished with a two-channel wireless isolated potentiostat (Pinnacle Technology, Inc., Lawrence, KS, USA). The potentiostat used had a sampling rate of 6.5 to 13 Hz (gain = 5,000,000 V/A, resolution = 47 fA). Sirenia software (Pinnacle Technology, Inc., Lawrence, KS, USA) was used for all data acquisition. Electrochemical measurements were taken at a working electrode potential of +1.000 V or +1.100 V vs. Ag/AgCl reference electrode (BASi, West Layfayette, IN, USA) for normal and reverse polarity, respectively. All data analysis was performed with Origin 8.6 software (OriginLab, Northhampton, MA, USA).

4.3. Results and Discussion

4.3.1. Glass Drilling Optimization

Osbourn *et al*. used a CO_2 laser etcher to drill holes into a microscope coverslip (~250 μm thick) for the decoupler array [8]. Therefore, initial attempts at drilling holes in 500 μm thick glass utilized a CO_2 laser etcher. The glass substrate used in this study was thicker than previously reported because the Pt or carbon ink microelectrode used for electrochemical detection was fabricated on the glass substrate and coverslips are too fragile to contain microelectrodes. Laser etching through this thicker glass proved problematic because of thermal stress. As the laser etched the glass, there was localized heating in the area around the laser resulting in slight glass expansion. Once completely etched, the thermal energy could not be properly dissipated and the glass cracks [9]. Attempts to solve this problem included heating the glass substrate and submersion of the glass substrate in water with additives during etching are described below.

Previous reports have shown that proper dissipation of the thermal energy through heating or liquid submersion can significantly reduce stress fractures in glass that occur during or after drilling [10-12]. First, heating the glass substrate was tested. The glass was heated to 350 °C on a ceramic hotplate and then etched while hot. This method allowed for etching at higher laser powers; however, cracking occurred while the glass was cooling down regardless of rate of temperature change (up to 3 hr cooldown times were tested).

Next, the glass substrate was submerged in water during laser etching. The water acts as a heat sink for the thermal energy as well as causes a convection force to continually cool and wash the area around the drilling area due to boiling water [10]. This method is very difficult to reproduce because it is dependent on the volume of water above the surface of the glass plate. This method still produced cracks, but they were much smaller than those produced during the other methods. The last attempt at laser drilling involved submerging the glass substrate in a solution of 5% (v/v) Triton-X in water. The addition of surfactant increases the viscosity of the liquid, which changes the convection forces of the cooling solution around the laser/glass interface to better dissipate thermal energy [11]. Unfortunately, this method also resulted in microcracks.

After laser etching was found to be ineffective for this application, sand blasting was tested for glass micro-sandblasting. Sandblasting provided very reproducible drilled holes without any microcracking. The holes drilled in this study had diameters of 500 to 800 μm. The diameter of the hole can be controlled by the size of the sandblaster nozzle and the length of the drill time; longer drill times result in larger diameter holes. The glass was covered with PDMS during the drilling process to protect the glass surface and electrode. It was observed that areas not covered with PDMS contained scratches after drilling. Most importantly, the working

(detection) electrode must be covered with PDMS to prevent stray sand from destroying the embedded electrode.

4.3.2. Decoupler Operation in Normal Polarity

The complete decoupler design was first tested in a normal polarity separation. A standard solution of 150 μM norepinephrine, 150 μM hydroquinone, and 100 μM ascorbic acid was separated in normal polarity with in-channel and off-channel aligned carbon ink working electrodes (Figure 4.2). Carbon ink was chosen for this separation because the analytes being tested produce a better electrochemical signal on carbon-based electrodes. In the presence of a decoupler, the peak height decreased about 2-fold for both norepinephrine and hydroquinone. This is most likely due to the band broadening occurring from diffusion after the electric field is removed from the separation channel by the decoupler. Unfortunately, due to the significant decrease in resolution, accurate measurements of the peak areas could not be obtained. Even though there was a 2-fold decrease in the peak height of the analytes, there was also a 6-fold decrease in the noise amplitude. Therefore, the S/N ratio is improved when using the decoupler. This decrease in noise is due to absence of noise produced by natural coupling of the working electrode with the high voltage separation field.

4.3.3. Effect of Decoupler on Noise in Reverse Polarity

To determine if the decoupler was working properly in a reverse polarity separation environment, the noise amplitude was measured with and without a decoupler present. Since the goal of this experiment was to observe the noise at the working electrode, the microchip used in this study only contained a straight 5 cm channel and no separation was performed. The channel was simply filled with run buffer and a high voltage was applied at one end. The voltage was

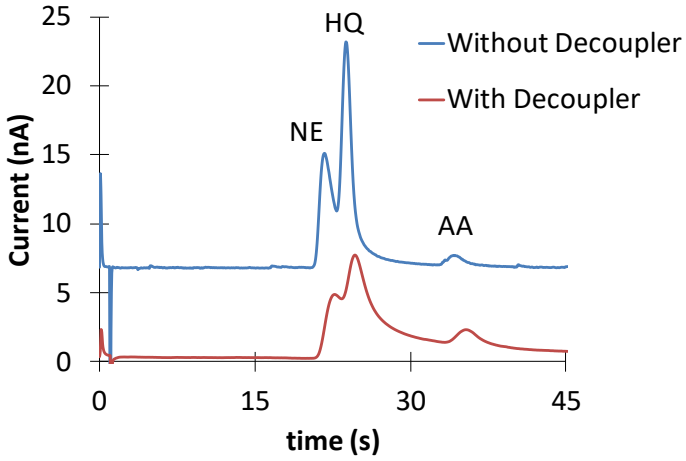

	Without Decoupler	With Decoupler
NE signal	8.29 nA	4.47 nA
HQ signal	16.75 nA	7.16 nA
AA signal	0.71 nA	1.03 nA
Noise	23 pA	4 pA

Figure 4.2. Electropherogram of 150 µM norepinephrine (NE), 150 µM hydroquinone (HQ), and 100 µM ascorbic acid (AA) in normal polarity with and without the presence of a decoupler. The table on the right displays the peak heights for each analyte peak as well as the amplitude of the noise with and without a decoupler.

either grounded at the other end (in-channel electrode alignment) or in the decoupler reservoir (off-channel electrode alignment). Figure 4.3 shows the average amplitude of the noise at the working electrode as a function of electrical field strength. When using in-channel alignment without a decoupler, the noise exponentially increases from 10 pA at 100 V/cm to more than 500 pA at 500 V/cm. Above 500 V/cm, the noise value could not be determined with this alignment because the background current was too high and maxed out the potentiostat. On the other hand, the presence of a decoupler prevented any significant noise increase or variation. From 100 V/cm to 1500 V/cm, the noise varies from 2 pA to 5 pA. This demonstrates that this type of decoupler is capable of successfully decoupling very large electric fields in reverse polarity.

4.3.4. Reverse Polarity Separation with Decoupler

To this point, no decoupler for a microfluidic platform has been reported to be capable of functioning in reverse polarity. In this experiment, a standard solution of 100 μM NO_2^-, 100 μM ascorbic acid, and 200 μM hydrogen peroxide was separated in reverse polarity and detected by EC with a cellulose acetate decoupler (Figure 4.4). All three analytes are fully resolved with good peak shape. However, the peak heights are significantly decreased (more than 50-fold) when compared with an in-channel aligned electrode. Possible explanations include leakage of solution from the separation channel due to improper sealing of the cellulose acetate membrane to the glass or PDMS, analyte binding to the membrane, or analytes penetrating the membrane. The molecules used in this study are very small, making them more susceptible to membrane penetration or leakage due to high diffusion rates. In the future, tests will be done to determine the cause of this signal decrease and attempt to remedy it.

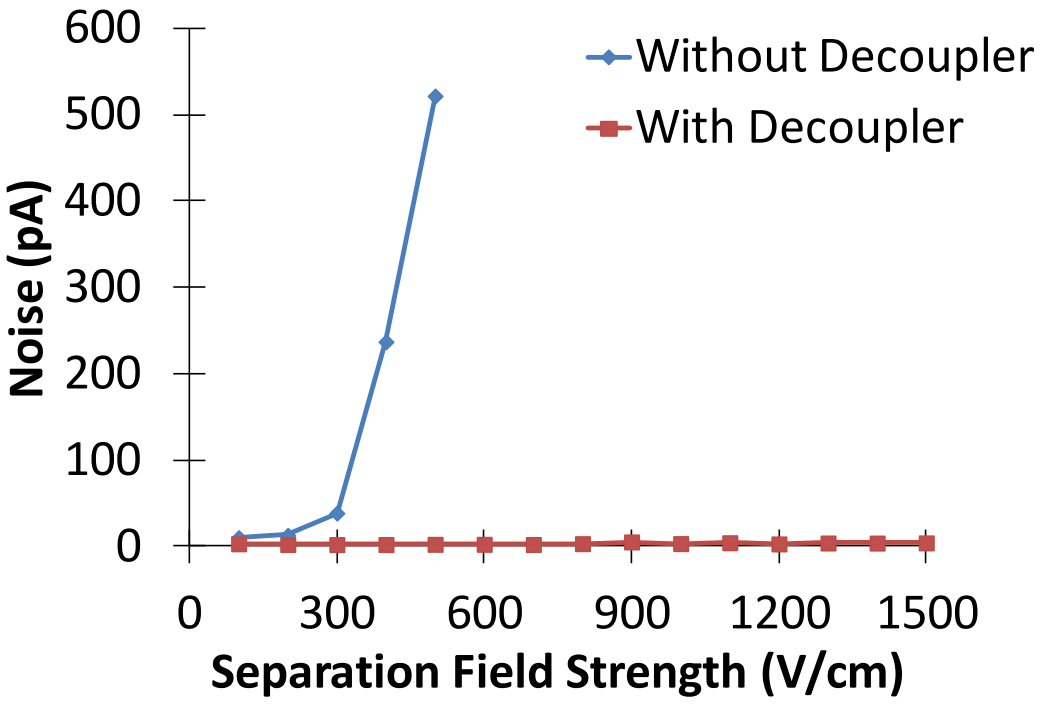

Figure 4.3. A graph of the noise amplitude as a function of separation field strength for a microchip with and without a decoupler.

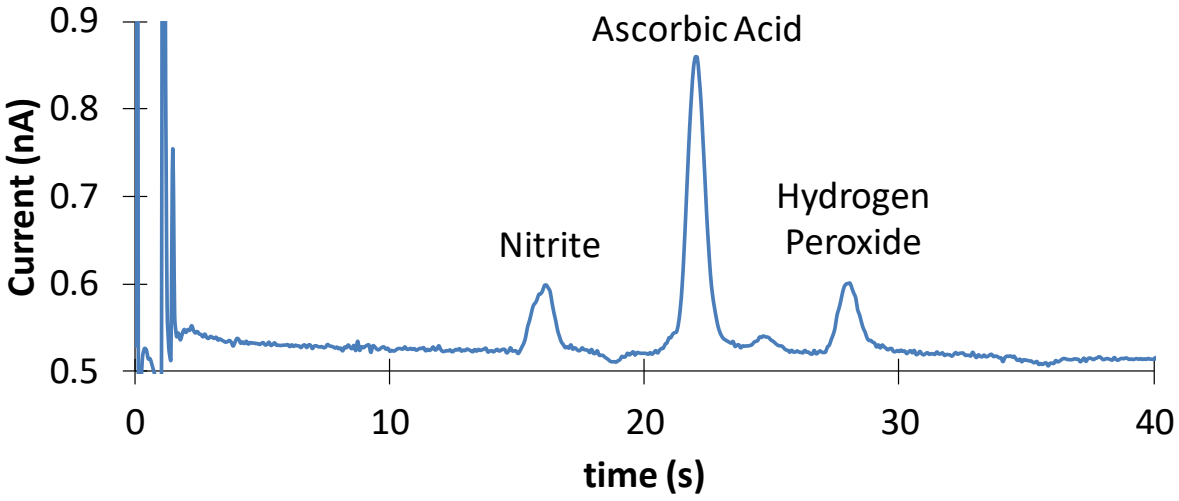

Figure 4.4. Electropherogram of the separation of 100 µM NO_2^-, 100 µM ascorbic acid, and 200 µM hydrogen peroxide in reverse polarity with a cellulose acetate decoupler.

4.4. Conclusions

A cellulose acetate-based decoupler was developed that is able to operate in both normal and reverse polarity separation fields with a variety of analytes. Additionally, it can function up to 1500 V/cm in reverse polarity, which allows the possibility of coupling very fast, high field strength microfluidic separations with electrochemical detection. Further optimization still must be done to reduce the amount of band broadening or analyte loss following the decoupler. Band broadening can be reduced by increasing the separation field strength, thereby increasing the velocity of the electroosmotic flow and decreasing the amount of time for analytes to diffuse after passing the decoupler. Other membrane materials will also be tested including Nafion and hydrogels to determine the mechanism and mitigate analyte loss.

4.5. References

1. Lacher, N.A.; Garrison, K.E.; Martin, R.S.; Lunte, S.M. Microchip Capillary Electrophoresis/ Electrochemistry. *Electrophoresis*. **2001**, *22*, 2526-36.

2. Lacher, N.A.; Lunte, S.M.; Martin, R.S. Development of a Microfabricated Palladium Decoupler/Electrochemical Detector for Microchip Capillary Electrophoresis Using a Hybrid Glass/Poly(Dimethylsiloxane) Device. *Anal Chem*. **2004**, *76*, 2482-91.

3. Bowen, A.L.; Scott Martin, R. Integration of Serpentine Channels for Microchip Electrophoresis with a Palladium Decoupler and Electrochemical Detection. *Electrophoresis*. **2009**, *30*, 3347-54.

4. Vickers, J.A.; Henry, C.S. Simplified Current Decoupler for Microchip Capillary Electrophoresis with Electrochemical and Pulsed Amperometric Detection. *Electrophoresis*. **2005**, *26*, 4641-7.

5. Chen, D.-C.; Hsu, F.-L.; Zhan, D.-Z.; Chen, C.-H. Palladium Film Decoupler for Amperometric Detection in Electrophoresis Chips. *Anal Chem*. **2001**, *73*, 758-62.

6. Gunasekara, D.B.; Wijesinghe, M.B.; Saylor, R.A.; Lunte, S.M. Fundamental Principles and Strategies for Microchip Electrophoresis with Amperometric Detection. In: Arrigan DWM, editor. Electrochemical Strategies in Detection Science. Cambridge, UK: The Royal Society of Chemistry; 2014.

7. Rossier, J.S.; Ferrigno, R.; Girault, H.H. Electrophoresis with Electrochemical Detection in a Polymer Microdevice. *J Electroanal Chem*. **2000**, *492*, 15-22.

8. Osbourn, D.M.; Lunte, C.E. On-Column Electrochemical Detection for Microchip Capillary Electrophoresis. *Anal Chem*. **2003**, *75*, 2710-4.

9. Allcock, G.; Dyer, P.E.; Elliner, G.; Snelling, H.V. Experimental Observations and Analysis of CO_2 Laser-Induced Microcracking of Glass. *J Appl Phys*. **1995**, *78*, 7295-303.

10. Chung, C.K.; Sung, Y.C.; Huang, G.R.; Hsiao, E.J.; Lin, W.H.; Lin, S.L. Crackless Linear through-Wafer Etching of Pyrex Glass Using liquid-Assisted CO_2 Laser Processing. *Appl Phys A*. **2008**, *94*, 927-32.

11. Chung, C.K.; Liao, M.W.; Lin, S.L. Effect of Nonionic Surfactant Addition on Pyrex Glass Ablation Using Water-Assisted CO_2 Laser Processing. *Appl Phys A*. **2010**, *99*, 285-90.

12. Meng-Hua, Y.; Ji-Yen, C.; Cheng-Wey, W.; Yung-Chuan, C.; Tai-Horng, Y. Rapid Cell-Patterning and Microfluidic Chip Fabrication by Crack-Free CO_2 Laser Ablation on Glass. *J Micromech Microeng*. **2006**, *16*, 1143-53.

Chapter 5:

Development of a Method to Monitor Oxidative Stress in RAW 264.7 Macrophage Cells

This work has been published in the following journal publication:

Richard P. S. de Campos, **Joseph M. Siegel**, Claudia G. Fresta, Giuseppe Caruso, José A. F. da Silva, Susan M. Lunte. "Indirect detection of superoxide in RAW 264.7 macrophage cells using microchip electrophoresis coupled to laser-induced fluorescence." Analytical and Bioanalytical Chemistry. 2015, 407, 7003-7012.

5.1. Introduction

In order to better understand the toxicity of excess superoxide ($O_2^{\bullet-}$) production, several strategies to measure this molecule in cells have been reported in the literature [1-3]. Experimentally, high concentrations of intracellular $O_2^{\bullet-}$ can be achieved in immune cells by incubating with a stimulant such as phorbol 12-myristate 13-acetate (PMA) [3-5]. PMA promotes the phosphorylation of NADPH oxidase by inducing the activation of protein kinase C and produces $O_2^{\bullet-}$ in the process [3]:

$$2NADPH + 2O_2 \rightarrow 2NADP^+ + 2O_2^{\bullet-} + 2H^+$$

Other methods of $O_2^{\bullet-}$ stimulation include the use of zymosan [1, 6, 7] and succinate [8].

The most common probes used for $O_2^{\bullet-}$ detection are based on hydroethidine (HE) and its derivatives. MitoSOX red, or MitoHE, is a commercially available mitochondrial targeted hydroethidine derivative that has been widely used [9-11]. As pointed out by Zielonka *et al*., it is important to have a separation step prior to detection of the fluorescent product in order to eliminate interferences from other HE derivatives [12]. The reaction of HE with $O_2^{\bullet-}$ leads to a specific hydroxylated product (2-OH-E^+, λ_{ex}/ λ_{em} = 475/580 nm), but other hydride acceptor molecules present in biological matrices can induce the formation of a second, non-specific product, ethidium (E^+, λ_{ex}/ λ_{em} = 495/590 nm) [13, 14]. Analogously, the same behavior can be observed with MitoHE [12]. Therefore, it is necessary to separate the two fluorescent products to determine the signal obtained due to the reaction with $O_2^{\bullet-}$ from that obtained from oxidizing interferences.

Strategies to separate the $O_2^{\bullet-}$-specific product from the non-specific ones generated by MitoHE and HE derivatives reactions in biological samples have been developed using high-performance liquid chromatography (HPLC) [15, 16] and capillary electrophoresis (CE) [8, 17].

For instance, Xu *et al*. developed a method for the determination of $O_2^{\bullet-}$ in single skeletal muscle fibers by individually lysing triphenylphosphonium hydroethidine treated cells in a nanowell [17]. Injection and separation were subsequently performed using micellar electrokinetic capillary chromatography with laser-induced fluorescence detection (MEKC-LIF) [17]. Meany *et al*. also used MEKC-LIF to separate and detect HE products in isolated mitochondria following stimulation with succinate [8].

This chapter focuses on the development of a microchip electrophoresis method with LIF detection for the measurement of $O_2^{\bullet-}$ production in native (untreated) and PMA stimulated RAW 264.7 macrophage cells using MitoHE as the fluorescent probe. Differences in intracellular $O_2^{\bullet-}$ generation due to the presence of the cytosolic SOD inhibitor, diethyldithiocarbamate (DDC), and mitochondrial SOD inhibitor, 2-methoxyestradiol (2-ME) prior to PMA stimulation versus non-stimulated samples (control) are measured with this technique. Finally, changes in intracellular $O_2^{\bullet-}$ concentration due to incubation of RAW 264.7 cells with a $O_2^{\bullet-}$ donor, 3-morpholino-sydnonimine (SIN-1) were also investigated.

5.2. Materials and Methods

5.2.1. Materials and Reagents

All chemicals used in this work were of analytical grade and purchased from Sigma (St. Louis, MO, USA), unless specified otherwise. MitoSOX Red (MitoHE) was purchased from Life Technologies (Carlsbad, CA, USA). Potassium nitrosodisulfonate was purchased as a 50-75% pure powder (Sigma). Dulbecco's Modified Eagle's Medium (DMEM), fetal bovine serum (FBS), L-glutamine, penicillin, and streptomycin were obtained from ATCC (Manassas, VA, USA). Polydimethylsiloxane (PDMS) microdevices were prepared from the Sylgard 184 Elastomer Kit (Ellsworth Adhesives, Germantown, WI, USA).

The pH values of solutions were adjusted using 1.5 M sodium hydroxide and 0.1 M hydrochloric acid solutions as needed.

5.2.2. Solution Preparation

5.2.2.1. MitoHE Stock Solution Preparation

MitoHE stock solution was prepared as specified by the manufacturer. Briefly, 13 µL of dimethyl sulfoxide (DMSO) were added to an individual vial containing 50 µg of probe. The vial was vortexed for 15 seconds and then centrifuged for 2 minutes at 7000 rpm, leading to a 5 mM MitoHE stock solution. All preparation and handling steps using MitoHE were performed in the dark. All MitoHE stock solutions were used in the experiments immediately after preparation.

5.2.2.2. 2-OH-MitoE$^+$ Standard Preparation

2-OH-MitoE$^+$ standards were prepared by the reaction of MitoHE with nitrosodisulfonate anion (NDS) as follows. A 1 mM NDS solution was prepared by dissolving potassium nitrosodisulfonate (Fremy's salt) in a 50 mM borate solution (pH = 9.2) containing 1 mM diethylene triamine pentaacetic acid (DTPA). The NDS solution used was always fresh, prior to each standard preparation.

The reaction was conducted by mixing the following reagents: 200 µL of 100 mM borate buffer (pH = 9.2), 40 µL of 1 mM DTPA, 8 µL of 5 mM MitoHE stock solution, 72 µL of nanopure water and 80 µL of 1 mM NDS solution. The reaction was allowed to proceed for 2 hours in the dark at room temperature. Afterwards, the reaction media containing 2-OH-MitoE$^+$ standard was simply diluted in ME run buffer and analyzed with the ME-LIF system.

5.2.2.3. Xanthine/Xanthine Oxidase Reaction

The xanthine/xanthine oxidase reaction (XA/XO) is well established method for *in situ* $O_2^{\bullet -}$ production [18, 19]. MitoHE was added to solution containing XA and XO in order to

produce 2-OH-MitoE$^+$. The reaction was performed in two different vials. The first vial contained 375 µL of 1 mM xanthine (XA), 7 µL of 0.5 U mL^{-1} xanthine oxidase (XO), 6 µL of 5 mM MitoHE stock solution and 612 µL of XO buffer. XO buffer consisted of 0.1 mM ethylenediaminetetraacetic acid in 50 mM phosphate buffer (pH = 7.4). The second vial was prepared with the same amount of XA, XO, and MitoHE with the addition of 50 µL of 5800 U mL^{-1} superoxide dismutase (SOD) and 562 µL of XO buffer. The contents of both vials were allowed to react for 3 hours in the dark at room temperature and then the contents of each vial were diluted in electrophoresis run buffer prior to analysis.

5.2.3. Cell Culture and Stimulation Protocol

RAW 264.7 macrophages cells obtained from American Type Culture Collection (ATCC® TIB-71™, Manassas, VA, USA) were cultured in DMEM supplemented with 10% (v/v) FBS, L-glutamine (2 mM), penicillin (0.3 mg mL^{-1}), and streptomycin (0.3 mg mL^{-1}). The cells were maintained in a humidified environment at 37 °C and 5% CO_2 and cultured in 25 cm^2 polystyrene culture flasks (Fisher Scientific, Waltham, MA, USA). Cells were passaged every 2 days to avoid overgrowth. Cells were grown until they reached approximately 50-60% confluence and then stimulated.

Stimulation of $O_2^{\bullet-}$ production in the macrophage cells was accomplished using PMA. PMA was added to healthy cells in a 25 cm^2 cell culture flask to obtain a final PMA concentration of 3.24 nM and then incubated for 24 hrs in a humidified environment at 37 °C and 5% CO_2. Untreated (native) RAW 264.7 cells from the same population were incubated under identical conditions and used as a control for each stimulation experiment. In order to increase $O_2^{\bullet-}$ detection, cells were treated with 1 mM DDC and 50 µM 2-ME, 1 h prior to PMA stimulation.

For SIN-1 incubation studies, healthy cells in a 25 cm^2 cell culture flask were first treated with 1 mM DDC for 1 hour in the same environment mentioned above and then incubated with 50 µM SIN-1 solution under the same conditions for 1 hour. An experiment without DDC addition was also performed. Native cells (not treated with SIN-1) from the same population were also incubated at the same conditions and used as a control.

5.2.4. Bulk Cell Lysate Preparation

Following stimulation or SIN-1 incubation, RAW 264.7 cells in their original medium were labeled with MitoHE. The stock dye solution was prepared in DMSO. A 6 µL aliquot of 5 mM MitoHE solution was added to each culture flask and allowed to react for 10 min in the dark inside the incubator. Then, the dye loaded cells were harvested using a cell scraper. The cell suspension was transferred to a 15 mL centrifuge tube and centrifuged at 1137 g for about 3 min. Before centrifugation, 100 µL of the cell solution were taken out for cell counting. The supernatant medium was then removed, leaving only the cell pellet, which was washed twice with 1 M phosphate buffered saline at pH 7.4. Next the cell pellet was lysed in 100 µl of lysing buffer (10 mM borate buffer, 40 mM Tris HCl, and 0.5% Triton X-100 at pH 9.2) and transferred into 500 µL vials. 25 µL of 10 mg mL^{-1} Proteinase K solution were added to the lysate followed by incubation for 45 min at 37 ºC. Then 13.5 µL of 10 mg mL^{-1} of DNase I were loaded into the vials for an additional 20 min. In order to remove any turbidity, the lysate solution was sonicated for 30 s and then centrifuged for 2 min at 7000 rpm. Lastly, the lysate solution was diluted 10-fold and loaded into the sample reservoir of the microchip for ME-LIF analysis.

5.2.5. Cell Viability

Cell viability was measured using the Trypan blue exclusion assay and a hemocytometer cell count (C-Chip disposable hemocytometer, Bulldog Bio, Inc., Portsmouth, NH, USA). The

RAW 264.7 cell suspension was diluted using 1:1 to 1:3 ratios (based on cell density) with a 0.4% trypan blue solution. The number of viable cells and cell density was determined using a 4 mm^2 total area hemocytometer. Native RAW cells typically had densities of about 6 million cells in a 25 cm^2 flask prior to passaging.

5.2.6. Microchip Fabrication and Instrumental Setup

The fabrication of the PDMS/glass microfluidic has been previously described by our group [20]. First, a SU-8 10 photoresist (Silicon, Inc., Boise, ID, USA) mold containing the microdevice design was fabricated using soft photolithography. Second, the PDMS substrate was prepared by mixing its pre-polymer and cross-linking agent in a 10:1 w/w ratio. The mixture was degassed under vacuum and poured over the SU-8 mold and cured in oven at 70 ºC for 3 hours. The cured PDMS device was peeled off the mold and access reservoirs were made using a 3 mm biopsy punch (Harris Uni-core, Ted Pella, Redding, CA, USA). Lastly, the PDMS substrate was reversibly sealed against flat borosilicate glass (Precision Glass and Optics, Santa Ana, CA, USA) to form the final microdevice with enclosed microchannels in which the electrophoresis separations were performed. The present work used a simple "T" microchip design with a 5 cm separation channel and 0.75 cm side arms for all experiments. The microchannel depth and width dimensions were 15 µm and 45 µm, respectively.

A dual channel high voltage power supply (HV Rack, Ultravolt Inc., Ronkonkoma, NY, USA) controlled by a homemade Labview program (National Instruments, Austin, TX, USA) was used in all experiments. Sample was introduced to the separation channel using a 1 s gated injection. Both injection and separation were performed using a high voltage power supply in positive polarity mode. For all separations, +2400 V and +2200 V were applied to the background electrolyte (BGE) and sample reservoir, respectively.

The PDMS/glass hybrid microchip was placed in an inverted microscope (Eclipse Ti-U, Nikon Instruments Inc., Melville, NY, USA) for fluorescence detection. A 488 nm diode laser (Spectra-Physics, Irvine, CA, USA) was used as the excitation source. Light was collected using a photomultiplier tube (Hamamatsu Corporation, Bridgewater, NJ, USA). The signal was amplified using a SR570 low noise current preamplifier at 1 μAV^{-1} (Stanford Research Systems, Sunnyvale, CA). Data acquisition and analysis were carried out using a D/A converter (National Instruments) and a custom Labview software program.

Prior to analysis, each microdevice was flushed with 0.1 M NaOH for 5 min, followed by a 10 min flush with electrophoresis BGE. The BGE used in all ME-LIF experiments consisted of 10 mM borate (pH = 9.2) and 3.5 mM sodium dodecyl sulfate (SDS). Cleaning runs were performed between each bulk cell lysate sample analysis by flushing the system for 30 s with electrophoresis BGE only. This setup made it possible to perform several consecutive runs for each sample, and it was also possible to easily realign the laser when needed.

5.3. Results and Discussion

One primary focus of our group has been developing methods using spectrometric and electrochemical detection to study biological reactive species, such as nitric oxide (NO) and peroxynitrite ($ONOO^-$), *in vitro*. Due to the complexity of biological samples, a separation method is needed to isolate the analytes of interest from interferences. In the case of $O_2^{\bullet-}$, the combination of a separation method with a fluorescent probe that generates a unique product with $O_2^{\bullet-}$ can ensure that a given signal is due only to $O_2^{\bullet-}$ production, and not other ROS, such as hydrogen peroxide. Therefore, the present study was focused on the development of a ME-LIF method that could be used for the detection of $O_2^{\bullet-}$ produced by native and stimulated RAW 264.7 macrophages cells.

The fluorescent probe used, Mito-HE, has been reported to react with intracellular $O_2^{\bullet -}$ to produce a 2-hydroxylated product, 2-OH-MitoE^+. Once inside a cell, MitoSOX can also react with other reactive species, such as $ONOO^-$, hydroxyl radical, and hydrogen peroxide, but these reactions generate a non-hydroxylated product, MitoE^+, that can be electrophoretically separated from 2-OH-MitoE^+ [12, 14, 21]. Therefore, under biological conditions, only $O_2^{\bullet -}$ will lead to the formation of 2-OH-MitoE^+, which gives a fluorescent signal useful for monitoring changes in its concentration (Figure 5.1).

5.3.1. Results from Standard Solutions

Although the reaction of $O_2^{\bullet -}$ and MitoHE inside RAW 264.7 cells generates a specific product, an alternative approach to obtain 2-OH-MitoE^+ outside the biological environment has been reported [22]. This involves the reaction of the fluorescent probe with nitrosodisulfonate anion (NDS). The previously discussed method was used to generate 2-OH-MitoE^+ standards and the calibration curve [21]. The reaction has a 1:2 stoichiometry and should give, under optimal conditions, a total conversion of the fluorescent probe to 2-OH-MitoE^+.

Following the optimization of the reaction and subsequent analysis of the product by ME-LIF, a calibration curve between 50 and 500 nM was obtained for 2-OH-MitoE^+ with a R^2 value of 0.97 (Figure 5.2). Under the reaction conditions specified in the experimental section for preparation of the standard, only one peak was observed in the electropherogram. Electropherograms containing two peaks were obtained when the reaction was performed using a limiting amount of NDS. In this case, the excess unreacted probe could autoxidize into the non-specific product MitoE^+, which was detected as a less intense peak in the electropherogram (Figure 5.3).

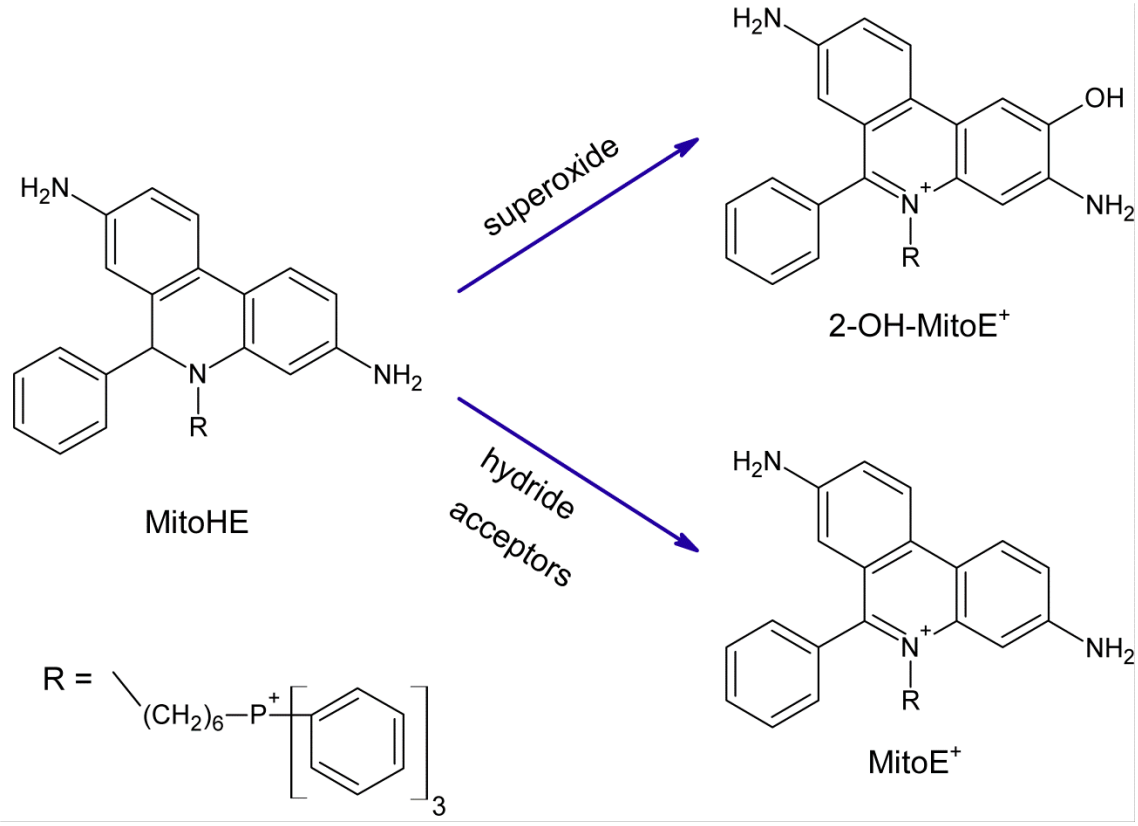

Figure 5.1. Reaction of MitoHE with $O_2^{\bullet-}$ and other ROS (adapted by permission from Macmillan Publishers Ltd: Nature Protocols, 2008.).

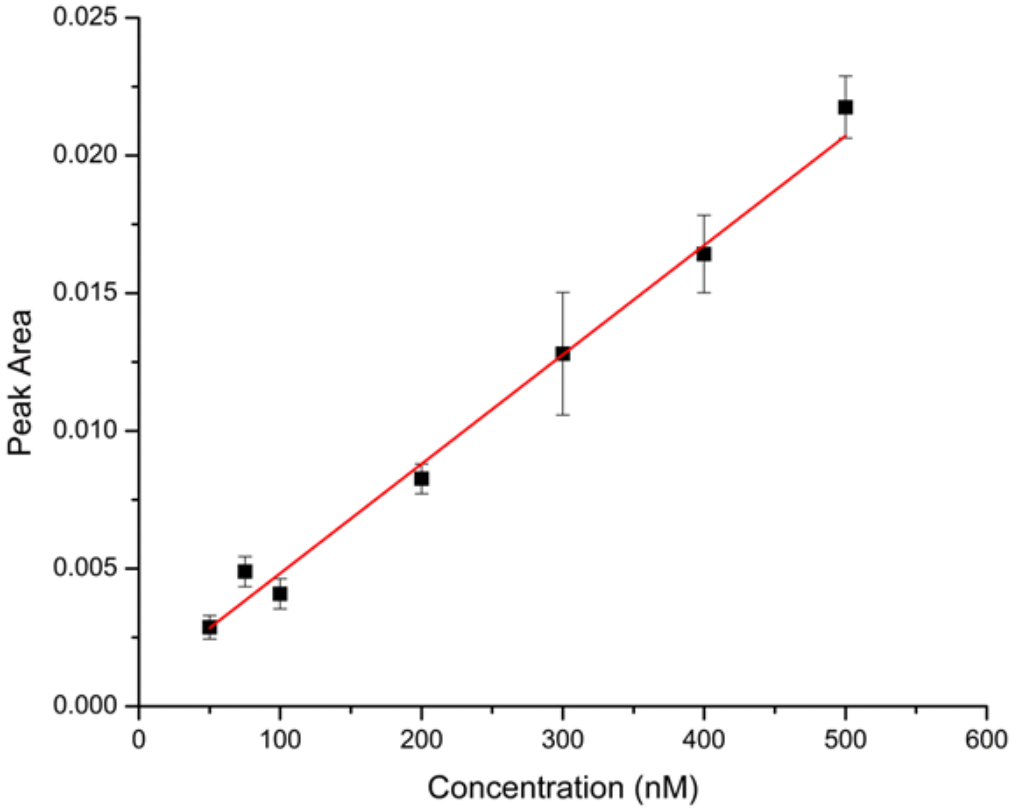

Figure 5.2. Calibration curve for 2-OH-MitoE^{+} obtained from the reaction between MitoHE and NDS. $R^2 = 0.97$. $y=8.6\times10^{-4} + (4.0\times10^{-5})\,x$

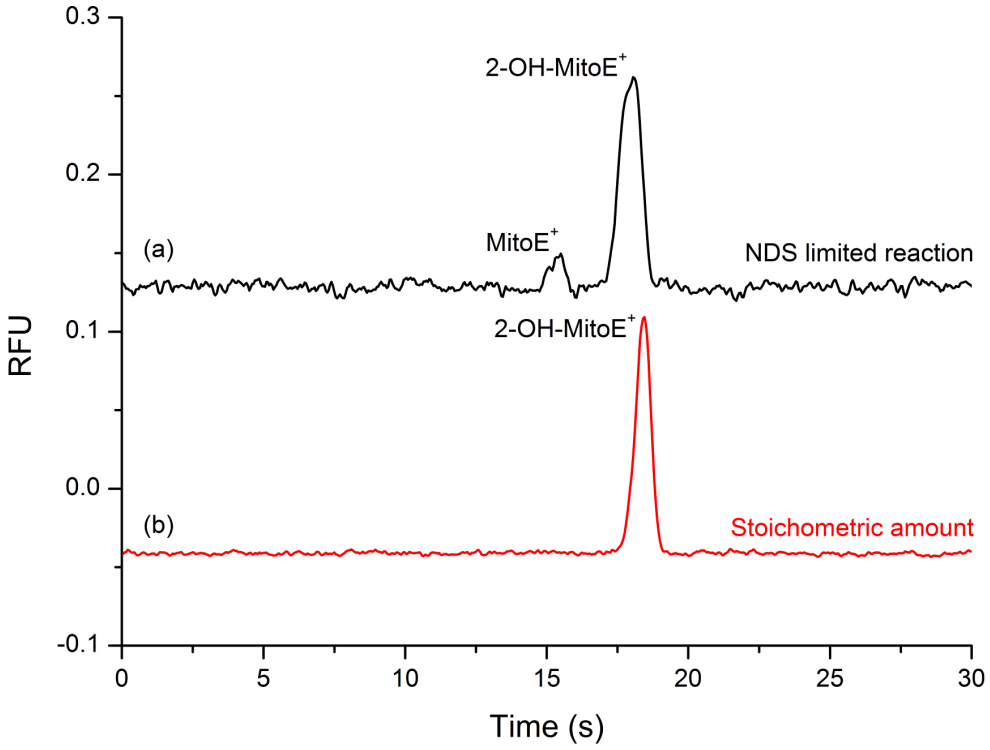

Figure 5.3. MitoHE reaction with NDS prepared using (a) 3.6 mg of potassium NDS (NDS limited reaction) and (b) using 4.0 mg of potassium NDS (stoichiometric amount) from a 67.5% pure Fremy's salt. Laser alignment at 2.3 cm

5.3.2. Peak Identification using XA/XO Reaction

The identity of the major peak at 18.1 s in standard runs (Figure 5.3) was assigned to 2-OH-MitoE$^+$ based on Fremy's salt reaction, sample electrophoretic mobility, and also by comparison with previously published work [8]. To further verify the identity, the xanthine/xanthine oxidase (XA/XO) system was employed to generate $O_2^{\bullet-}$ *in situ* which then reacted with MitoHE. The conversion of XA to uric acid is catalyzed by XO and the generation of $O_2^{\bullet-}$ occurs as part of the regeneration of XO into its oxidizing form. The amount of $O_2^{\bullet-}$ produced is dependent on the concentration of XA, XO, and oxygen present in the medium [18]. By making the XA/XO reaction media with and without the presence of SOD, we were able to account for the specificity of the reaction between $O_2^{\bullet-}$ and MitoHE as well as provide a means for peak identification.

These reactions were allowed to proceed for 3 hours in the dark in open vials to ensure access to atmospheric oxygen. The reaction products were then analyzed by the ME-LIF system. The results are shown in Figure 5.4. Figure 5.4a represents the XA/XO reaction media without SOD. In this case, two fluorescent products were formed mainly due to the reaction of MitoHE with $O_2^{\bullet-}$ and hydrogen peroxide. Electropherogram (b) in Figure 5.4 shows the data for the reaction media containing SOD. In this case, SOD scavenges $O_2^{\bullet-}$ from the system and the second peak disappears. Therefore, it is possible to conclude that the peak at 21 seconds is indeed due to 2-OH-MitoE$^+$ and is formed from the reaction of MitoHE and $O_2^{\bullet-}$. The slight difference in the migration time of the 2-OH-MitoE$^+$ found in these experiments compared to the standards can be attributed to the use of a different PDMS microchip and small variations in the laser alignment on the separation channel. Moreover, the migration order obtained in this

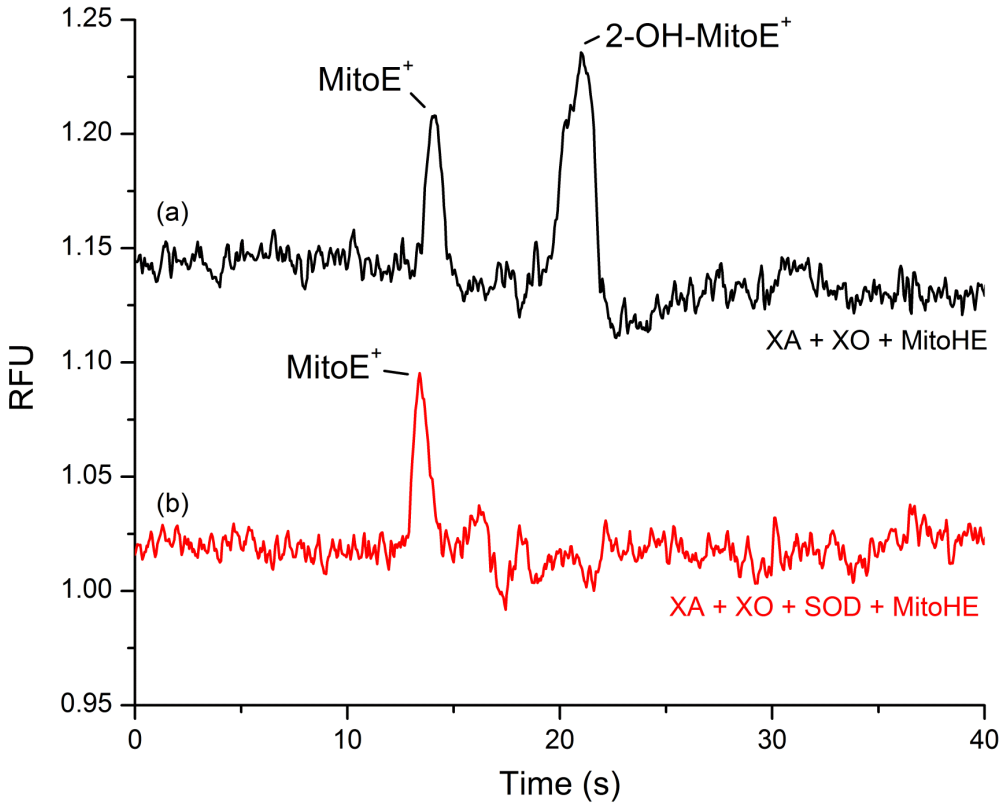

Figure 5.4. Electropherograms for the injection of XA/XO reaction media + MitoHE with and without SOD.

experiment was comparable to that obtained during the analysis of the previously prepared standards, indicating that the initial peak identifications were correct.

5.3.3. Bulk Cell Analysis of SIN-1 Incubated RAW 264.7 Macrophages

Before monitoring $O_2^{\bullet-}$ production in RAW 264.7 cells, it was crucial to ensure that the method will generate a measurable and reproducible signal in complex matrices such as cell lysates. Several factors needed to be taken into account that might influence the ability to detect the target analyte by ME-LIF including the experimental setup, the stimulation protocol used, the presence of SOD, and the reactions between the target analyte and biomolecules present in the biological media.

In order to monitor 2-OH-MitoE$^+$ signal in the presence of the cell lysate using the proposed experimental setup, we first decided to study the electropherograms obtained for RAW 264.7 cells incubated with SIN-1, a well-known $ONOO^-$ donor, and the fluorescent probe MitoHE before lysis. SIN-1 decomposition to SIN-1C is triggered by the addition of NaOH, producing both $O_2^{\bullet-}$ and NO (Figure 5.5) [23, 24]. These two molecules can then react with each other to form $ONOO^-$. It is possible to monitor the production of $O_2^{\bullet-}$ by SIN-1 in vitro by adding MitoHE to the mixture and monitoring the increase in the 2-OH-MitoE$^+$ peak as the $O_2^{\bullet-}$ indicator. Figure 5.6 shows the use of ME-LIF to continuously monitor $O_2^{\bullet-}$ production by the SIN-1 reaction in vitro.

From these results, it is possible to observe the increase in 2-OH-MitoE$^+$ concentration over time due to continuous $O_2^{\bullet-}$ production. The concentration keeps increasing until about 1750 s, after which the signal intensity starts to drop, eventually reaching a constant plateau. A possible explanation for this observation is that $O_2^{\bullet-}$ levels keep increasing until there is an

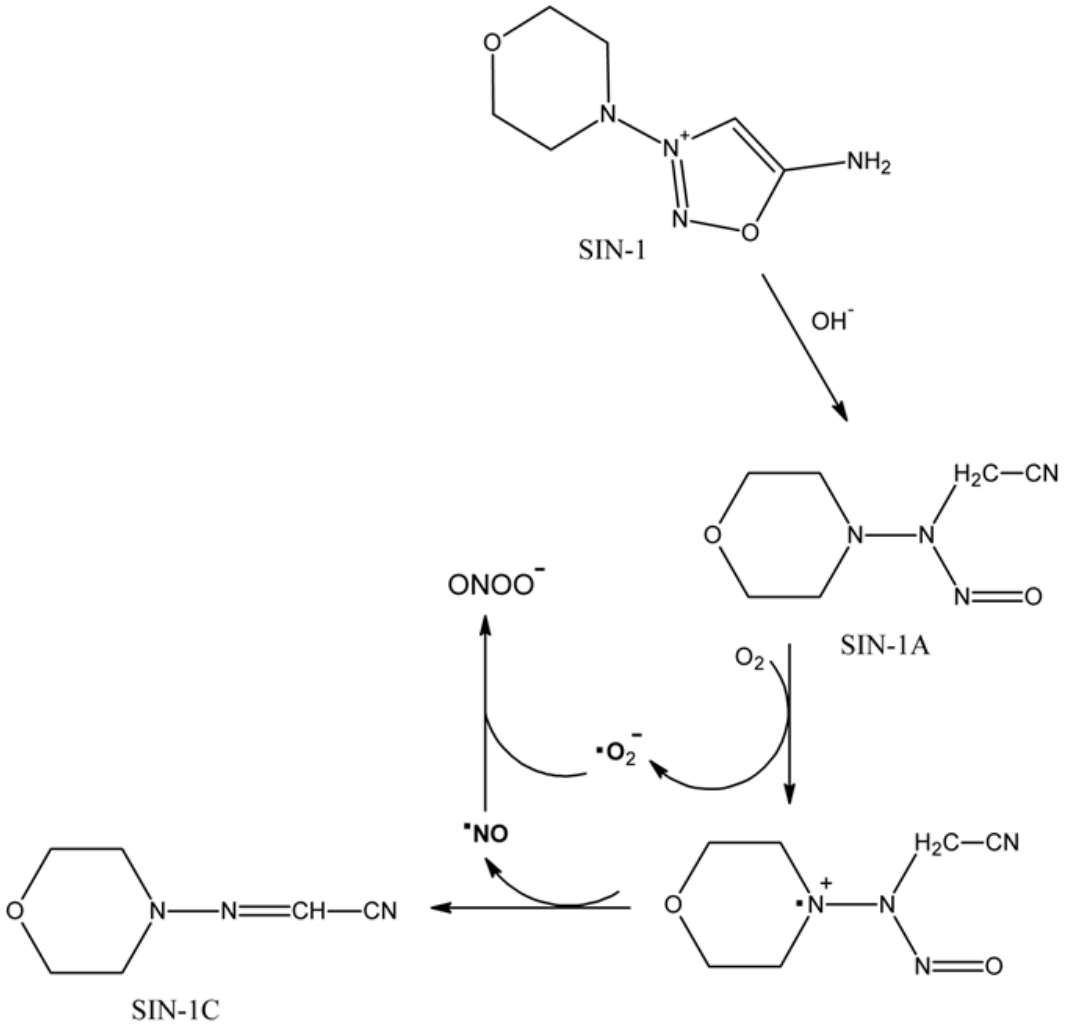

Figure 5.5. SIN-1 decomposition in presence of OH^-. The reaction generates NO and $O_2^{\bullet -}$ that will react to form $ONOO^-$. Once inside a cell, esterases can also trigger a similar reaction pathway, producing SIN-1C and the byproducts NO, $O_2^{\bullet -}$, and $ONOO^-$. Reprinted with permission from Hulvey, M.K.; Frankenfeld, C.N.; Lunte, S.M. *Anal Chem*. **2010**, *82*, 1608-11. Copyright 2010 American Chemical Society.

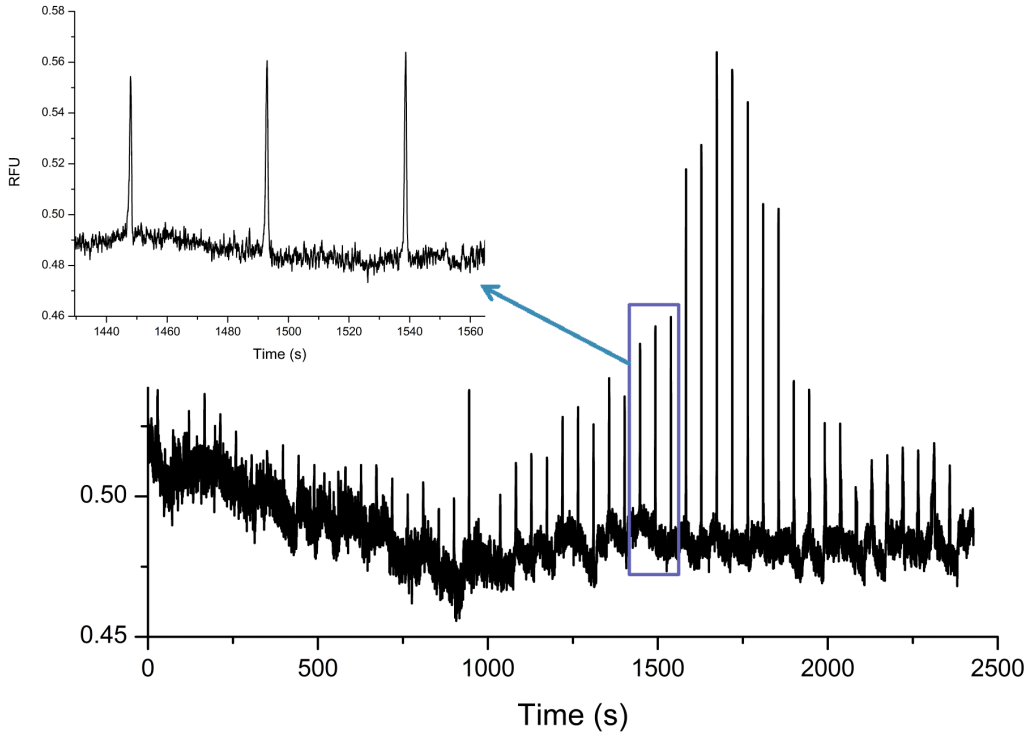

Figure 5.6. Monitoring of $O_2^{\bullet-}$ release during SIN-1 conversion to SIN-1C as a function of time.

excess of NO, which is also produced in the reaction. The presence of NO will cause the formation of $ONOO^-$ and the amount of free $O_2^{\bullet-}$ will therefore decrease as $ONOO^-$ is formed. This hypothesis will be further investigated by monitoring $ONOO^-$ concentration by using $ONOO^-$-specific fluorescent probes such as HK-Green 3 and HK-Green 4 [25, 26]. For the time being, it is important to state that SIN-1 decomposition and $O_2^{\bullet-}$ production can be monitored using MitoHE.

To reproduce this reaction *in vivo*, RAW 264.7 cells were incubated with 50 µM SIN-1 for 1 hour with subsequent addition of 7 µM MitoHE and incubation for an additional 10 minutes. Once inside the cellular environment, esterases hydrolyze SIN-1 and trigger its conversion into SIN-1C, generating $O_2^{\bullet-}$ that will then react with the MitoHE. In the initial experiments, the electropherogram of the cell lysate analysis consisted of a constant baseline, with no detectable peak for 2-OH-MitoE^+, for both native (Figure 5.7a) and SIN-1 incubated cells (Figure 5.7b). It was surmised that this was due to the presence of SOD in the cell cytosol. SOD reacts faster with $O_2^{\bullet-}$ than MitoHE causing any native or induced $O_2^{\bullet-}$ to be immediately converted to hydrogen peroxide and molecular hydrogen. To circumvent this problem, RAW 264.7 cells were first treated with DDC, an inhibitor for cytosolic SOD prior to the introduction of the SIN-1. Under these conditions, $O_2^{\bullet-}$ was detected in the electropherogram as seen in Figure 5.7c and d.

The peaks in the electropherograms for 2-OH-MitoE^+ were integrated and the areas obtained were 0.015 ± 0.001 and 0.055 ± 0.007, for SIN-1 incubated and native RAW 264.7, respectively. To estimate the 2-OH-MitoE^+ concentration in a single cell, 2-OH-MitoE^+ concentration for each electropherogram was calculated based on four parameters: the external

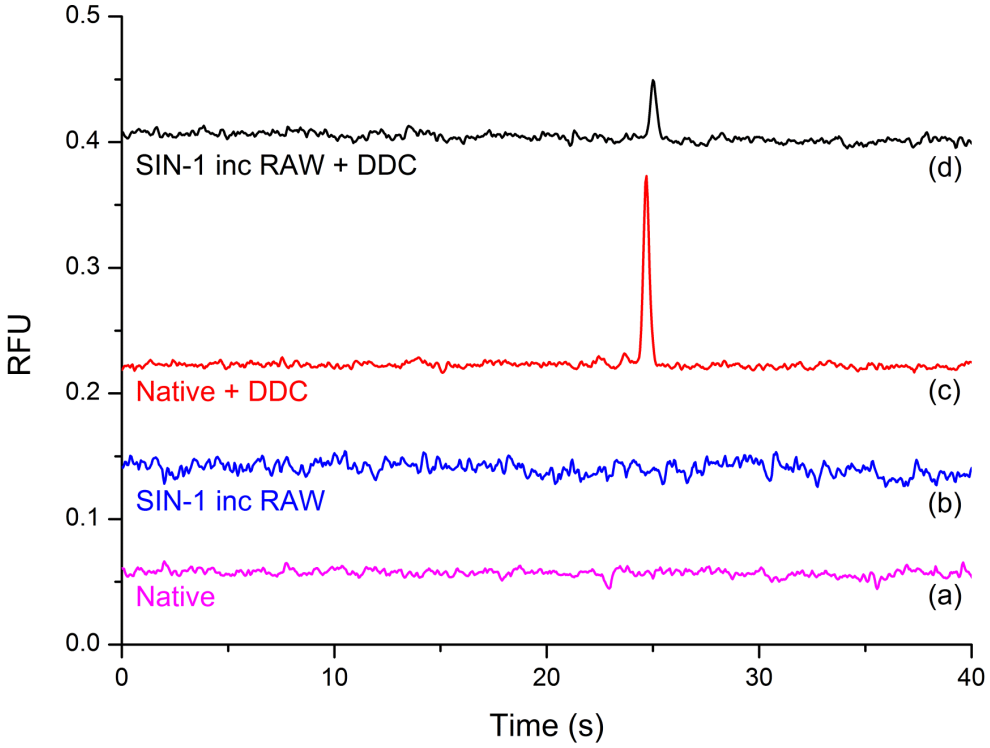

Figure 5.7. Electropherogram obtained for native and SIN-1 incubated RAW 264.7 macrophage cells. (a) Native RAW 264.7 macrophage cells; (b) SIN-1 incubated RAW 264.7 macrophage cells; (c) Native RAW 264.7 macrophage cells in presence of DDC; (d) SIN-1 incubated RAW 264.7 macrophage cells in presence of DDC. Detection point = 4.5 cm from T intersection

calibration curve, the volume of cell lysis buffer, the estimated volume of an individual macrophage cell (0.05 pL) [27], and the number of cells present in each cell culture flask. Therefore, each SIN-1 incubated cell produced, on average, 0.061 ± 0.006 fmol (0.12 ± 0.01 mM) of 2-OH-MitoE^+, while native cells produced 0.23 ± 0.03 fmol (0.45 ± 0.05 mM) of 2-OH-MitoE^+ (both treated with DDC). The results indicate that after incubation with SIN-1 the detected amount of $O_2^{\bullet-}$-specific fluorescent probe is less than those detected in native (not treated with SIN-1) cells inhibited with DDC. Once again, the hypothesis built from observations to explain this behavior is that the reaction between NO and $O_2^{\bullet-}$ will be favored over the reaction between $O_2^{\bullet-}$ and MitoHE. This is primarily due to the faster reaction kinetics of the NO/$O_2^{\bullet-}$ reaction. Notably, the experiment demonstrated the importance of using a SOD inhibitor to minimize the loss of $O_2^{\bullet-}$ through biological pathways. Moreover, the experiment also proved that the system can detect the $O_2^{\bullet-}$ signal generated in such a complex matrix.

5.3.4. Indirect $O_2^{\bullet-}$ Detection in PMA Stimulated RAW 264.7 Macrophage Cells

Chronic and acute stimulation protocols were both evaluated for the production of $O_2^{\bullet-}$. Bulk cell lysates were analyzed by ME-LIF. Experiments were performed without the addition of SOD inhibitors, proteinase K, or DNase I and the cell pellets were lysed using electrophoresis BGE, containing SDS. We obtained fluorescent images for stimulated and control cells (Figure 5.8a and b) and an electropherogram with a low intensity 2-OH-MitoE^+ peak for the stimulated cells (Figure 5.8c).

Although the fluorescence signal for stimulated cells can be clearly distinguished from the control cell sample, the peak obtained from the cell lysate exhibited very low intensity and it

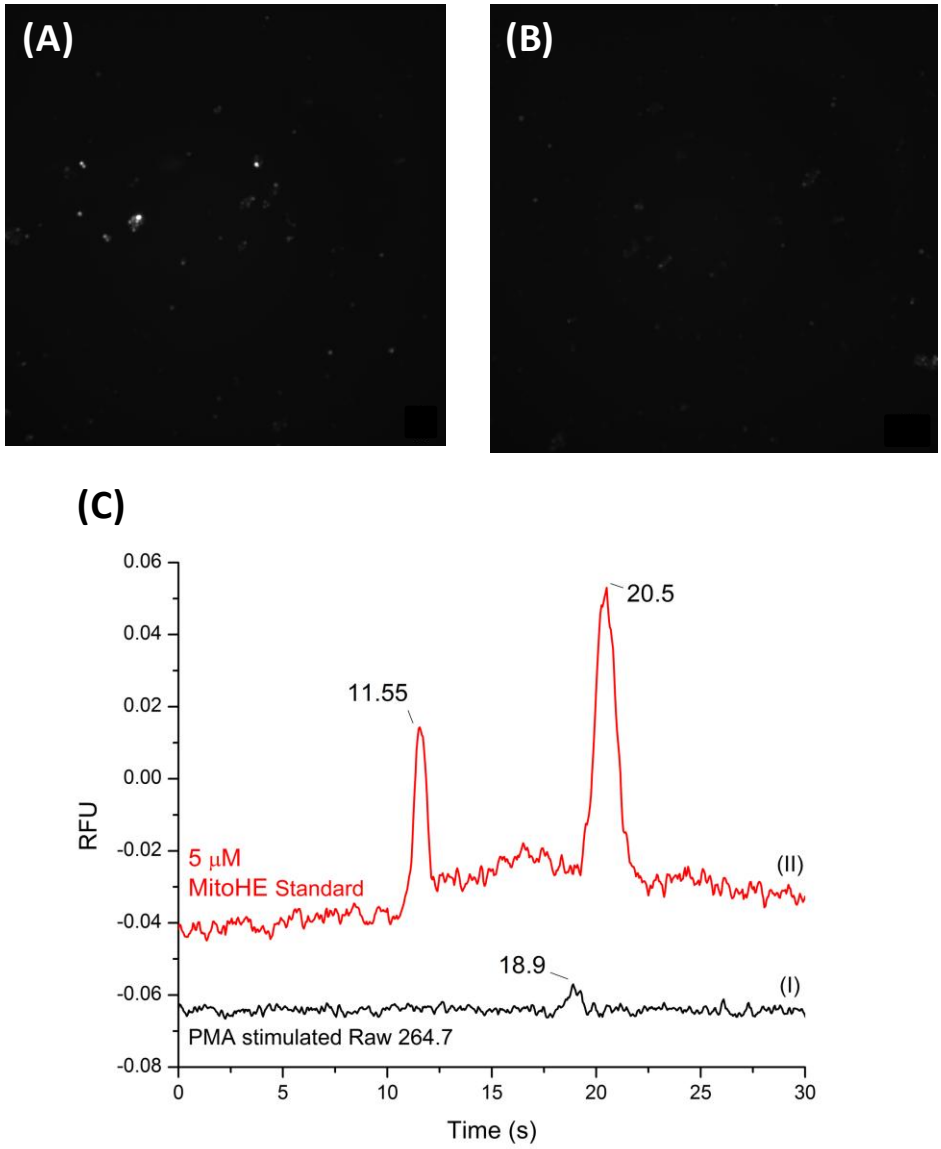

Figure 5.8. Stimulation optimization. RAW 264.7 macrophage cells were stimulated with 2 ng/mL PMA for 12 hours and then incubated with 6 uL of 5mM MitoHE for 10 minutes. (a) Fluorescence image of stimulated cells and (b) fluorescence image of native/control cells after stimulation protocol. (c) Electropherogram for (I) stimulated RAW 264.7 in comparison to (II) standard containing $MitoE^+$ and 2-OH-$MitoE^+$. Detection point = 2.5 cm from T intersection.

is evident from Figure 5.8a that not all cells will respond equally to the stimulation. Therefore in order to increase the amount of $O_2^{\bullet-}$ produced by cells, the incubation time was increased from 12 h to 24 h, without compromising cell viability.

Sample preparation was also a determining factor for the signal intensity. Previously, our group developed a method for the detection of NO in Jurkat cells using ME-LIF. In these studies, a similar sample preparation method was employed using SDS in the lysing buffer and then filtering the lysate with a 3 kDa MWCO PES centrifuge filter [20]. Although this method was satisfactory for measurement of NO with DAF-FM, the use of the centrifuge filter affected the results for $O_2^{\bullet-}$ analysis. This is because 2-OH-MitoE^+ binds to DNA [12], which causes most of target analyte to be stuck to the PES filter during centrifugation. Furthermore, attempts to analyze the lysate sample without centrifugation caused an irreproducible EOF and led to easily clogged channels due to the highly viscous lysate solution obtained when SDS and cell debris are present. Thus, in order to obtain a less viscous lysate capable of being analyzed without a centrifugation step, we decided to switch from a lysing solution containing SDS to a 0.5% Triton X-100 solution in borate buffer.

The migration times for 5 µM 2-OH-MitoE^+ standards in the presence of SDS and Triton X-100, with the detection point at 4.5 cm down from the T intersection of the simple T microchip, were 26.5 and 27.2 s, respectively. The average peak area obtained for standards in SDS was 0.24 with a RSD of 10.2%, while those in Triton X-100 were 0.25 with a RDS of 7.2%. Both results are not statistically different at a 95% confidence level. Thus, a less viscous lysate that can be diluted in electrophoresis BGE prior to injection in the ME-LIF system, without drastically altering the analytes electrophoretic properties, was identified. Additionally, since the interaction between 2-OH-MitoE^+ and DNA will alter the electrophoretic mobility and

fluorescence yield of the 2-OH-MitoE$^+$, proteinase K and DNase I were employed as part of the sample preparation to break up DNA and eliminate this interaction [8].

Another important factor to take into account is the presence of both cytosolic and mitochondrial SOD in the macrophage cells. As discussed previously, SOD can scavenge $O_2^{\bullet-}$ faster than MitoHE, and this will cause a decrease in signal intensity. This way, the system would only provide information regarding excess $O_2^{\bullet-}$ production instead of total $O_2^{\bullet-}$ production. In order to minimize the effects of SOD on the analysis, cytosolic and mitochondrial SOD inhibitors (DDC and 2-ME, respectively) were added to the cells prior to PMA incubation. Thus, the optimized protocol for PMA stimulation was achieved.

The electropherograms obtained for stimulated and native RAW 264.7 cells using the optimized protocol described above are showed in Figure 5.9. 6-Carboxyfluorescein (6-CF) was added to the cell lysate samples as an internal standard to ensure injection reproducibility. The results show the difference between the concentration of 2-OH-MitoE$^+$ due to the reaction with natively present $O_2^{\bullet-}$ and PMA-stimulated produced. The average peak area, cell count, average number of moles of [2-OH-MitoE+] per cell ($n_{[2\text{-OH-MitoE+}]}$), average 2-OH-MitoE$^+$ concentration per cell, and RSD for each electropherogram are detailed in Table 5.1.

These results clearly show that $O_2^{\bullet-}$ production increases following chronic PMA stimulation, represented by the increase in 2-OH-MitoE$^+$ from 0.08 ± 0.01 fmol (0.17 ± 0.03 mM) in native cells to 1.26 ± 0.06 fmol (2.5 ± 0.1 mM) after PMA treatment. The presence of both SOD inhibitors makes it possible to indirectly detect $O_2^{\bullet-}$ even in native cells. Assuming the cell volume as 0.5 pL, the average 2-OH-MitoE$^+$ concentration per cell was 15-fold higher in stimulated cells compared to native/control cells, which corresponds to increased

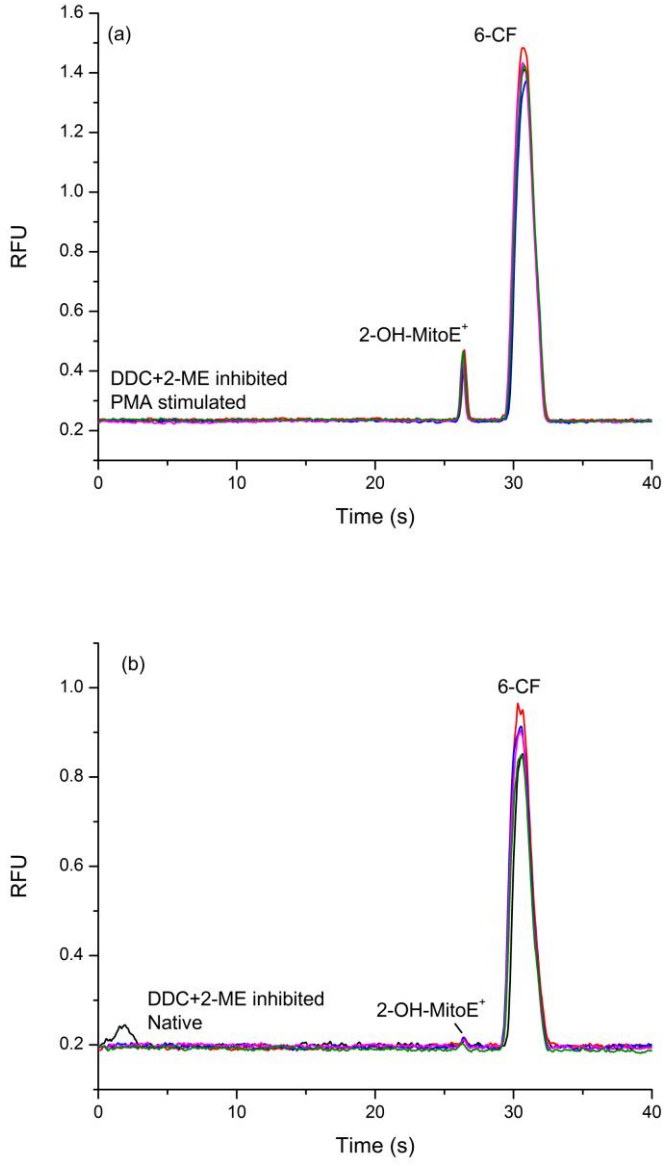

Figure 5.9. Electropherograms for RAW 264.7 lysate samples. Samples were prepared and diluted by a factor of 10 prior to injection. n = 5. (a) Lysate from 24 h PMA stimulated cells in presence of both DDC and 2-ME. (b) Lysate from cells incubated with DDC and 2-ME without PMA stimulation (native/control).

Table 5.1. Results for RAW 264.7 lysate samples: Average peak area, cell count, average number of moles of [2-OH-MitoE+] per cell, average 2-OH-MitoE$^+$ concentration per cell, and RSD.

	PMA stimulated DDC + 2-ME inhibited	**Native DDC + 2-ME inhibited**
Avarage peak area	0.086	0.007
St. Dev	0.004	0.001
RSD	4.62%	15.14%
Cell count (10^6)	2.34	4.00
[2-OH-MitoE$^+$]/cell	9.13 pM	0.36 pM

$O_2^{\bullet-}$ production due to the presence of PMA. Moreover, the results obtained with both inhibitors for the control cells (Figure 5.9b) show that the amount of $O_2^{\bullet-}$ that is naturally produced was not detectable without the presence of the inhibitors due to the scavenging action of SOD.

Finally, the electropherograms shown in Figure 5.9 for stimulated and native RAW 264.7 cell samples generated two peaks; the first is due to 2-OH-MitoE^+ and the second represents 6-CF. However, later it was observed that some samples started to develop a faster migrating and less intense additional peak. This peak was caused by the formation of the non-specific product MitoE^+ (Figure 5.10). Its formation could be due to the reaction of free MitoHE with other oxidizing species present in the sample or due to probe auto-oxidation. The presence of this interfering peak highlights the importance of using a separation method as a method to distinguish the fluorescence signal generated from the $O_2^{\bullet-}$-specific product from the signal generated by the presence of MitoE^+.

5.4. Conclusions

The development and evaluation of a ME-LIF method for the indirect detection of $O_2^{\bullet-}$ in RAW 264.7 macrophage cells using MitoSOX Red as a specific fluorescent probe was reported. The separation step is important to eliminate potential fluorescent side products and interferences that could provide exaggerated results for $O_2^{\bullet-}$ generation. The stimulation protocol using PMA in the presence of DDC and 2-ME as SOD inhibitors showed an increase of 15-fold in 2-OH-MitoE^+ concentration per cell, when compared to native cells. Cell stimulation and sample preparation protocols were optimized for the detection of the product of MitoHE with $O_2^{\bullet-}$. Additionally, the monitoring of SIN-1 driven $O_2^{\bullet-}$ production inside and outside a biological environment by ME-LIF was also presented. In the future, the cell heterogeneity observed after

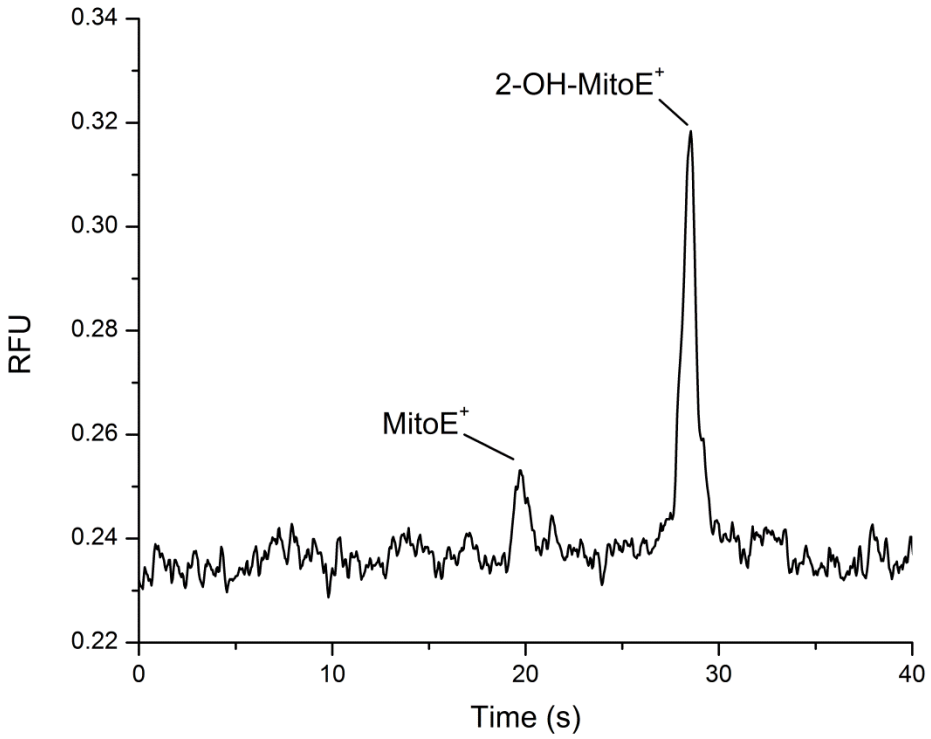

Figure 5.10. Bulk cell lysate analysis of 24 h PMA stimulated RAW 264.7 in the presence of both DDC and 2ME inhibitors. Run showing the separation both MitoE+ and in 2-OH-MitoE^+ peaks produced due to prolonged reaction between free MitoHE with oxidizing species other than $O_2^{\bullet-}$ or due to probe auto-oxidation.

PMA stimulation can be further evaluated by performing single cell analysis. Other $O_2^{\bullet-}$-specific fluorescent probes can be tested using the proposed PMA stimulation protocol to evaluate probe-to-probe variability. Additional cell lines can also be studied. This method complements our previously reported methods for NO detection using fluorescence and electrochemical detection [20, 27] as it allows an effective way to study a second reactive species, $O_2^{\bullet-}$, using ME-LIF. The ultimate goal is to develop microanalytical methods that are capable of simultaneously monitoring the production of NO, $O_2^{\bullet-}$, and $ONOO^-$ to better evaluate oxidative damage in different biological conditions at bulk and single cell levels.

5.5. References

1. Kagan, V.E.; Tyurina, Y.Y.; Tyurin, V.A.; Konduru, N.V.; Potapovich, A.I.; Osipov, A.N.; Kisin, E.R.; Schwegler-Berry, D.; Mercer, R.; Castranova, V.; Shvedova, A.A. Direct and Indirect Effects of Single Walled Carbon Nanotubes on RAW 264.7 Macrophages: Role of Iron. *Toxicol Lett*. **2006**, *165*, 88-100.

2. Li, H.; Li, Q.; Wang, X.; Xu, K.; Chen, Z.; Gong, X.; Liu, X.; Tong, L.; Tang, B. Simultaneous Determination of Superoxide and Hydrogen Peroxide in Macrophage RAW 264.7 Cell Extracts by Microchip Electrophoresis with Laser-Induced Fluorescence Detection. *Anal Chem*. **2009**, *81*, 2193-8.

3. Abbas, K.; Hardy, M.; Poulhès, F.; Karoui, H.; Tordo, P.; Ouari, O.; Peyrot, F. Detection of Superoxide Production in Stimulated and Unstimulated Living Cells Using New Cyclic Nitrone Spin Traps. *Free Radical Biol Med*. **2014**, *71*, 281-90.

4. So, H.-S.; Park, R.; Oh, H.-M.; Pae, H.-O.; Lee, J.-H.; Chai, K.-Y.; Chung, S.-Y.; Chung, H.-T. The Methanol Extract of Spiraea Prunifolia Var. Simpliciflora Root Inhibits the Generation of Nitric Oxide and Superoxide in Raw 264.7 Cells. *J Ethnopharmacol*. **1999**, *68*, 209-17.

5. Ambrozova, G.; Pekarova, M.; Lojek, A. The Effect of Lipid Peroxidation Products on Reactive Oxygen Species Formation and Nitric Oxide Production in Lipopolysaccharide-Stimulated Raw 264.7 Macrophages. *Toxicol In Vitro*. **2011**, *25*, 145-52.

6. Cohen, H.; Newburger, P.; Chovaniec, M.; Whitin, J.; Simons, E. Opsonized Zymosan-Stimulated Granulocytes-Activation and Activity of the Superoxide-Generating System and Membrane Potential Changes. *Blood*. **1981**, *58*, 975-82.

7. Suzuki, K.; Yamaguchi, T.; Oshizawa, T.; Yamamoto, Y.; Nishimaki-Mogami, T.; Hayakawa, T.; Takahashi, A. Okadaic Acid Induces Both Augmentation and Inhibition of Opsonized Zymosan-Stimulated Superoxide Production by Differentiated Hl-60 Cells. Possible Involvement of Dephosphorylation of a Cytosolic 21k Protein in Respiratory Burst. *Biochim Biophys Acta*. **1995**, *1266*, 261-7.

8. Meany, D.L.; Thompson, L.; Arriaga, E.A. Simultaneously Monitoring the Superoxide in the Mitochondrial Matrix and Extramitochondrial Space by Micellar Electrokinetic Chromatography with Laser-Induced Fluorescence. *Anal Chem*. **2007**, *79*, 4588-94.

9. Robinson, K.M.; Janes, M.S.; Pehar, M.; Monette, J.S.; Ross, M.F.; Hagen, T.M.; Murphy, M.P.; Beckman, J.S. Selective Fluorescent Imaging of Superoxide in Vivo Using Ethidium-Based Probes. *Proc Natl Acad Sci USA*. **2006**, *103*, 15038-43.

10. Mukhopadhyay, P.; Rajesh, M.; Hasko, G.; Hawkins, B.J.; Madesh, M.; Pacher, P. Simultaneous Detection of Apoptosis and Mitochondrial Superoxide Production in Live Cells by Flow Cytometry and Confocal Microscopy. *Nat Protocols*. **2007**, *2*, 2295-301.

11. Robinson, K.M.; Janes, M.S.; Beckman, J.S. The Selective Detection of Mitochondrial Superoxide by Live Cell Imaging. *Nat Protocols*. **2008**, *3*, 941-7.

12. Zielonka, J.; Kalyanaraman, B. Hydroethidine- and Mitosox-Derived Red Fluorescence Is Not a Reliable Indicator of Intracellular Superoxide Formation: Another Inconvenient Truth. *Free Radical Biol Med*. **2010**, *48*, 983-1001.

13. Zhao, H.; Kalivendi, S.; Zhang, H.; Joseph, J.; Nithipatikom, K.; Vásquez-Vivar, J.; Kalyanaraman, B. Superoxide Reacts with Hydroethidine but Forms a Fluorescent Product That Is Distinctly Different from Ethidium: Potential Implications in Intracellular Fluorescence Detection of Superoxide. *Free Radical Biol Med*. **2003**, *34*, 1359-68.

14. Gomes, A.; Fernandes, E.; Lima, J.L.F.C. Fluorescence Probes Used for Detection of Reactive Oxygen Species. *J Biochem Bioph Methods*. **2005**, *65*, 45-80.

15. Kalyanaraman, B.; Dranka, B.P.; Hardy, M.; Michalski, R.; Zielonka, J. Hplc-Based Monitoring of Products Formed from Hydroethidine-Based Fluorogenic Probes — the Ultimate Approach for Intra- and Extracellular Superoxide Detection. *Biochim Biophys Acta*. **2014**, *1840*, 739-44.

16. Michalski, R.; Michalowski, B.; Sikora, A.; Zielonka, J.; Kalyanaraman, B. On the Use of Fluorescence Lifetime Imaging and Dihydroethidium to Detect Superoxide in Intact Animals and Ex Vivo Tissues: A Reassessment. *Free Radical Biol Med*. **2014**, *67*, 278-84.

17. Xu, X.; Thompson, L.V.; Navratil, M.; Arriaga, E.A. Analysis of Superoxide Production in Single Skeletal Muscle Fibers. *Anal Chem*. **2010**, *82*, 4570-6.

18. Lvovich, V.; Scheeline, A. Amperometric Sensors for Simultaneous Superoxide and Hydrogen Peroxide Detection. *Anal Chem*. **1997**, *69*, 454-62.

19. Chen, J.; Rogers, S.C.; Kavdia, M. Analysis of Kinetics of Dihydroethidium Fluorescence with Superoxide Using Xanthine Oxidase and Hypoxanthine Assay. *Ann Biomed Eng*. **2013**, *41*, 327-37.

20. Mainz, E.R.; Gunasekara, D.B.; Caruso, G.; Jensen, D.T.; Hulvey, M.K.; Fracassi Da Silva, J.A.; Metto, E.C.; Culbertson, A.H.; Culbertson, C.T.; Lunte, S.M. Monitoring Intracellular Nitric Oxide Production Using Microchip Electrophoresis and Laser-Induced Fluorescence Detection. *Anal Methods*. **2012**, *4*, 414-20.

21. Zielonka, J.; Vasquez-Vivar, J.; Kalyanaraman, B. Detection of 2-Hydroxyethidium in Cellular Systems: A Unique Marker Product of Superoxide and Hydroethidine. *Nat Protocols*. **2008**, *3*, 8-21.

22. Zielonka, J.; Zhao, H.; Xu, Y.; Kalyanaraman, B. Mechanistic Similarities between Oxidation of Hydroethidine by Fremy's Salt and Superoxide: Stopped-Flow Optical and Epr Studies. *Free Radical Biol Med*. **2005**, *39*, 853-63.

23. Singh, R.J.; Hogg, N.; Joseph, J.; Konorev, E.; Kalyanaraman, B. The Peroxynitrite Generator, SIN-1, Becomes a Nitric Oxide Donor in the Presence of Electron Acceptors. *Arch Biochem Biophys*. **1999**, *361*, 331-9.

24. Hulvey, M.K.; Frankenfeld, C.N.; Lunte, S.M. Separation and Detection of Peroxynitrite Using Microchip Electrophoresis with Amperometric Detection. *Anal Chem*. **2010**, *82*, 1608-11.

25. Peng, T.; Yang, D. HKGreen-3: A Rhodol-Based Fluorescent Probe for Peroxynitrite. *Org Lett*. **2010**, *12*, 4932-5.

26. Peng, T.; Wong, N.-K.; Chen, X.; Chan, Y.-K.; Ho, D.H.-H.; Sun, Z.; Hu, J.J.; Shen, J.; El-Nezami, H.; Yang, D. Molecular Imaging of Peroxynitrite with HKGreen-4 in Live Cells and Tissues. *J Am Chem Soc*. **2014**, *136*, 11728-34.

27. Gunasekara, D.B.; Siegel, J.M.; Caruso, G.; Hulvey, M.K.; Lunte, S.M. Microchip Electrophoresis with Amperometric Detection Method for Profiling Cellular Nitrosative Stress Markers. *Analyst*. **2014**, *139*, 3265-73.

Chapter 6:

Simultaneous Detection of Nitric Oxide and Superoxide in RAW 264.7 Macrophage Cells

This work has been published in the following journal publication:

Giuseppe Caruso, Claudia G. Fresta, **Joseph M. Siegel**, Manjula B. Wijesinghe, Susan M. Lunte. "Microchip electrophoresis with laser-induced fluorescence detection for the determination of the ratio of nitric oxide to superoxide production in macrophages during inflammation." Analytical and Bioanalytical Chemistry. *Accepted*.

6.1. Introduction

Macrophages are cells involved in the primary immune defense mechanism that, when activated *in vivo* under pro-inflammatory conditions, can lead to a higher expression of inducible NOS (iNOS) coupled to the production of a large amount of NO and, thus, RNOS [1, 2]. It is well known that a combination of lipopolysaccharides (LPS) and interferon-gamma (IFN-γ) results in the stimulation of macrophages to produce a large amount of NO via iNOS [3]. In addition, high amounts of intracellular $O_2^{\bullet-}$ can be generated by incubating macrophages with phorbol 12-myristate 13-acetate (PMA) [4].

In this chapter, the use of ME-LIF for the simultaneous detection of intracellular NO and $O_2^{\bullet-}$ in RAW 264.7 macrophage cells is reported. These RNOS are detected by ME-LIF in the cell lysates of macrophages following incubation of the cells with both 4-amino-5-methylamino-2',7'-difluorofluorescein diacetate (DAF-FM DA) and MitoSOX Red for NO and $O_2^{\bullet-}$, respectively. Changes in the NO/$O_2^{\bullet-}$ ratio was then investigated under physiological and pro-inflammatory conditions. The resulting method provides an additional tool for understanding the physiopathological role of RNOS in oxidative stress-driven disorders.

6.2. Materials and Methods

6.2.1. Materials and Reagents

Murine RAW 264.7 cells (ATCC® TIB71™), Dulbecco's Modified Eagle's Medium (DMEM), phenol red-free DMEM, fetal bovine serum (FBS), and penicillin/streptomycin antibiotic solution were purchased from American Type Culture Collection (ATCC, Manassas, VA, USA). L-carnosine, diethyldithiocarbamate (DDC), 2-methoxyestradiol (2-ME), phorbol 12-myristate 13-acetate (PMA), anhydrous dimethyl sulfoxide (DMSO), phosphate-buffered saline (PBS), Trypan blue solution, lipopolysaccharides (LPS), sodium dodecyl sulfate (SDS),

calcium chloride, and bovine serum albumin (BSA) were all supplied by Sigma-Aldrich (St. Louis, MO, USA). Sodium hydroxide (NaOH), hydrochloric acid (HCl), 25 mL polystyrene culture flasks, boric acid, ethanol (95%), and C-Chip disposable hemocytometers were obtained from Fisher Scientific (Pittsburgh, PA, USA). Interferon-γ (IFN-γ) was supplied by Calbiochem (Gibbstown, NJ, USA). 4-Amino-5-methylamino-2',7'-difluorofluorescein diacetate (DAF-FM DA) and MitoSOX Red were purchased from Life Technologies (Carlsbad, CA, USA). Polyethersulfone (PES) membrane (3 kDa) centrifuge filters were purchased from VWR International (West Chester, PA, USA). Polydimethylsiloxane (PDMS) microdevices were prepared from the Sylgard 184 Elastomer Kit (Ellsworth Adhesives, Germantown, WI, USA). All water used was ultrapure (18.3 MΩ cm) (Milli-Q Synthesis A10, Millipore, Burlington, MA, USA).

6.2.2. Cell Culture and Preparation

RAW 264.7 macrophage cells were cultured in DMEM containing 10% (v/v) FBS, L-glutamine (2 mM), penicillin (50 IU mL^{-1}), and streptomycin (0.3 mg mL^{-1}). The cells were cultured in 25 cm^2 polystyrene culture flasks at a density of 5×10^6 cells/flask, maintained in a humidified environment at 37 °C, 5% CO_2, and 95% air, and passaged every 2 or 3 days depending on the cell confluence to avoid overgrowth.

6.2.2.1. Stimulation Protocol for the Detection of NO and $O_2^{\bullet-}$

The protocol used for cell sample preparation is shown in Figure 6.1. The day of the experiment, cells were harvested using a cell scraper, counted with a C-Chip disposable hemocytometer, and plated at a density of 1.2×10^7 cells/flask. Stock solutions of 1 mg/mL LPS and 200,000 U/mL IFN-γ were prepared in 10 mM PBS and 10 mM PBS with 0.1% BSA,

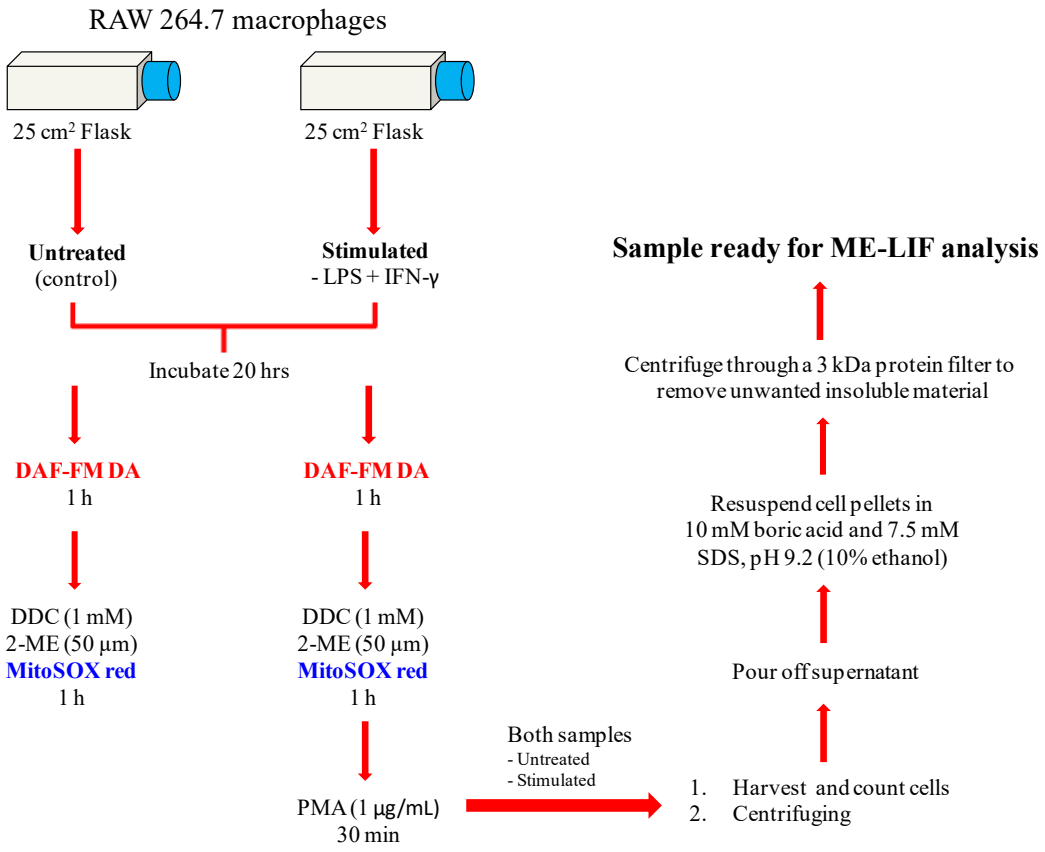

Figure 6.1. Flowchart of the protocol used for the preparation of RAW 264.7 cell lysates.

respectively. Once the cells adhered to the flask surface, they were stimulated to increase the production of NO by diluting the stock solutions to 100 ng/mL LPS and 600 U/mL INF-γ in 5 mL of cell culture medium. Immediately after the stimulation, the macrophages were incubated for 20 h in a humidified environment at 37 °C, 5% CO_2, and 95% air. A stock solution of 5 mM DAF-FM DA was prepared in 99% sterile DMSO. After the 20-h incubation with LPS + INF-γ, the medium was replaced with 5 mL of phenol red-free DMEM containing 10 µL of DAF-FM DA for 60 min (10 µM DAF-FM DA final concentration) [5]. A 5 mM MitoSOX Red stock solution was prepared in 99% sterile DMSO [6]. Additionally, a stock solution of 100 mM DDC was prepared in 10 mM PBS and stock solutions of 16.5 mM 2-ME and 1 mg/mL PMA were prepared in DMSO. Each flask of cells containing 5 mL of culture medium was then incubated for 1 h with a combination of the cytosolic SOD inhibitor DDC (1 mM final concentration), mitochondrial SOD inhibitor 2-ME (50 µM final concentration), and MitoSOX Red (10 µM MitoSOX final concentration). Finally, the cells were stimulated with PMA (1 µg/mL final concentration) for 30 min. During the incubation of the macrophages with DAF-FM DA and MitoSOX Red, the flasks were covered with aluminum foil to minimize any photo-bleaching of the dyes.

Native untreated cells from the same population were used as a control. These were incubated under the same conditions as the cells above, except that no stimulants were added. Another set of untreated cells was incubated in the presence of both SOD inhibitors (to increase the detectable concentration of $O_2^{\bullet-}$).

At the end of the stimulation process, the cells were harvested, and 100 µL of the cell suspension was removed for cell counting. The suspension was then centrifuged at 1,137 × *g* for 4 min. The supernatant was removed, and the cell pellet was washed twice with 1 mL of cold 10

mM PBS at pH 7.4. Cells were lysed with 50 µL of pure ethanol. The lysate solution was filtered using a 3 kDa molecular weight cut-off filter with centrifugation at 18,690 × *g* for 10 min. Then 10 µL of the filtered cell lysates were added to a 90 µL solution of 10 mM boric acid and 7.5 mM SDS at pH 9.2 (10% ethanol final concentration) and immediately analyzed with the microfluidic device**.** Peak identification of NO or $O_2^{\bullet-}$ was accomplished by using the same stimulation protocol, except that the cells were incubated in the presence of DAF-FM DA or MitoSOX Red only.

6.2.2.2. Alternative Stimulation Protocol

The effect of specific NO or $O_2^{\bullet-}$ stimulation procedures was evaluated through the analysis of changes in the NO/$O_2^{\bullet-}$ ratio in the macrophage cells. The protocol used for this analysis is the same as that described for the simultaneous detection of both analytes, except that the cells were stimulated with LPS + INF-γ (NO stimulation) or PMA ($O_2^{\bullet-}$ stimulation) only.

6.2.2.3. Pre-Treatment with Carnosine or Ca^{2+}

To investigate changes in the NO/ $O_2^{\bullet-}$ ratio due to the presence of carnosine or calcium ions, cells were incubated with either carnosine (10 µL of 500 mM stock solution in 10 mM PBS; 1 mM final concentration) 1 h prior to the stimulation with LPS + INF-γ or calcium chloride (25 µL of 200 mM stock solution in DI water; 1 mM final concentration) 1 h prior to the stimulation with PMA. Native untreated (nonstimulated) cells from the same population were incubated under identical conditions, in the presence of carnosine or calcium chloride, and used as controls.

6.2.2.4. Cell Density and Viability

Cell density and viability were measured using a C-Chip disposable hemocytometer and Trypan blue exclusion assay, respectively. The cell suspension was diluted either 1:3 or 1:5 (stimulated and untreated, respectively) with 0.4% Trypan blue solution.

6.2.3. Microchip Fabrication and Instrumental Setup

The fabrication of hybrid PDMS-glass microfluidic devices has been described previously [5]. Briefly, a silicon master containing the design of the microchip was fabricated with SU-8 photoresist and soft lithography. A 10:1 (w/w) PDMS pre-polymer to curing agent mixture was degassed in a vacuum desiccator and poured onto the master. The PDMS was cured overnight in an oven at 70 °C. Then the cured PDMS was peeled off the master and 3 mm reservoirs were punched in the substrate with a biopsy punch (Harris Uni-core, Ted Pella, Redding, CA, USA). To make the final microfluidic device, the PDMS substrate was reversibly bonded to a borosilicate glass substrate (Precision Glass and Optics, Santa Ana, CA, USA). For these experiments, a microchip with a simple-T design was employed with a 5 cm separation channel, 0.75 cm side arms, and 40 μm by 15 μm channels throughout.

Prior to operation, the microchip was conditioned with 0.1 M NaOH and run buffer. The run buffer utilized in these experiments consisted of 10 mM boric acid and 7.5 mM SDS at pH 9.2. A separation field was generated with a high voltage power supply (Ultravolt Inc., Ronkonkoma, NY, USA). A 1 s gated injection was used for sample introduction. A gate was established by applying +2400 V and +2200 V to the buffer and sample reservoirs, respectively.

For LIF detection, the microchip was placed on the stage of an Eclipse Ti-U inverted microscope (Nikon Instruments Inc., Melville, NY, USA). A 488 nm diode laser (Spectra-Physics, Irvine, CA, USA) was aligned 3.75 cm below the sample/buffer intersection as the

excitation source. Fluorescence signals were collected with a photomultiplier tube (Hamamatsu Corporation, Bridgewater, NJ, USA) and amplified with a SR570 low noise preamplifier at 1 μA V^{-1} (Stanford Research Systems, Sunnyvale, CA). Data were acquired with a D/A converter (National Instruments, Austin, TX, USA) and a homemade LabView program (National Instruments, Austin, TX, USA). Data analysis was accomplished with Origin 8.6 software (OriginLab, Northhampton, MA, USA).

6.2.4. Comparison of the Sensitivity of DAF-FM DA and MitoSOX Red

The fluorescence quantum yield of DAF-FM is ~0.005, but increases about 160-fold to ~0.81 after reacting with NO [7]. In the case of MitoSOX Red, the literature does not present a uniform view of the fluorescence quantum yield before and after reaction with $O_2^{\bullet-}$. To ensure that the ratio accurately depicts the relative concentration of NO to $O_2^{\bullet-}$ in the cell, the response factors for the products of the two probes were determined as described previously in [5] and [6]. The ratio of the slope of the response curve for DAF-FM T (NO-specific product) to that of 2-OH-MitoE^+ ($O_2^{\bullet-}$-specific product) was determined to be 1.2 (Figure 6.2). All NO/ $O_2^{\bullet-}$ ratios were corrected for the difference in sensitivity (quantum yield) between the two products. This provided a more accurate assessment of the relative amounts that are produced.

6.3. Results and Discussion

6.3.1. Optimization of the Stimulation Protocol and Electrophoretic Separation

Before monitoring the NO/ $O_2^{\bullet-}$ ratio, it was crucial to ensure that the method would be able to generate separable, measurable, and reproducible signals for both NO and $O_2^{\bullet-}$ in complex matrices such as RAW 264.7 macrophage cell lysates. Several factors needed to be considered because of their possible influence on the ability to detect both analytes by ME-LIF.

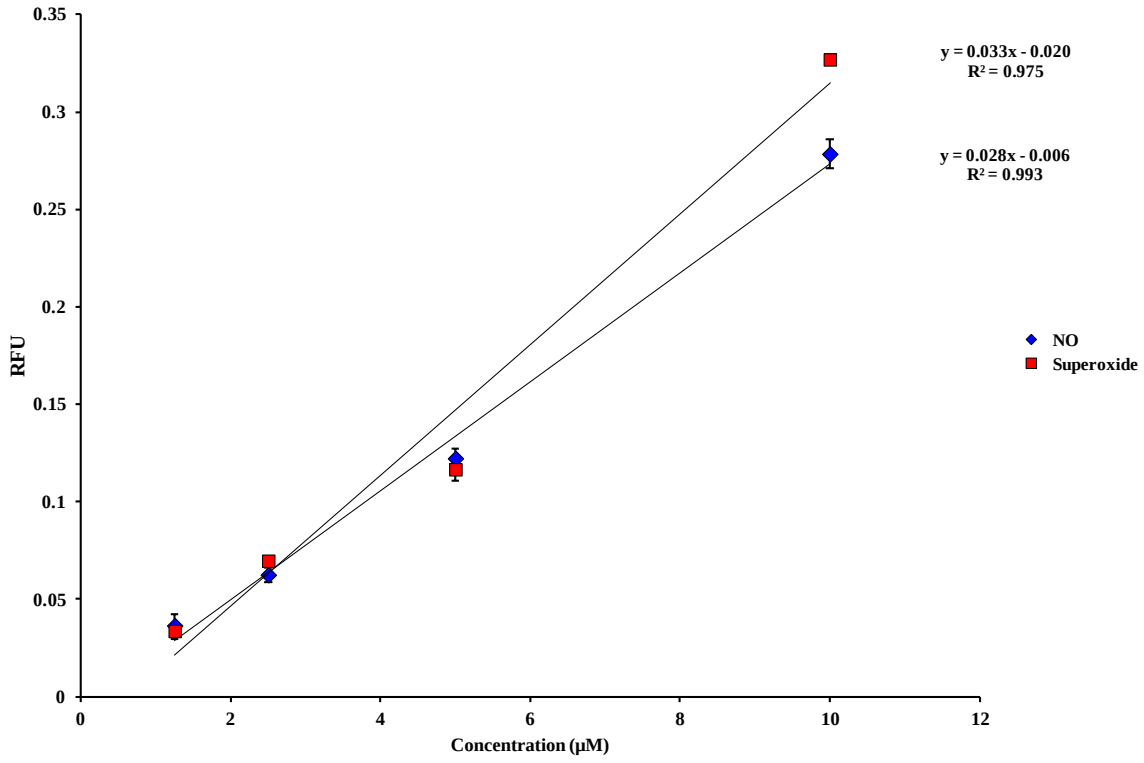

Figure 6.2. Calibration curves for DAF-FM T (NO-specific fluorescent product) and 2-OH-MitoE$^+$ ($O_2^{\bullet -}$-specific fluorescent product). Standard deviations are represented by vertical bars.

Initially, the cell stimulation protocol was optimized for generation of NO and $O_2^{\bullet-}$. In the first studies, cells were stimulated for 20 h with LPS + IFN-γ, followed by the addition of PMA (500 ng/mL final concentration) and incubation for an additional 60 min. However, this protocol was not optimal in terms of cell viability and NO and $O_2^{\bullet-}$ production. The PMA-stimulation time was then decreased from 60 to 30 min and the concentration was doubled to 1 µg/mL. The MitoSOX probe was incubated with cells for 1 h prior to stimulation with PMA. This new protocol was found to be the best for cell viability and NO and $O_2^{\bullet-}$ production.

Once the optimal cell stimulation protocol was established, attention was focused on the separation and detection conditions. Our group previously reported the detection of NO using DAF-FM and ME-LIF using a run buffer consisting of 10 mM boric acid and 7.5 mM SDS at pH 9.2 [5]. A separate method was developed for $O_2^{\bullet-}$ that employed a similar run buffer but with a lower SDS concentration (3.5 mM) [6]. In order to determine the optimal concentration of SDS needed for the simultaneous detection of NO and $O_2^{\bullet-}$, several SDS concentrations (3.5, 5.5, and 7.5 mM) in combination with 10 mM boric acid at pH 9.2 were investigated as background electrolytes. It was found that 7.5 mM SDS provided the best resolution for DAF-FM-T, 2-OH-MitoE^+, and potential interferences.

The previous ME-LIF methods mentioned above used a detection distance of 4.5 cm from the T intersection of the simple T microchip. Therefore, initial experiments in these studies used the same detection distance. However, it was found in these experiments that a distance of 3.5 cm provided a faster separation and better resolution, so it was used for all further studies.

The migration times for DAF-FM T and 2-OH-MitoE^+ under the different experimental conditions are reported in Table 1. The RSD for migration times was below 5% for both DAF-

Table 6.1. Migration times for DAF-FM T and 2-OH-MitoE$^+$ for untreated and stimulated cells.

	Migration time (s)	
Cell treatment	**DAF-FM T**	**2-OH-MitoE$^+$**
Untreated	21.82 ± 0.11	27.87 ± 0.15
Unstimulated + SOD inhibitors	22.81 ± 0.59	29.41 ± 0.45
LPS + IFN-γ + PMA + SOD inhibitors	23.64 ± 1.13	30.90 ± 1.42

FM T and 2-OH-MitoE$^+$ within sample type. However, there was a drift to longer migration times with the stimulated samples, which could be due to changes in the sample matrix effects and fouling of the PDMS substrate. The final optimized method including sample preparation is described in detail in the experimental section.

6.3.2. Simultaneous Detection of NO and $O_2^{\bullet-}$ in Macrophage Cell Lysates

Prior to the investigation of the effect of inflammation on the NO/$O_2^{\bullet-}$ ratio in macrophage cell lysates, the identity of the NO- and $O_2^{\bullet-}$-product-specific fluorescence peaks had to be verified. Figure 6.3a shows representative electropherograms of the simultaneous detection of NO and $O_2^{\bullet-}$ in RAW 264.7 macrophage cell lysates. The identification of NO and $O_2^{\bullet-}$ peaks was performed by incubating stimulated cells in the presence of one probe (DAF-FM DA or MitoSOX Red for NO and $O_2^{\bullet-}$, respectively). DAF-FM T and 2-OH-MitoE$^+$ represent the fluorescence reaction products of DAF-FM DA with NO and MitoSOX with $O_2^{\bullet-}$ [5, 6], respectively. Although DAF-FM is very selective for NO, it has been shown that it can react with dehydroascorbate (DHA), giving DAF-FM DHA [8-10]. In earlier studies, the DAF-FM DHA peak was effectively separated from the NO-specific peak in cell lysates [5]. In these studies, a peak for DAF-FM DHA was observed only in the electropherogram of a stimulated cell sample (Figure 6.3c).

Figure 6.3a shows a representative electropherogram for untreated macrophage cells. As can be seen by this electropherogram, the amount of NO and $O_2^{\bullet-}$ produced by native macrophages is very small due to the natural occurrence of endogenous intracellular scavenging molecules, such as SOD. Cytosolic and mitochondrial SOD regulates the intracellular concentration of $O_2^{\bullet-}$, which can make $O_2^{\bullet-}$ difficult to detect in the cell lysate samples [11]. Therefore, to reduce the degradation of intracellular $O_2^{\bullet-}$ by SOD, two different SOD inhibitors,

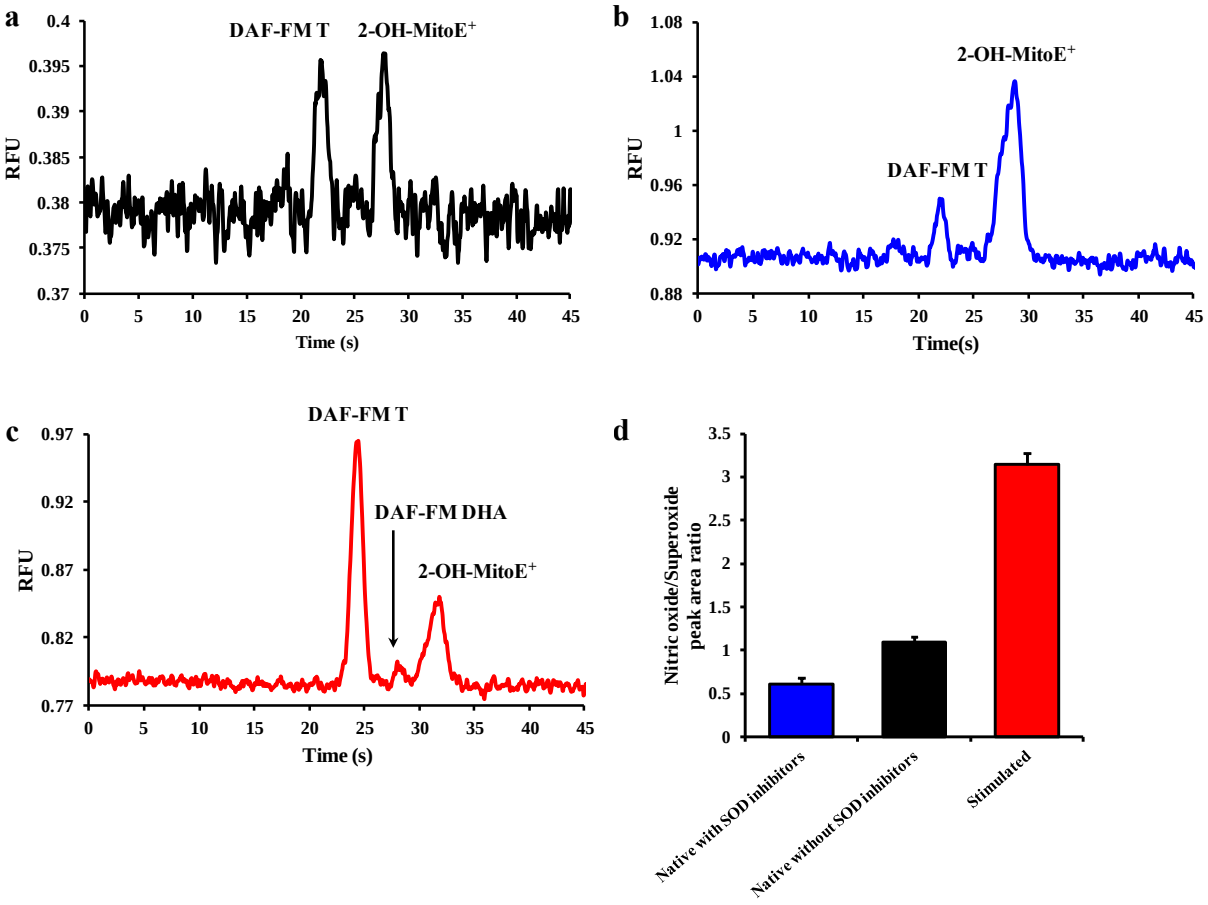

Figure 6.3. Representative electropherograms of (a) a native macrophage cell lysate, (b) macrophage cell lysate treated with DDC and 2-ME, and (c) cell lysate stimulated with LPS + IFN-γ + PMA in the presence of SOD inhibitors. (d) A histogram comparing the $NO/O_2^{\bullet-}$ peak area ratios between unstimulated cells in the presence or absence of SOD inhibitors, and cells stimulated with LPS + IFN-γ + PMA in the presence of SOD inhibitors. Standard deviations are represented by vertical bars.

2-ME and DDC, were introduced into the cells, along with MitoSOX Red, and incubated for an hour prior to analysis (Figure 6.1). Figure 6.3b shows a representative electropherogram obtained for unstimulated macrophages pre-treated with 2-ME and DDC, with a corresponding increase in the 2-OH-MitoE$^+$ peak in relation to the DAF-FM T peak. An electropherogram of the cell lysate obtained for cells stimulated with LPS, IFN-γ, and then PMA in the presence of SOD inhibitors is shown in Figure 6.3c. In this case, the products for both NO and $O_2^{\bullet-}$ signals were increased, indicating an expected enhancement in intracellular production of both species, with a greater amount of NO being produced. This yielded a higher NO/$O_2^{\bullet-}$ ratio than for the SOD inhibitors alone.

A bar graph showing the comparison of the NO/$O_2^{\bullet-}$ ratios obtained under the different experimental conditions is provided in Figure 6.3d. The ratios obtained for unstimulated cells pre-treated with SOD inhibitors (0.60 ± 0.07), unstimulated cells without SOD inhibitors (1.08 ± 0.06), and stimulated (3.14 ± 0.13) macrophages show that, along with peak areas, the ratio of NO to $O_2^{\bullet-}$ changes as a function of the stimulation conditions. In these experiments, the number of viable cells was determined prior to analysis because the stimulation process can reduce the amount of cell division [12], increase cell differentiation [13], and also cause cell death [14]. Figure 6.4 shows the variation in cell numbers as a function of the different stimulation protocols used in this study.

6.3.3. Changes in the NO/$O_2^{\bullet-}$ Ratio for LPS + IFN-γ-Stimulated Versus PMA-Stimulated Macrophages

NO [15] and $O_2^{\bullet-}$ [16] have been implicated in the development of several neurodegenerative disorders and cardiovascular disease. Therefore, a series of experiments was

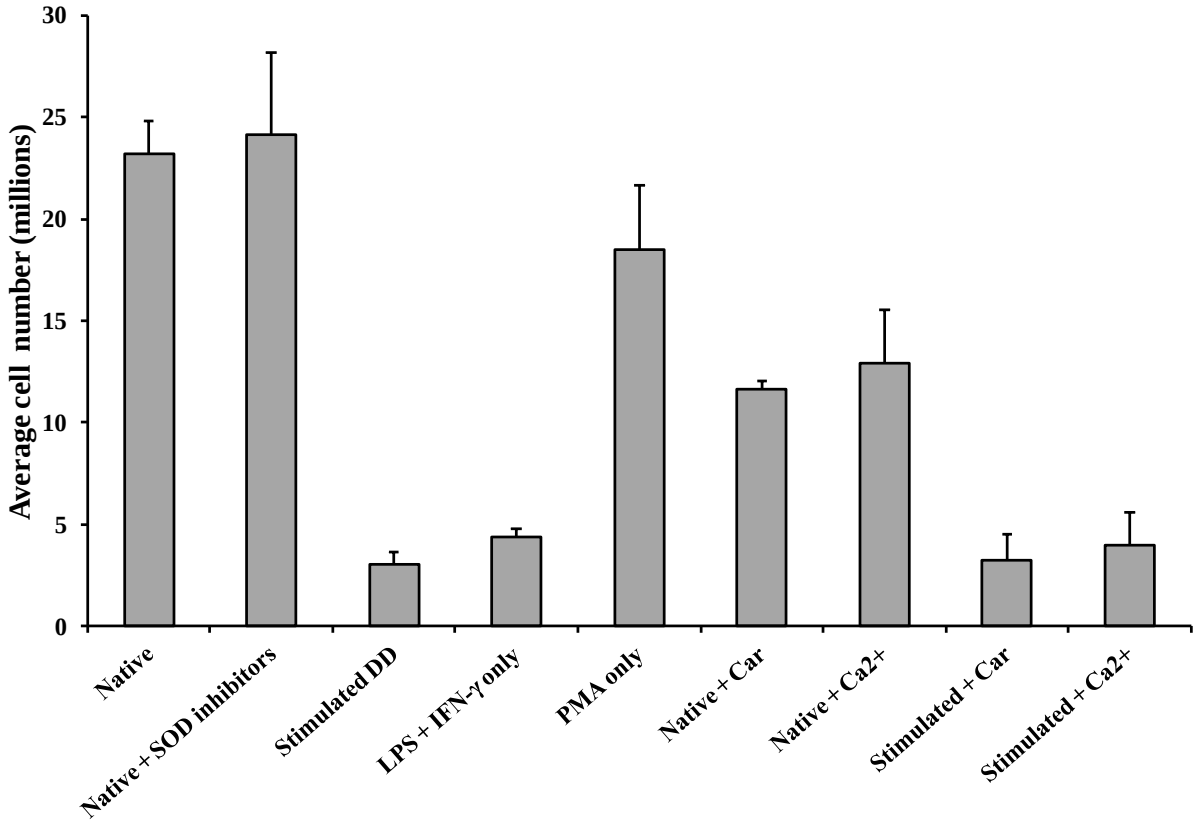

Figure 6.4. Variation of cell number as a function of the different stimulation protocols. Standard deviations are represented by vertical bars.

performed to investigate the effect of two different stimulation protocols on the intracellular $NO/O_2^{\bullet-}$ ratio. Figure 6.5a shows the comparison between NO and $O_2^{\bullet-}$ peak areas obtained for cells stimulated with LPS + INF-γ (NO stimulation) or PMA ($O_2^{\bullet-}$ stimulation) only. As expected, the NO peak area was higher than that of $O_2^{\bullet-}$ for the samples stimulated with LPS + INF-γ, while an opposite situation was observed for samples treated with only PMA. Interestingly, the average $O_2^{\bullet-}$ peak area was more than 3 times higher in the case of iNOS-activated cells (LPS + INF-γ) than with cells stimulated by PMA alone. These data imply that increased NO production or iNOS activation may catalyze $O_2^{\bullet-}$ production, which agrees with previous reports in the literature [17-20].

A bar graph showing the effect of stimulation protocol on the $NO/O_2^{\bullet-}$ ratio is shown in Figure 6.5b. The $NO/O_2^{\bullet-}$ value for cells stimulated with LPS + INF-γ was 2.31 ± 0.41 while the value for cells treated with PMA alone was 0.19 ± 0.06.

6.3.4. Effect of Carnosine or Ca^{2+} on the $NO/O_2^{\bullet-}$ Ratio in Native and Stimulated Macrophages

Carnosine is an endogenous dipeptide that exhibits antioxidant properties and protects cells against free radicals. It has been clearly demonstrated that carnosine is able to scavenge RNOS [21]. Recently, Caruso *et al.* have reported that carnosine can catalyze the conversion of NO into NO_2^-, thereby causing a decrease in the apparent intracellular NO concentration [22]. We have also shown that significant amounts of carnosine are taken up by macrophages when it is incorporated in the cell culture medium [23]. In these studies, the effect of Ca^{+2} on the $NO/O_2^{\bullet-}$ ratio was also investigated. Ca^{2+} is an intracellular second messenger involved in signal transduction and many pathological processes [24]. Calcium, along with RNOS, participates in

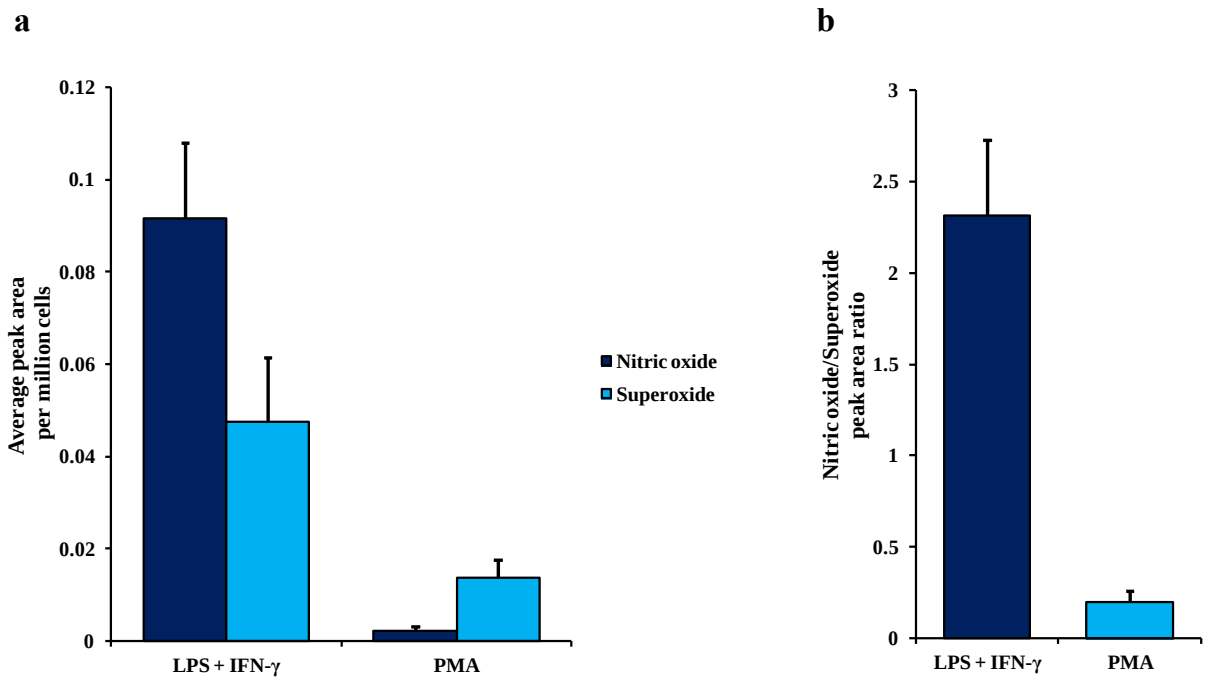

Figure 6.5. (a) The average peak area per million cells of NO and $O_2^{\bullet-}$ in cell lysate samples only stimulated with LPS + INF-γ (NO stimulation) or PMA ($O_2^{\bullet-}$ stimulation). (b) A comparison of the NO/$O_2^{\bullet-}$ peak area ratios between the two different stimulation protocols. Standard deviations are represented by vertical bars.

the regulation and integration of many cellular functions [25]. Increases in cytoplasmic Ca^{2+} have been correlated with increased $O_2^{\bullet-}$ [25-27].

In this study, the effect of pretreatment of the cells with either carnosine or Ca^{2+} on the $NO/O_2^{\bullet-}$ ratio in macrophage cell lysates was investigated under native and pro-inflammatory conditions. Figure 6.6 depicts the change in $NO/O_2^{\bullet-}$ ratio due to pretreatment of the cells with carnosine or Ca^{2+} in unstimulated (Figure 6.6a) and stimulated (Figure 6.6b) cells. When compared to the control (unstimulated cells), the samples pre-treated with carnosine showed a decrease in the $NO/O_2^{\bullet-}$ ratio (from 0.60 ± 0.07 to 0.35 ± 0.04). This ratio decrease was even more prominent for cells pre-treated with Ca^{2+} (from 0.60 ± 0.07 to 0.29 ± 0.05). A comparable trend was observed for stimulated samples, where the difference in the $NO/O_2^{\bullet-}$ ratio between each sample was slightly lower (from 3.1 ± 0.1 for cells stimulated with LPS + INF-γ + PMA to 2.3 ± 0.2 and 1.9 ± 0.1 for cells challenged with the same stimuli and pre-treated with carnosine or Ca^{2+}, respectively).

We believe that the decrease in the $NO/O_2^{\bullet-}$ ratio produced by pre-treatment with carnosine is due to a decrease in NO production (with little or no change in $O_2^{\bullet-}$ production). Previous studies by our group and others have shown that carnosine reduces iNOS-facilitated NO production in cells [22, 28, 29]. In contrast, it is proposed that Ca^{2+} pre-treatment caused a decrease in the $NO/O_2^{\bullet-}$ ratio due to an increase in intracellular $O_2^{\bullet-}$ (and not a decrease in NO). High intracellular Ca^{2+} concentrations have been shown to enhance the production of $O_2^{\bullet-}$ in the both the cytoplasm and mitochondria [25-27].

6.4. Conclusions

In this investigation, ME-LIF was employed for the simultaneous detection of NO and

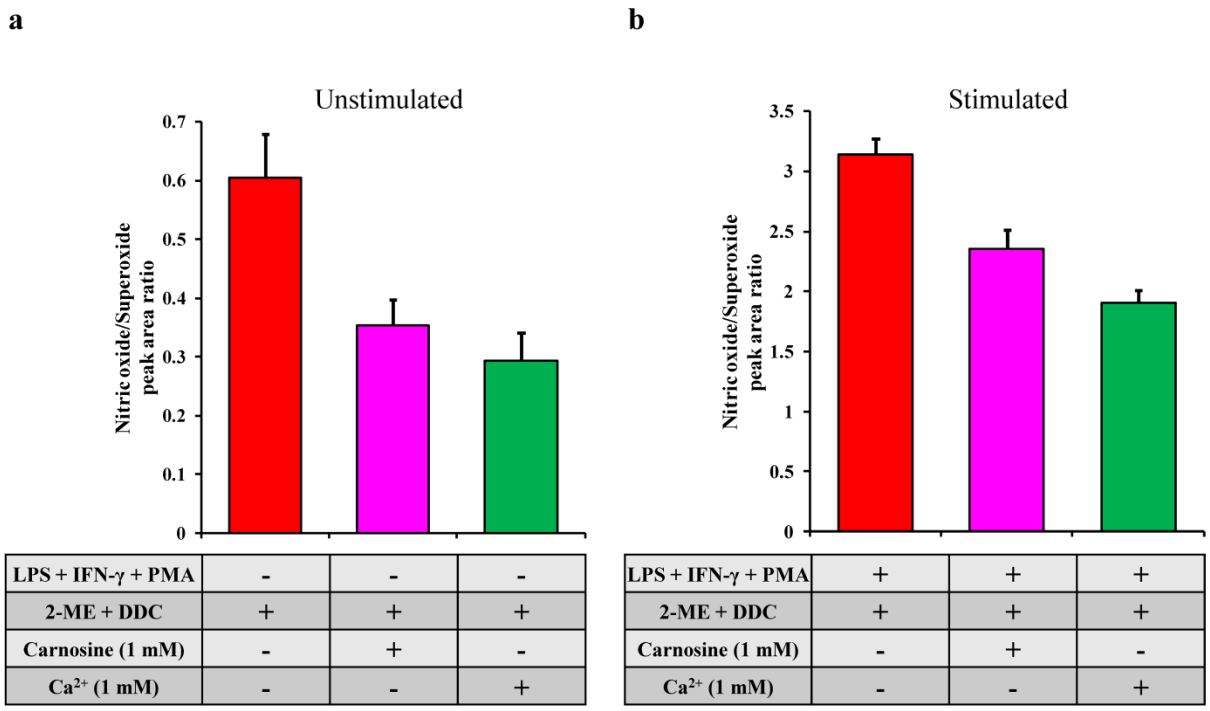

Figure 6.6. Changes in the $NO/O_2^{\bullet-}$ ratio due to pre-treatment with carnosine or Ca^{2+} in (a) unstimulated and (b) LPS + IFN-γ + PMA-stimulated cells. Standard deviations are represented by vertical bars.

$O_2^{\bullet-}$ using the fluorescent probes DAF-FM DA and MitoSOX. This method was also employed to study the variations of the $NO/O_2^{\bullet-}$ ratio in RAW 264.7 macrophage cell lysates under physiological and pro-inflammatory conditions. Additionally, the effect of the natural antioxidant carnosine and the second messenger Ca^{2+} in modulating this ratio was investigated. These results highlight the roles played by different stimulation protocols in influencing the release and bioavailability of NO with respect to $O_2^{\bullet-}$. It is well known that NO and $O_2^{\bullet-}$ production is related to many nitrosative and oxidative stress-driven disorders; thus, the development of new cell stimulation protocols along with the application of this method in single cell analysis formats will provide new perspectives that can be used for a better understanding of the role of RNOS in neurodegenerative and cardiovascular disease.

6.5. References

1. Chi, D.S.; Qui, M.; Krishnaswamy, G.; Li, C.; Stone, W. Regulation of Nitric Oxide Production from Macrophages by Lipopolysaccharide and Catecholamines. *Nitric Oxide*. **2003**, *8*, 127-32.

2. Panaro, M.A.; Brandonisio, O.; Acquafredda, A.; Sisto, M.; Mitolo, V. Evidences for iNOS Expression and Nitric Oxide Production in the Human Macrophages. *Curr Drug Targets Immune Endocr Metabol Disord*. **2003**, *3*, 210-21.

3. Seminara, A.R.; Ruvolo, P.P.; Murad, F. LPS/Ifn-γ-Induced RAW 264.7 Apoptosis Is Regulated by Both Nitric Oxide–Dependent and –Independent Pathways Involving JNK and the Bcl-2 Family. *Cell Cycle*. **2007**, *6*, 1772-8.

4. Abbas, K.; Hardy, M.; Poulhès, F.; Karoui, H.; Tordo, P.; Ouari, O.; Peyrot, F. Detection of Superoxide Production in Stimulated and Unstimulated Living Cells Using New Cyclic Nitrone Spin Traps. *Free Radical Biol Med*. **2014**, *71*, 281-90.

5. Mainz, E.R.; Gunasekara, D.B.; Caruso, G.; Jensen, D.T.; Hulvey, M.K.; Silva, J.A.F.; Metto, E.C.; Culbertson, A.H.; Culbertson, C.T.; Lunte, S.M. Monitoring Intracellular Nitric Oxide Production Using Microchip Electrophoresis and Laser-Induced Fluorescence Detection. *Anal Methods*. **2012**, *4*, 414-20.

6. Campos, R.P.S.; Siegel, J.M.; Fresta, C.G.; Caruso, G.; Silva, J.A.F.; Lunte, S.M. Indirect Detection of Superoxide in RAW 264.7 Macrophage Cells Using Microchip Electrophoresis Coupled to Laser-Induced Fluorescence. *Anal Bioanal Chem*. **2015**, *407*, 7003-12.

7. Kojima, H.; Urano, Y.; Kikuchi, K.; Higuchi, T.; Hirata, Y.; Nagano, T. Fluorescent Indicators for Imaging Nitric Oxide Production. *Angew Chem Int Ed*. **1999**, *38*, 3209-12.

8. Kim, W.-S.; Ye, X.; Rubakhin, S.S.; Sweedler, J.V. Measuring Nitric Oxide in Single Neurons by Capillary Electrophoresis with Laser-Induced Fluorescence: Use of Ascorbate Oxidase in Diaminofluorescein Measurements. *Anal Chem*. **2006**, *78*, 1859-65.

9. Balcerczyk, A.; Soszynski, M.; Bartosz, G. On the Specificity of 4-Amino-5-Methylamino-2′,7′-Difluorofluorescein as a Probe for Nitric Oxide. *Free Radical Biol Med*. **2005**, *39*, 327-35.

10. Zhang, X.; Kim, W.-S.; Hatcher, N.; Potgieter, K.; Moroz, L.L.; Gillette, R.; Sweedler, J.V. Interfering with Nitric Oxide Measurements: 4,5-Diaminofluorescein Reacts with Dehydroascorbic Acid and Ascorbic Acid. *J Biol Chem*. **2002**, *277*, 48472-8.

11. Fukai, T.; Ushio-Fukai, M. Superoxide Dismutases: Role in Redox Signaling, Vascular Function, and Diseases. *Antioxid Redox Signal*. **2011**, *15*, 1583-606.

12. Vadiveloo, P.K.; Keramidaris, E.; Morrison, W.A.; Stewart, A.G. Lipopolysaccharide-Induced Cell Cycle Arrest in Macrophages Occurs Independently of Nitric Oxide Synthase Ii Induction. *Biochim Biophys Acta*. **2001**, *1539*, 140-6.

13. Daigneault, M.; Preston, J.A.; Marriott, H.M.; Whyte, M.K.B.; Dockrell, D.H. The Identification of Markers of Macrophage Differentiation in Pma-Stimulated THP-1 Cells and Monocyte-Derived Macrophages. *PLoS One*. **2010**, *5*, e8668.

14. Nishio, K.; Horie, M.; Akazawa, Y.; Shichiri, M.; Iwahashi, H.; Hagihara, Y.; Yoshida, Y.; Niki, E. Attenuation of Lipopolysaccharide (LPS)-Induced Cytotoxicity by Tocopherols and Tocotrienols. *Redox Biology*. **2013**, *1*, 97-103.

15. Togo, T.; Katsuse, O.; Iseki, E. Nitric Oxide Pathways in Alzheimer's Disease and Other Neurodegenerative Dementias. *Neurol Res*. **2004**, *26*, 563-6.

16. Wu, Z.; Zhao, Y.; Zhao, B. Superoxide Anion, Uncoupling Proteins and Alzheimer's Disease. *J Clin Biochem Nutr*. **2010**, *46*, 187-94.

17. Xia, Y.; Roman, L.J.; Masters, B.S.S.; Zweier, J.L. Inducible Nitric-Oxide Synthase Generates Superoxide from the Reductase Domain. *J Biol Chem*. **1998**, *273*, 22635-9.

18. Heinzel, B.; John, M.; Klatt, P.; Böhme, E.; Mayer, B. Ca^{2+}/Calmodulin-Dependent Formation of Hydrogen Peroxide by Brain Nitric Oxide Synthase. *Biochem J*. **1992**, *281*, 627-30.

19. Pou, S.; Keaton, L.; Surichamorn, W.; Rosen, G.M. Mechanism of Superoxide Generation by Neuronal Nitric-Oxide Synthase. *J Biol Chem*. **1999**, *274*, 9573-80.

20. Pou, S.; Pou, W.S.; Bredt, D.S.; Snyder, S.H.; Rosen, G.M. Generation of Superoxide by Purified Brain Nitric Oxide Synthase. *J Biol Chem*. **1992**, *267*, 24173-6.

21. Hipkiss, A.R. Chapter 3 Carnosine and Its Possible Roles in Nutrition and Health. Advances in Food and Nutrition Research. Academic Press; 2009. p. 87-154.

22. Caruso, G.; Fresta, C.G.; Martinez-Becerra, F.; Antonio, L.; Johnson, R.T.; De Campos, R.P.S.; Siegel, J.M.; Wijesinghe, M.B.; Lazzarino, G.; Lunte, S.M. Carnosine Modulates

Nitric Oxide in Stimulated Murine RAW 264.7 Macrophages. *Mol Cell Biochem*. **2017**, doi:10.1007/s11010-017-2991-3.

23. Fresta, C.G.; Hogard, M.L.; Caruso, G.; Melo Costa, E.E.; Lazzarino, G.; Lunte, S.M. Monitoring Carnosine Uptake by RAW 264.7 Macrophage Cells Using Microchip Electrophoresis with Fluorescence Detection. *Anal Methods*. **2017**, *9*, 402-8.

24. Nicholls, D.G. Mitochondrial Calcium Function and Dysfunction in the Central Nervous System. *Biochim Biophys Acta*. **2009**, *1787*, 1416-24.

25. Yan, Y.; Wei, C.-L.; Zhang, W.-R.; Cheng, H.-P.; Liu, J. Cross-Talk between Calcium and Reactive Oxygen Species Signaling. *Acta Pharmacol Sin*. **2006**, *27*, 821-6.

26. Scully, S.P.; Segel, G.B.; Lichtman, M.A. Relationship of Superoxide Production to Cytoplasmic Free Calcium in Human Monocytes. *J Clin Invest*. **1986**, *77*, 1349-56.

27. Valentin, F.; Bueb, J.L.; Capdeville-Atkinson, C.; Tschirhart, E. Rac-1-Mediated O_2 Secretion Requires Ca^{2+} Influx in Neutrophil-Like Hl-60 Cells. *Cell Calcium*. **2001**, *29*, 409-15.

28. Fleisher-Berkovich, S.; Abramovitch-Dahan, C.; Ben-Shabat, S.; Apte, R.; Beit-Yannai, E. Inhibitory Effect of Carnosine and N-Acetyl Carnosine on LPS-Induced Microglial Oxidative Stress and Inflammation. *Peptides*. **2009**, *30*, 1306-12.

29. Nicoletti, V.G.; Santoro, A.M.; Grasso, G.; Vagliasindi, L.I.; Giuffrida, M.L.; Cuppari, C.; Purrello, V.S.; Stella, A.M.G.; Rizzarelli, E. Carnosine Interaction with Nitric Oxide and Astroglial Cell Protection. *J Neurosci Res*. **2007**, *85*, 2239-45.

Chapter 7:

Conclusions and Future Directions

7.1. Conclusions

The ultimate goal of this research is to develop separation-based methods using microfluidic platforms to monitor the reactive nitrogen and oxygen species (RNOS) production in macrophage cells under nitrosative and oxidative stress conditions. To achieve this goal, methods utilizing microchip electrophoresis coupled with either electrochemical detection (ME-EC) or laser induced-fluorescence (ME-LIF) were developed. First, a method was developed to detect nitrite (NO_2^-), a major product of nitric oxide (NO) metabolism, in bulk macrophage cell lysates with ME-EC. Electrochemical detection is advantageous because it has the ability to detect multiple electrochemically active molecules, including some RNS and intracellular antioxidants. To demonstrate this, the ME-EC method was used to separate and detect NO_2^-, iodide (internal standard), tyrosine, and hydrogen peroxide standards in reverse polarity with a run buffer consisting of 10 mM boric acid at pH 10 with 2 mM TTAC. Then, NO_2^- and glutathione were separated and detected in lipopolysaccharide (LPS)-stimulated and native macrophages. Using the method of standard additions, the concentration of NO_2^- in a single macrophage cell was estimated to be 1.41 mM and 4.00 mM in native and LPS-stimulated cells, respectively. There was no change in intracellular glutathione. Additionally, NO was directly detected in LPS-stimulated cells and identified by its quick degradation and comigration with the neutral marker.

This ME-EC method was then improved upon through the addition of transient isotachophoresis (t-ITP) and a Pt black modified working electrode. First, it was determined that increasing the TTAC concentration from 2 mM to 5.5 mM in the run buffer helped improve peak-to-peak resolution, especially between NO_2^- and azide (interference). Stacking of the NO_2^- peak was accomplished through the addition of 10 mM NaCl to the run buffer while keeping the

sample buffer at 10 mM boric acid at pH 10 with 5.5 mM TTAC. The use of t-ITP provided a 5-fold decrease in the NO_2^- LOD without changing the ascorbic acid and hydrogen peroxide peaks. On the other hand, a Pt black modified working electrode did not improve the LOD of NO_2^-, but did enhance the NO_2^- sensitivity 2.5-fold. Lastly, t-ITP and a Pt black modified working electrode were used to separate and detect NO_2^- in native and LPS-stimulated macrophages, which produced a much more reliable NO_2^- signal.

Next, a cellulose acetate (CA)-based decoupler that is capable of operating in both polarities was developed and evaluated for ME-EC. The decoupler membrane was constructed by using a sandblaster to drill a hole in a glass substrate containing an embedded electrode and then filling that reservoir with a solution of 5% cellulose acetate in dioxane and heating. First, this decoupler platform was tested in normal polarity by separating and detecting norepinephrine, hydroquinone, and ascorbic acid at a carbon ink working electrode. The use of the cellulose acetate decoupler reduced the noise at the working electrode but caused significant band broadening. Next, a planar Pt working electrode was placed in a 5 cm straight channel containing run buffer with and without a decoupler to determine the effect of varying electric field strengths on the noise. The amplitude of the noise remained nearly constant up to 1500 V/cm when a decoupler was present, whereas the noise is dramatically increased without a decoupler and the background current maxed out the detector above 500 V/cm. Finally, a standard solution of NO_2^-, ascorbic acid, and hydrogen peroxide was separated in reverse polarity on the device and successfully detected electrochemically without significant band broadening after the cellulose acetate decoupler. However, the signals were significantly decreased after the decoupler, implying leakage around the membrane or possible analyte penetration through the cellulose acetate membrane.

A ME-LIF method was also developed to detect intracellular superoxide ($O_2^{\bullet-}$) in macrophages. This method used the fluorescent probe MitoSOX Red, which selectively reacts with $O_2^{\bullet-}$ to form the fluorescent product 2-OH-MitoE^+. However, this probe can also react with other ROS to form the product MitoE^+, which is also fluorescent, so a separation method is necessary to accurately measure the 2-OH-MitoE^+. The $O_2^{\bullet-}$-specific product was identified by using the xanthine/xanthine oxidase reaction to produce $O_2^{\bullet-}$. Next, SIN-1, a NO and $O_2^{\bullet-}$ donor, was added to cells and the $O_2^{\bullet-}$ production was monitored over a period of 40 min. Superoxide dismutase (SOD) inhibitors were also added to the cell culture to obtain a better intracellular $O_2^{\bullet-}$ signal. This prevented the intracellular $O_2^{\bullet-}$ from being immediately scavenged in the cell before the MitoSOX could react with it. Lastly, the intracellular $O_2^{\bullet-}$ concentration was determined to be 0.17 mM and 2.5 mM for native and phorbol 12-myristate 13-acetate (PMA)-simulated macrophage cells, respectively, also incubated with SOD inhibitors.

This ME-LIF method for detecting $O_2^{\bullet-}$ was then coupled with a method to fluorescently detect NO with DAF-FM DA. This allowed for the simultaneous detection of $O_2^{\bullet-}$ and NO in macrophage cells under nitrosative and oxidative stress conditions. NO and DAF-FM DA react to form the NO-specific fluorescent product DAF-FM T. DAF-FM T and 2-OH-MitoE^+ were separated while using a run buffer consisting of 10 mM boric acid at pH 9.2 with 7.5 mM SDS. Detection of these molecules occurred 3.5 cm after the injection intersection of the microchip to obtain optimal resolution. Both fluorescent products were successfully detected in native, SOD incubated, and SOD incubated with LPS, interferon-γ (IFN-γ), and PMA stimulated macrophage cells. Stimulation with only PMA resulted in oxidative stress and the production of $O_2^{\bullet-}$ was increased, with no significant change in the NO production. On the other hand, stimulation with only LPS and IFN-γ (nitrosative stress conditions) caused both the NO and $O_2^{\bullet-}$ production to

increase. The ratio of NO to $O_2^{\bullet-}$ for cells stimulated with LPS and IFN-γ as well as those stimulated with PMA were found to be 2.31 and 0.19, respectively, indicating that more NO was produced under nitrosative stress conditions and more $O_2^{\bullet-}$ was produced under oxidative stress conditions. Lastly, the effects of carnosine as well as calcium on the $NO/O_2^{\bullet-}$ ratio was tested on cells incubated with SOD inhibitors and cells incubated with SOD and stimulated with LPS, IFN-γ, and PMA. A decrease in the ratio was observed for both the carnosine and calcium incubations.

7.2. Future Directions

7.2.1. Immediate Goals

7.2.1.1. Detection of $ONOO^-$ with HKGreen-3

HKGreen-3 is a peroxynitrite ($ONOO^-$)-selective fluorescent probe developed by Peng *et al.* [1]. This probe is not commercially available, and was synthesized at the University of Kansas. To determine the intercellular concentration of $ONOO^-$, HKGreen-3 was modified to include an acetate group (HKGreen-3A), allowing it to travel across cell membranes. Inside the cell, esterases cleave off the acetate group, recreating HKGreen-3, which can then react with $ONOO^-$ to form the fluorescent product N-methylrhodol (Figure 7.1). All three forms of the fluorescent probe were found to exhibit similar excitation and emission wavelengths (512 and 535 nm, respectively), so a separation method was necessary to detect N-methylrhodol without HKGreen-3 and HKGreen-3A interfering. An electrophoretic separation was developed on a hybrid PDMS/glass microchip with a simple-t design containing a 5 cm separation channel and a run buffer of 12.5 mM boric acid and 7 mM sodium dodecyl sulfate at pH 9.2. To ensure that $ONOO^-$ only reacted with HKGreen-3 and not its acetylated form, HKGreen-3A was added to a

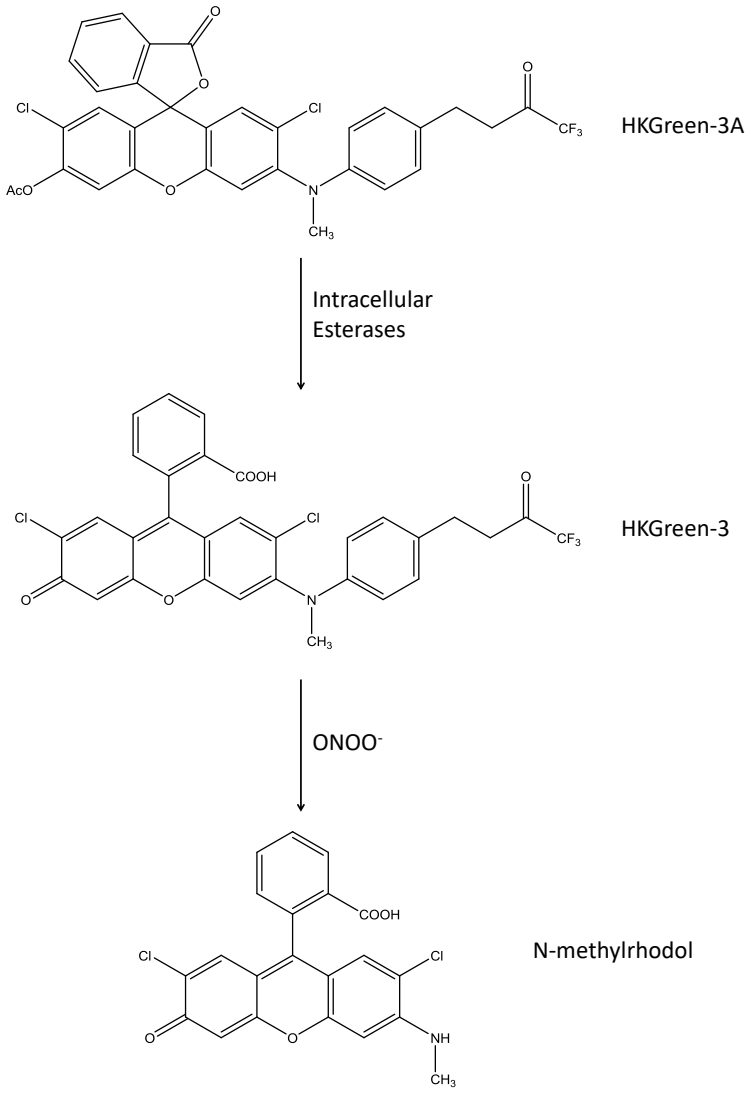

Figure 7.1. Reaction scheme of HKGreen-3.

concentrated sample of $ONOO^-$ (Figure 7.2a). As expected, N-methylrhodol was not produced. Esterase was then manually added to the sample in order to convert the probe into HKGreen-3. A large N-methylrhodol peak was subsequently observed (Figure 7.2b), indicating that $ONOO^-$ would only react with the probe once inside a cell.

To study the production of $ONOO^-$ *in vitro*, RAW 264.7 macrophage cells were used. The cells successfully took up the acetylated probe and converted it into HKGreen-3. It was found that both HKGreen-3A and HKGreen-3 associated with the cell membrane, so the cells were lysed with pure ethanol to prepare them for ME-LIF analysis. The next step is to detect the intracellular $ONOO^-$ produced through the stimulation of macrophage cells with LPS, IFN-γ, and PMA.

7.2.1.2. Optimization of the Cellulose Acetate Decoupler

The cellulose acetate-based decoupler developed in Chapter 4 still requires optimization before it can be practically applied to a separation system. Two issues need to be addressed: band broadening and analyte loss or leakage. Band broadening can be reduced by increasing the separation field strength, which would increase the velocity of the electroosmotic flow. Increasing the bulk flow of the system would decrease the time analytes travel from the decoupler to the working electrode, thereby limiting diffusion. Increasing the separation field strength can be achieved by switching from a gated injection system, which requires two high voltage sources, to a one high voltage source injection or a pressure injection. Gated injections are very useful for ME separations because of their reproducibility; however, in order to create a gate, two large electric fields that are similar in strength must be present (e.g. 2400 V and 2200 V applied to the buffer and sample reservoirs, respectively, in a simple-t microchip). Therefore,

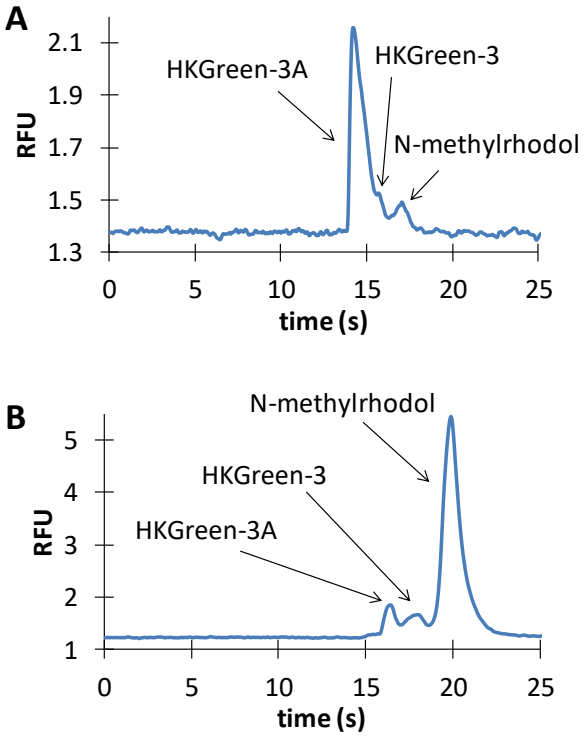

Figure 7.2. Electropherograms of a mixture of HKGreen-3A and concentrated $ONOO^-$ (A) before and (B) after the addition of esterase to convert HKGreen-3A to HKGreen-3.

increasing the separation field past 350 V/cm becomes difficult because the voltages being supplied become so large that Joule heating can occur. This Joule heating primarily occurs between the sample and sample waste reservoirs in a simple-t microchip because the length of channel that potential is applied over is much shorter than the distance from the buffer to buffer waste. However, in a one electrode separation system, a large separation field can be more easily produced because there is no need for a junction potential.

Bowen *et al*. utilized a set of on-chip PDMS pumps to hydrodynamically inject sample into a separation channel, thereby removing the need for two applied electrical potentials [2]. Sahore *et al*. developed a microchip system that used a set of PDMS valves to move the sample to the separation channel and another set to control the injection volume [3]. Once the sample was loaded into the injection space, an electric potential was applied across the channel for the separation and valves were opened for sample injection and separation [3]. Not only did these systems only need one high voltage source, but they also provided larger sample injection volumes, thereby increasing analyte signals.

To solve the problem of analyte not reaching the working electrode after the decoupler, other types of membranes should be tested. Known membranes, such as Nafion, can be used, however care must be taken that certain analytes are not removed from the separation channel because the membrane can act as a ion-exchange membrane [4]. Another possibility is to use hydrogels or xerogels because of their conductivity, which allows for charge transfer, their pore size variations, and their modification options for specific applications [5, 6]. Additionally, PDMS could be used as a possible membrane material if the pore size is increased. Normally, a PDMS membrane is too resistive and will not allow charge to travel across it [4]. However, Gabriel *et al*. found that PDMS mixed with powdered sugar, cured, and subsequently sonicated

in water to dissolve the sugar provided a membrane that allows charge transfer [7]. This porous PDMS membrane was used in a membrane-based decoupler, but the decoupler was only tested up to 200 V/cm [7]. So, additional testing would have to be done to determine versatility of this membrane in higher field strengths.

7.2.2. Long Term Goals

7.2.2.1. Studying Nitrosative and Oxidative Stress in Single Cells

Single cell analysis (SCA) provides an opportunity to study cellular heterogeneity. Since immune cells can be activated into inflammatory (M1) and anti-inflammatory (M2) phenotypes, it is important to understand the molecules produced by each phenotype under various nitrosative and oxidative stress-inducing environments. A SCA device and method was developed by Metto *et al*. to monitor NO in single Jurkat cells using DAF-FM DA and 6-CFDA (internal standard for cell volume) [8]. This device was then improved with the implementation of a PDMS pump system to better control fluidic and cell movement throughout the device [9]. The next step in this process is to combine electrochemical detection (EC) with the SCA device to allow for multiple analytes to be detected simultaneously within a separation without the need for expensive fluorescent probes. The design of this device is shown in Figure 7.3.

The difficulty in coupling SCA with EC is the high electric field necessary for cell lysis. Cell lysis on a chip can be achieved at an electric field strength of 600 to 700 V/cm. Since this electric field is also used as the separation field, an in-channel working electrode alignment cannot be used because the electrode or potentiostat would break. End-channel alignment would effectively decouple the electric field from the working electrode, but the decrease in resolution would significantly limit the number of measureable analytes in the separation. Off-channel

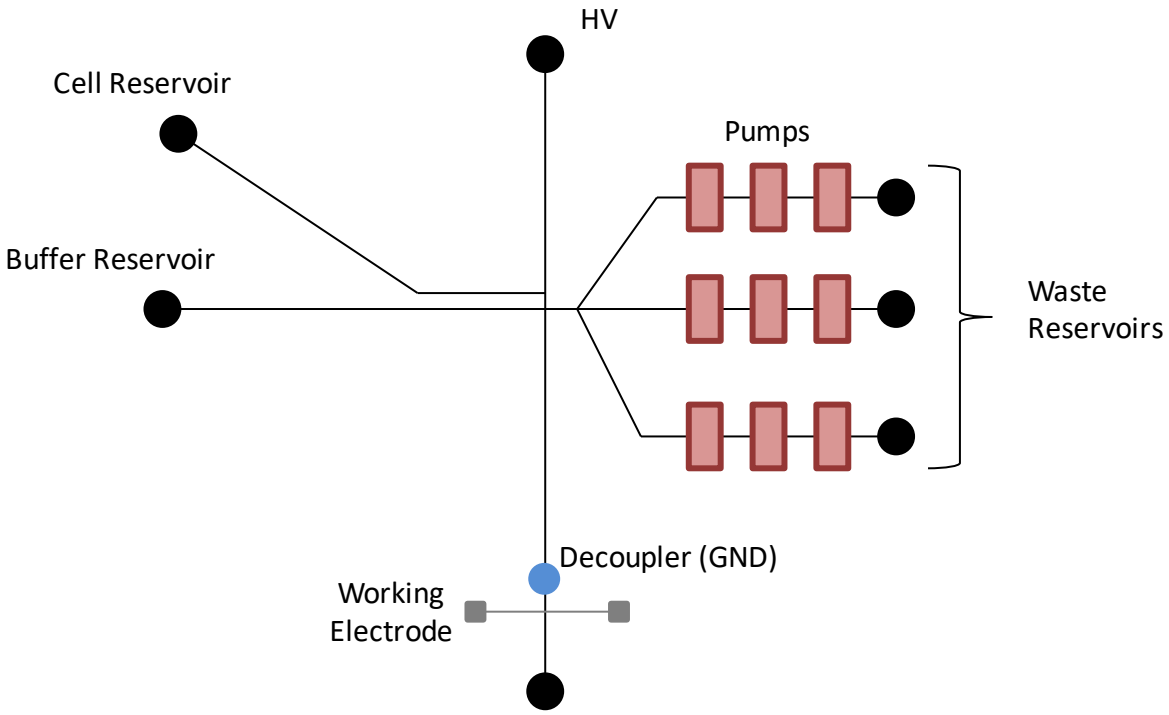

Figure 7.3. A schematic of the SCA device coupled with EC.

alignment with the use of a decoupler would provide optimal conditions for EC on this device. Therefore, once optimized, a cellulose acetate-based decoupler will be coupled with this SCA device. The cellulose-acetate-based decoupler is desirable because it can be used in reverse polarity, thereby allowing the separation of very small, negative molecules such as RNOS.

The ultimate goal is to use this device to obtain a better understanding of the role nitrosative and oxidative stress as well as cellular heterogeneity play in neurodegeneration. The SCA-EC device will be tested first with Jurkat cells and then RAW 264.7 macrophages. Jurkat cells are a good preliminary cell line because they are non-adherent and are less likely to attach to the channel walls and form clogs. Once shown to be fully operational, RNOS will be monitored in single BV-2 microglial cells after incubation with neurodegenerative disease markers, such as amyloid-β or α-synuclein for Alzheimer's and Parkinson's disease, respectively.

7.3. References

1. Peng, T.; Yang, D. HKGreen-3: A Rhodol-Based Fluorescent Probe for Peroxynitrite. *Org Lett*. **2010**, *12*, 4932-5.

2. Bowen, A.L.; Martin, R.S. Integration of On-Chip Peristaltic Pumps and Injection Valves with Microchip Electrophoresis and Electrochemical Detection. *Electrophoresis*. **2010**, *31*, 2534-40.

3. Sahore, V.; Kumar, S.; Rogers, C.I.; Jensen, J.K.; Sonker, M.; Woolley, A.T. Pressure-Actuated Microfluidic Devices for Electrophoretic Separation of Pre-Term Birth Biomarkers. *Anal Bioanal Chem*. **2016**, *408*, 599-607.

4. Osbourn, D.M.; Lunte, C.E. On-Column Electrochemical Detection for Microchip Capillary Electrophoresis. *Anal Chem*. **2003**, *75*, 2710-4.

5. Hrubesh, L.W. Aerogel Applications. *J Non-Cryst Solids*. **1998**, *225*, 335-42.

6. Schmidt, M.; Schwertfeger, F. Applications for Silica Aerogel Products. *J Non-Cryst Solids*. **1998**, *225*, 364-8.

7. Gabriel, E.F.M.; Coltro, W.K.T.; Garcia, C.D. Fast and Versatile Fabrication of PMMA Microchip Electrophoretic Devices by Laser Engraving. *Electrophoresis*. **2014**, *35*, 2325-32.

8. Metto, E.C.; Evans, K.; Barney, P.; Culbertson, A.H.; Gunasekara, D.B.; Caruso, G.; Hulvey, M.K.; Silva, J.A.F.; Lunte, S.M.; Culbertson, C.T. An Integrated Microfluidic

Device for Monitoring Changes in Nitric Oxide Production in Single T-Lymphocyte (Jurkat) Cells. *Anal Chem*. **2013**, *85*, 10188-95.

9. Patabadige, D.E.W.; Mickleburgh, T.; Ferris, L.; Brummer, G.; Culbertson, A.H.; Culbertson, C.T. High-Throughput Microfluidic Device for Single Cell Analysis Using Multiple Integrated Soft Lithographic Pumps. *Electrophoresis*. **2016**, *37*, 1337-44.